**ISTANBUL TECHNICAL UNIVERSITY ★ GRADUATE SCHOOL OF
SCIENCE ENGINEERING AND TECHNOLOGY**

**HIGH STRAIN RATE CHARACTERIZATION OF ENGINEERING
MATERIALS**

M.Sc. THESIS

M. Burak YEGIN

Department of Mechanical Engineering

Solid Mechanics Programme

JUNE 2013

ISTANBUL TECHNICAL UNIVERSITY ★ GRADUATE SCHOOL OF SCIENCE ENGINEERING AND TECHNOLOGY

HIGH STRAIN RATE CHARACTERIZATION OF ENGINEERING MATERIALS

M.Sc. THESIS

M. Burak YEGIN
(503101502)

Department of Mechanical Engineering

Solid Mechanics Programme

Thesis Advisor: Emin SUNBULOGLU, Ph. D.

JUNE 2013

M. Burak Yegin, a **M.Sc.** student of ITU **Graduate School of Science, Engineering and Technology** student ID 503101502, successfully defended the **thesis** entitled "**HIGH STRAIN RATE CHARECTERIZATION**", which he/she prepared after fulfilling the requirements specified in the associated legislations, before the jury whose signatures are below.

Thesis Advisor :   **Prof. Dr. Emin SÜNBÜLOĞLU**   ....
                         İstanbul Technical University

Jury Members :   **Prof. Dr. Ahmet ARAN**   ....
                       Isik University

                       Prof. Dr. Ekrem TÜFEKÇİ   ....
                       İstanbul Technical University

Date of Submission :   **03 May 2013**
Date of Defense :   **07 June 2013**

To my late grand family,

FOREWORD

This thesis study would not have been possible great deal of support and friendship.

May 2013   M. Burak Yegin
                                                                  (Mechanical Engineer)

x

TABLE OF CONTENTS

ABBREVIATIONS

AISI   **:** American Iron and Stel Institute
SHPB   **:** Split-Hopkinson Pressure Bar

LIST OF TABLES

LIST OF FIGURES

HIGH STRAIN RATE CHARACTERIZATION OF ENGINEERING MATERIALS

SUMMARY

Determining of mechanical properties of engineering materials is one of the oldest research area of mechanical engineering. There has been a significant demand for engineering materials that are stronger, lighter and durable especially for automobile, aerospace and military industries. In addition to this, identification of the mechanical properties mainly requires experimental tests. It is the fact that experimental methods are very expensive for identification of mechanical properties. Nowadays, computer simulation which simulates real world are popular in scientific and engineering world especially for material behavior. In order to simulate material behavior, constitutive models which links the flow stress to incremental strain, strain rate and temperature should be used.

One of the most popular constitutive models used in computer simulation is Johnson – Cook strength model. This model includes three terms and five constants in order to describe stress as a function of strain rate, strain, temperature.

In the present work, five parameters of Johnson – Cook constitutive model are determined for material characterization. For this purpose, three test types were performed. Initially, quasi-static ($10^{-3} s^{-1}$) tensile tests are performed for determining yield strength and strain hardening parameters of Johnson – Cook Model. In addition to this, quasi–static temperature tests at $80 \, ^{\circ}C$ and $260 \, ^{\circ}C$ were performed in order to find thermal softening parameter.

Finally, the high strain rate tests were performed to characterize material behavior at strain rates. For this purpose, Split Hopkinson Pressure Bar apparatus was used. This device is used to obtain stress – strain behavior of materials under impact loading conditions. In SHPB, a specimen is sandwiched between two pressure bars which are called incident and transmitted bars. Then, a striker bar is accelerated with a gas gun or pressure bar in order to strike incident bar. At the same time, two strain gages on the pressure bars measure the strains on the bars.

In the present study, the test methods in order to determine Johnson – Cook material parameters are searched and applied three types of steel which are AISI 1040, AISI 1045 and AISI 4140. After necessary tests were performed, the obtained data is analyzed via MATLAB and Microsoft Excel for determining Johnson – Cook parameters.

The determined parameters for AISI 1040 were found to be well agreed with literature study. The thermal softening parameter could not be accurately determined because of not using extensometer at tests concducted at $260 \, ^{\circ}C$. For AISI 1045 and AISI 4140 steels, the test results were not seen to be compatible with available literature based on "normalized" material. Thus, it has seen that materials tested had an unknown "strain history", and this effects the material behavior considerably.

MÜHENDİSLİK MALZEMELERİNİN YÜKSEK ŞEKİL DEĞİŞTİRME HIZINDA KARAKTERİZASYONU

ÖZET

Malzemelerin mekanik özelliklerinin belirlenmesi makine mühendisliğinin en eski araştırma alanlarından birisidir. Piyasadaki rekabet dolayısıyla özellikle otomotiv, havacılık ve askeri endüstri malzemelerin daha hafif, daha dayanıklı olmasını istemektedir. Bu sebeple malzemlerin geliştirme alanındaki çalışmalar günümüzde hızla devam etmektedir.

Malzemelerin mekanik özellikleriyle ilgili en önemli bilgiye gerilme – birim şekil değiştirme eğrilerinden ulaşılır. Bilim adamları ve mühendisler yüzyıllarca malzemelerin maruz kaldıkları yükler altında nasıl davrandığı hakkında araştırmalar yapmıştır. Günümüzde bir çok sektörde malzeme seçimlerinde gerilme – birim şekil değiştirme eğrileri önemli rol oynamaktadır.

Malzemelerin gerilme – birim şekil değiştirme eğrileri deneysel yöntemlerle elde edilir. Fakat deneysel yöntemlerin pahalı ve zaman olarak uzun süreler aldığı bilinmektedir. Bu nedenle son yıllarda bilgisayarların da gelişmesiyle birlikte malzemeleri belirlenen yüklerde teste tabi tutmak yerine bilgisayar ortamında modelleyerek sonuçları görmek zaman ve ucuzluk açısından tercih edilmektedir.

Yapıların yükleme koşullarındaki davranışını bilgisayar ortamında modelleyebilmek için kullanılan malzemenin mekanik özelliklerinin bilinmesi ve bilgisayar programına verilmesi gereklidir. Elastisite modülü ve akma mukavemeti gibi malzeme özellikleri bir çok firma tarafından bilinmekle beraber, bu özellikler özellikle çarpma, patlama gibi yüksek sıcaklık ve yüksek birim şekil değiştirme hızı içeren olaylarda malzemenin davranışını belirlemek açısından yeterli değildir.

Plastisite teorisine göre bir malzemenin akma mukavemeti uygulanan birim şekil değiştirme miktarına, birim şekil değiştirme hızına ve sıcakığa bağlı olarak değişmektedir. Artan şekil değiştirme hızıyla malzemenin mukavemeti artmakta, artan sıcaklıkla beraber mukavemet azalmaktadır. Malzemenin bu gibi durumlarda davranışının belirlenebilmesi için standart çekme testlerinin yanında yüksek birim şekil değiştirme hızında ve yüksek sıcaklıklarda teste tabi tutulması gerekmektedir.

Malzemelerin yüksek birim şekil değiştirme hızı ve sıcaklıklardaki davranışını modelleyebilmek için mukavemet modellerine ihtiyaç duyulmaktadır. Mukavemet modelleri basit olarak mevcut birim şekil değiştirme miktarı, birim şekil değiştirme hızı ve sıcaklığa bağlı olarak gerilme değerinin hesaplanmasında kullanılmaktadır. Malzemenin elastik ve plastik bölgedeki davranışı malzemeye özgü çeşitli parametrelerle ifade edilir. Her malzeme için farklı olan bu değerler bilgisayar ortamına girilerek yapıların istenilen koşullar altında nasıl bir yapısal performans göstereceği belirlenebilir.

Viskoplastik mukavemt modellerinden en çok kullanılanı Johnson ve Cook tarafından 1983 yılında mermilerin yüksek hızda deformasyonuyla ilgili çalışmasında kullanılmak üzere buldukları Johnson – Cook mukavemet modelidir. Bu model malzemenin akma mukavemeti ve pekleşme özelliklerini, yüksek şekil değiştime sırasındaki davranışını ve yüksek sıcaklıktaki davranışını ifade eden üç ana çarpan ve beş parametreden oluşmaktadır. Bu beş parametreye karar vermek için çeşitli testler gerçekleştirilir. Bu testlerden standart çekme ve basma testleri

malzemenin akma mukavemeti ve pekleşme özelliklerinin bulunması açısından basit ve kullanışlı testlerdir. Yüksek sıcaklıkla ilgili parametre de yine çekme testlerinin yüksek sıcaklıklarda yapılmasıyla elde edilmektedir.

Malzemenin yüksek şekil değiştirme hızındaki davranışı ise ancak özel düzeneklerle test edilebilmektedir. Bu düzeneklerden en yaygın olarak kullanılanı Split Hopkinson Pressure Bar dinamik test aparatıdır. Bu düzenekte malzeme özellikleri öğrenilmek istenilen numune yüksek mukavemetli uzun silindirik barlar arasında sıkıştırılır. Daha sonra başka bir silindirik çubuk basınçlı bir sistemle hızlandırılarak ilk uzun çubuğa çarptırılır. Silindirler üzerinde ilerleyen gerilme ve gerinme dalgalarını ölçmek maksadıyla birinci ve ikinci barların yüzeylerine strain gageler konulmak suretiyle numune üzerinden iletilen ve geri yansıyan dalgalar hesaplanır. Bir boyutlu dalga denklemleri ve kuvvet eşitliği ilkelerinin uygulanılmsıyla malzemenin gerilme – gerinme eğrisi elde edilir. Günümüzde malzemelerin yüksek hızlı deformasyonlarındaki davranışını incelemek için en güvenilir düzenek bu düzenektir.

Bu çalışmada, 1040, soğuk çekme 1045 ve 4140 (CR42Mo4) çelikleri olmak üzere üç adet malzemenin Johnson – Cook mukavemet model parametrelerinin belirlenmesi hedeflenmiştir. Bu kapsamda öncelikle malzemenin akma mukavemeti ve pekleşme özellikleri, yüksek şekil değiştirme hızı ve yüksek sıcaklıktaki davranışını belirleyebilmek için üç ana test yapılır. Bunlardan ilki standar çekme testidir. Her malzeme için 5 adet çekme testi gerçekleştirilmiştir. Elde edilen sonuçlar MATLAB ve Microsoft Excel veri analizi programları yardımyla gerinme – gerilme grafikleri çizdirilmek vasıtasıyla akma mukavemeti ve pekleşme üsteli hesaplanır. Bu hesaplama deneyse sonuçlara modelin içerdiği parametrelerle birlikte en küçük kareler metodu ve regrassion analizi kullanılarak en iyi eğrinin uydurulmasına dayanır.

Malzemenin yüksek sıcaklık etkisini içeren parametreyi bulmak için çekme testleri 80 °C ve 260 °C olmak üzere iki farklı sıcaklıkta her malzeme için tekrarlandı. Buradan elde edilen eğriler oda sıcaklığında elde edilen çekme testi sonuçları baz alınarak ısıl yumuşama katsayısı elde edilmiştir. Yüksek sıcaklıklardaki testleri yaparken birim şekil değiştirme hızının etkisinin bulunmadığı varsayımı yapılarak Johnson – Cook mukavemet modelindeki bu terim dikkate alınmamıştır.

Mukavemet model parametrelerinin belirlenmesinde kullanılan son test tekniği Split Hopkinson Pressure Bar dinamik test yöntemidir. Her malzeme için üç adet silindirik numune kullanılarak farklı basınçlarda çarpma testi yapılmıştır. Bu yolla malzemelerin çarpma anındaki gerilme – şekil değiştirme eğrileri 400 kHz işleme frekansına sahip bir veri toplama cihazıyla belirlendikten sonar MATLAB veri analizi programlarıyla elde edilmiştir.Yüksek hızda çarpma test sonuçlarına, daha önceki testlerde elde edilen akma mukavemeti, pekleşme üsteli ve ısıl yumuşama katsayıları kullanılarak Johnson – Cook mukavemet modelinin son değişkeni olan birim şekil değiştirme katsayısı bulunmuştur.

Elde edilen sonuçlarda 1040 çeliği için özellikle literatüdeki yayınlarla uyumlu sonuçlar elde edilmiştir. 1045 ve 4140 çelikleri ise askeri uygulamlarda kullanılmak üzere ısıl işlem ve soğuk çekme uygulandığı için kırılgan davranış gösterip sünememiştir.

Malzemelerin yüksek sıcaklıkta akma mukavemetlerinin düştüğü gözlemlenmiştir. Bu düşme gözlemlenmekle beraber testlerin gerçekleştirildiği sıcaklıklar malzemelerin erime sıcaklıklarının çok altında olduğundan ısıl yumuşama etkisi

1040 ve 4140 çelikleri için tam olarak gözlemlenememiştir. Yüksek sıcaklıklarda extansiyometre kullanılmadığından dolayı eğriler 260 $°C$ için uyumsuzluklar göstermektedir.

Yüksek sıcaklıkta yapılan test sonuçlarında ise birim şekil değiştirme katsayısı üç test incelenerek elde edilmiştir. Elde edilen değerler literatürde bulunan değerlerle uyumlu olmaklar beraber malzemenin çekme ve basma durumunda farklılıklar gösterebilmesi nedeniyle Elastisite modülünde farklılıklar gözlemlenmiştir.

Bu çalışma kapsamında İTÜ BİYOMEKANİK VE MUKAVEMET LABARATUVARI akademisyenleri tarafından tasarlanan Split Hopkinson Pressure Bar dinamik test düzeneği malzemelerin çarpma anındaki davranışlarını belirleyebilmek amacıyla kullanılmıştır. Bunun yanında sonlu eleman yazılımlarda kullanılan malzeme modellerinin oluşturulması için gerekli testler araştırılıp çeşitli malzemeler için uygulanmıştır. Test tekniğinin gelişmesi öğrenilmesi ve sonlu elemanlar programları vasıtasıyla doğrulanmasıyla birlikte labaratuvar bünyesinde bulunan düzenek çarpma testlerinde başarıyla kullanılabilecektir. Uygulamalar sadece otomotiv, havacılık ve savunma sanayii gibi alanlarda değil mühendislikle tıbbın kesişim noktası olan biyomekanik alanında da önemli faydalar sağlayacaktır.

1. INTRODUCTION

Research on mechanical properties of engineering materials is one of the oldest scientific endeavors for mechanical engineering. There has been a significant demand for engineering materials that are stronger, lighter and durable especially for automobile, aerospace and military industries. In addition to this, identification of the mechanical properties mainly requires experimental tests. It is the fact that experimental methods are very expensive for identification of mechanical properties. The cost of identification of mechanical and chemical properties such as metallography, chemical composition and stress – strain curve is 1000-1250 €. Furthermore, if the strain rate dependent properties related crash tests are desired, the cost may increase to 5000-7000 € [1]. Since experimental tests are so expensive in order to characterize material properties of structure, the need for computational tools that describe the structural response of material has been increase day by day.

With improvement in computer skills, research facilities remarkably oriented to computational simulations. Development of CAE softwares allowed scientists and companies to reduce expenditures on research and avoiding too much testing [2]. For providing mechanical response of any material in computational simulations, material models known as constitutive equations are required. Indeed, all mechanical analysis of engineering materials needs for constitutive models that link the states of stress and strain [3]. For most of metals, in elastic regime, the stress linearly increases with respect to incremental strain until yield point. After the yield point, work hardening occurs and materials show a nonlinear stress increase respect incremental strain for most of metals. Furthermore, the rate of deformation and temperature are also effective in stress state.

It has been observed by experimental test that yield strength of many metals increases with increasing strain rate. In other words, metals resist to more deformation when the deformation rate is higher. Vice versa, metals resist to less deformation when the temperature is higher. Therefore, any constitutive model

should include the rate of deformation and temperature effects in order to simulate material behavior correctly.

1.1 Purpose of Thesis

The purpose of this thesis to characterize and model of mechanical behavior of three materials under quasi–static and dynamic loadings. The materials are AISI 1040, AISI 1045 cold rolled, AISI 4140 (Cr42Mo4) steels. These materials are not chosen for a specific project, they are chosen according to abundance and cost issues. For modeling material behavior, Johnson – Cook constitutive model is selected in this study. This rate – dependent constitutive model is chosen due to relative ease of parameters for this constitutive material model compared to other models.

After, an available constitutive law is described with different parameters, it is crucial to identify each of these parameters in order to define it. For this purpose, experimental tests are inevitable to evaluate these parameters. In this study, numerous quasi-static tension and Split Hopkinson Pressure Bar tests are performed to characterize mechanical behavior of materials. For performing dynamic test, Split Hopkinson Pressure Bar apparatus in ITU BIOMECHANICS AND STRENGTH OF MATERIALS LABORATORY is used. By identifying parameters of Johnson – Cook strength model, flow stress of any material can be described as a function of strain, strain rate and temperature as long as the material behavior is compatible.

The general information about elastic-plastic behavior and constitutive equations is presented in Chapter 2. The testing methods include quasi–static and dynamic tests are given in Chapter 3. The historical perspective and general theory of Split Hopkinson Pressure bar are also presented in this chapter. The results of different test such as quasi-static tension test, quasi-static tension test at high temperature and dynamic compression tests will be presented in Chapter 4. Finally, the conclusion and recommendations for future works are discussed in Chapter 5.

1.2 Literature Review

Engineering phenomenas occur usually at various strain and temperature. In other words, they are time-dependent and non-linear. It is known that materials exhibits different mechanical response at different strains and temperatures. Testing of

materials at these different conditions are remarkably expensive. Therefore, constitutive equations were developed in order to link the flow stress to strain, strain rate and temperature. Constitutive equations have the general form to characterize dynamic events as below,

$$\sigma = f(\varepsilon, \dot{\varepsilon}_p, T) \tag{1.1}$$

where σ, ε, $\dot{\varepsilon}_P$, T are the stress, strain and strain rate and temperature respectively. For metals, the constitutive equation given by equation **(1.1)** is called rate–dependent viscoplasticity model. In early 1900's, Ludwik (1909) proposed a model which strain hardening effect was taken into account as given equation **(1.2)**.

$$\sigma = \sigma_0 + K\varepsilon_p^{\ n} \tag{1.2}$$

where σ_0, K and n are yield strength of material, strength coefficient and strain hardening exponent respectively. It should be noted that strain measure must be true plastic strain. This concept will be explained in next chapters with details. Hollomon simplfies Ludwik's Law so that stress is not function of yield strength of material.

$$\sigma = K\varepsilon_p^{\ n} \tag{1.3}$$

In 1980's, two important material models were presented which includes basic relationship between strain hardening, strain rate and thermal softening. Johnson and Cook proposed a phenomenological model in which the flow stress is a function of equivalent plastic strain, strain rate and temperature as descibed in equation **(1.4)** [4].

$$\sigma = (A + B\varepsilon_p^{\ n})(1 + C\ln(\frac{\dot{\varepsilon}_p}{\dot{\varepsilon}_0}))(1 - T^{*m}) \tag{1.4}$$

A, B, C, m and n are material constants which are explained in details following chapters. $\dot{\varepsilon}_0$ is also a material parameter which describes strain rate at onset of yielding.This strain rate value is generally taken 1.0 s^{-1} and T^* is the homologous temperature as given by equation **(1.5)**.

$$T^* = \frac{T_{inst} - T_{ref}}{T_{melt} - T_{ref}} \tag{1.5}$$

where T_{inst}, T_{ref} and T_{melt} are instanteneous temperature, room temperature ($25\,C^\circ$) and melting temperature of material[5]. Zerilli and Armstrong proposed a physical based constitutive law, that takes two different form depending on microstructure of material[5]. For face centered cubic (fcc) material, the flow stress is descibed as given in equation **(1.6)**.

$$\sigma = C_0 + C_2\varepsilon^{1/2}\exp(-C_3 T + C_4 T \ln \dot{\varepsilon}) \tag{1.6}$$

For body – centered – cubic materials (bcc), the model takes the form as presented in equation **(1.7)**.

$$\sigma = C_0 + C_2\varepsilon^{1/2}\exp(-C_3 T + C_4 T \ln \dot{\varepsilon}) + C_5\varepsilon^n \tag{1.7}$$

For both equations, ε, $\dot{\varepsilon}$, T are the equivalent plastic strain, strain rate and temperature and C_i are material constants. In 1988, Holmquist and Johnson shows that both constitutive models gives good results for cylindirical impact tests at low strains while the results lost accuracy at high strains [6]. Holmquist and Johnson made a comparison between two constitutive models for cylindirical impact tests and depicted both models are consistent with test results. However, they recommended that obtained parameters in simulations where strains and strain rates should be similar values found in impact test [6]. Nobel and Harding compared two model by using Split Hopkinson Tension Bar Apparaturs and reported that Zerilli – Armstrong model gave better results [7]. In 1992, Tanimura proposed a modified model which includes a term that couples strain and strain rate together.

To determine strain rate parameters, Split Hopkinson Pressure Bar apparatus is usually used. Bertamd Hopkinson invented this apparatus and Kolsky developed it. Nowadays, many types of Hopkinson bars are used for characterizing material behavior at high strain rates. The detailed historical information about this apparatus will be presented in Chapter 3.

2. ELASTIC – PLASTIC BEHAVIOR OF METALLIC MATERIALS

2.1 Material Behavior in Elastic Region

The three major types of deformation that occur in engineering materials are elastic, plastic and creep deformation. In engineering applications, mathematical equations describing stress – strain behavior, called stress – strain relationships, or constitutive equations, are usually required [8]. In order to obtain these significant equations, mathematical preliminaries and concepts of material behavior must be known. If the material is in elastic region, stress usually changes linearly related with strain. Generalized Hooke's Law can be written in terms of incremental stress as a result of incremental strain. For a simple uniaxial loading, elastic behavior of a material can be described as given equation (**2.1**).

$$\sigma_x = E\varepsilon_X \tag{2.1}$$

where σ_x and E are stress in x-direction which is axial direction and Young (Elasticity) Modulus of materials respectively. However, elastic deformation in other directions occur as a result of uniaxial loading as stated in equations (**2.2**) and (**2.3**).

$$\varepsilon_y = -\upsilon \frac{\sigma_x}{E} \tag{2.2}$$

$$\varepsilon_z = -\upsilon \frac{\sigma_x}{E} \tag{2.3}$$

where υ is the Poisson ratio of material. If the three axial loading condition is considered, generalized Hooke's Laws called also Constitutive Equations of Elasticity are obtained as presented below equations.

$$\varepsilon_x = \frac{1}{E}[\sigma_x - \upsilon(\sigma_y + \sigma_z)] \tag{2.4}$$

$$\varepsilon_y = \frac{1}{E}[\sigma_y - \upsilon(\sigma_x + \sigma_z)] \tag{2.5}$$

$$\varepsilon_z = \frac{1}{E}[\sigma_z - \upsilon(\sigma_x + \sigma_y)] \tag{2.6}$$

As the same analogy, the shear strain can be described as equation **(2.7)**.

$$\gamma_{xy} = \frac{\tau_{xy}}{G}, \gamma_{yz} = \frac{\tau_{yz}}{G}, \gamma_{zx} = \frac{\tau_{zx}}{G} \tag{2.7-2.7a}$$

In equation **(2.7)**, G is called shear modulus and it is related with Young Modulus, E, as presented in equation **(2.8)** for homogeneous isotropic materials.

$$G = \frac{E}{2(1+\upsilon)} \tag{2.8}$$

2.2 Material Behavior in Plastic Region

If the material is deformed beyond the point of yielding, this deformation called plastic deformation that occurs in many engineering applications such as crash penetration, impact phenomena and so on. In plastic regime, stresses are not proportional to strains. Plastic flow of a material occurs if a certain stress combination exceeds a definite limit value [9]. The condition for plastic flow can be written in terms of principle stress as

$$f(\sigma_1, \sigma_2, \sigma_3) = 0 \tag{2.9}$$

where σ_1, σ_2 and σ_3 are principal stress values in principle stress directions. The plastic flow begins when the limit value is exceeded(f=0). If $f(\sigma_1, \sigma_2, \sigma_3) < 0$, the material is in elastic region. Yield condition must be independent of the choice of the coordinates and it is used for the limit value for the plastic flow [10]. According to many plasticity books, the rate of plastic strain is proportional to stress deviator [11].

6

$$\dot{\varepsilon_1} = \dot{\lambda}\,\sigma_1 \qquad\qquad (2.10)$$

$$\dot{\varepsilon_2} = \dot{\lambda}\,\sigma_2 \qquad\qquad (2.10a)$$

$$\dot{\varepsilon_3} = \dot{\lambda}\,\sigma_3 \qquad\qquad (2.10b)$$

where $\dot{\varepsilon_i}$ are plastic strain rates and $\dot{\lambda}$ is the plastic flow rate parameter. In equation (**2.11**), stresses are not rate dependent but they are proportional to rate dependent constant. During the plastic deformation, total volume is assumed to remain constant vice versa of elastic deformation. In other words, sum of plastic strains are equal to zero during plastic deformation, which is called plastic incompressibility.

$$\varepsilon_1{}^p + \varepsilon_2{}^p + \varepsilon_3{}^p = 0 \qquad\qquad (2.11)$$

The total strain due to any loading equals to sum of recovery elastic strains and permanent plastic strains.

$$\varepsilon_i = \varepsilon_i{}^e + \varepsilon_i{}^p \qquad\qquad (2.12)$$

The elastic portion of strain is recoverable, however the plastic portion is assumed permanent as in Figure 2.1.
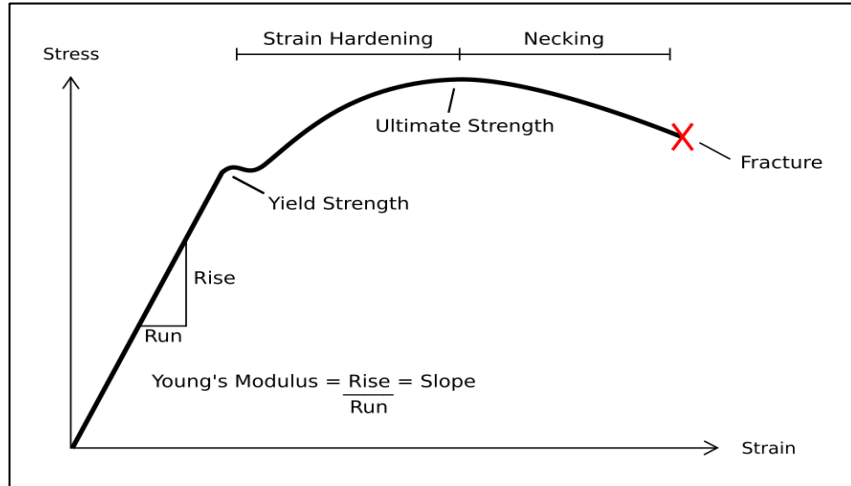
Figure 2.1 : Typical stress-strain curve of a ductile material [12].

2.2.1 Yield phenomena and yield criteria

When the combination of stress components exceeds a threshold value, it is assumed that yield phenomena begins. In order to define the onset of yielding, a "Yield Criteria" is needed. In past century many scientists proposed various yield criterias.

However, the most famous and widely accepted yield criteria is Von Mises Yield Criteria, which is based on maximum distortion energy theory. According to this theory, if the energy sourced by all combined stress at a point reaches the energy that causes to yielding of tensile test specimen, yielding is assumed to begin at this point. Total distortional energy at a point can be calculated as presented in equation **(2.13)**.

$$U_d = \frac{1}{12G}[(\sigma_{xx} - \sigma_{yy})^2 + (\sigma_{yy} - \sigma_{zz})^2 + (\sigma_{zz} - \sigma_{xx})^2 + 6(\tau_{xy}{}^2 + \tau_{yz}{}^2 + \tau_{xz}{}^2)]$$ **(2.13)**

where U_d is distortional energy [13].

The maximum distortional energy at yield point of simple tension test specimen can be given as.

$$(U_d)_{\sigma_0} = \frac{1+v}{3E}(\sigma_0)^2 = \frac{1}{6G}(\sigma_0)^2$$ **(2.14)**

where σ_0 is stress where yielding starts in the tension test.

It can be seen from two equations above that plastic flow begins when the elastic distortion energy reaches a threshold value. During the plastic flow, distortional energy remains constant and all distortion will result in plastic work [13]. When the material deforms plastically and then unloaded; only the elastic energy can be recovered [13]. Von Mises Yield Criteria can be derived by combining equations **(2.13)** and **(2.14)** in terms of distortional energy theory.

$$(\sigma_{xx} - \sigma_{yy})^2 + (\sigma_{yy} - \sigma_{zz})^2 + (\sigma_{zz} - \sigma_{xx})^2 + 6(\tau_{xy}{}^2 + \tau_{yz}{}^2 + \tau_{xz}{}^2) = 2(\sigma_0)^2$$ **(2.15)**

Von Mises Yield Criterion can be also written as in terms of principal stress as.

$$(\sigma_1 - \sigma_2)^2 + (\sigma_2 - \sigma_3)^2 + (\sigma_3 - \sigma_1)^2 = 2(\sigma_0)^2$$ **(2.16)**

Equation **(2.16)** defines a circular cylinder in σ_1, σ_2 and σ_3 space as depicted in Figure 2.2. The axis of cylinder equally inclined to the principal axis system of coordinates [11].
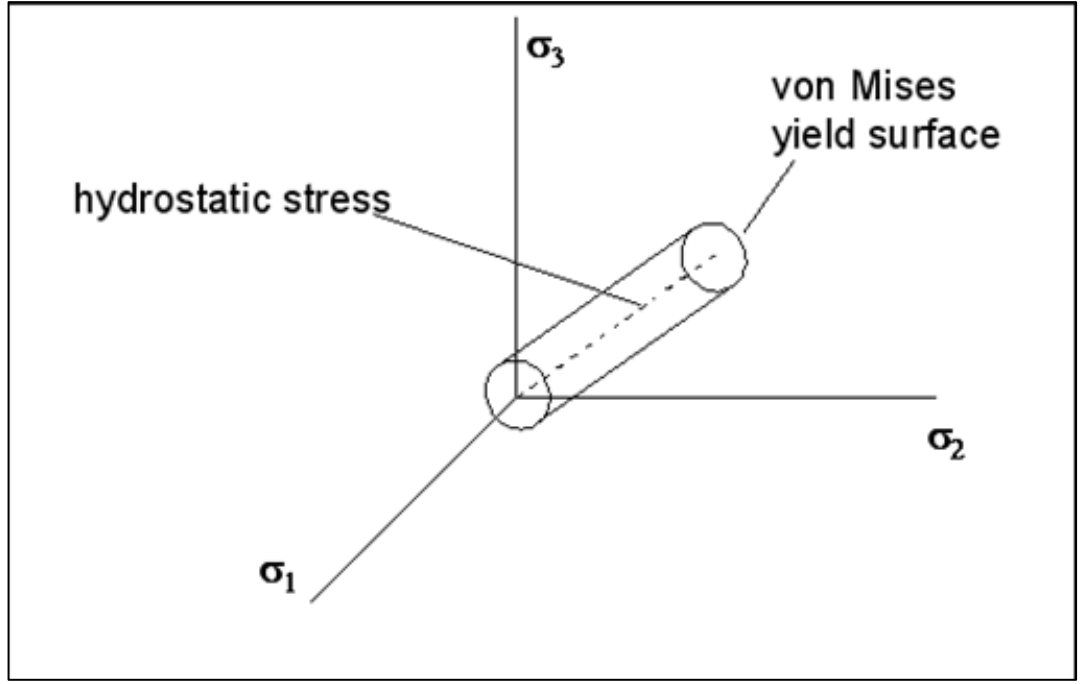
Figure 2.2 : Von Mises yield surface in principle stress space [14].

By using equations **(2.17)** and **(2.18)**, effective stress can be defined as.

$$\sigma_{eff} = \frac{1}{\sqrt{2}} \sqrt{(\sigma_{xx} - \sigma_{yy})^2 + (\sigma_{yy} - \sigma_{zz})^2 + (\sigma_{zz} - \sigma_{xx})^2 + 6(\tau_{xy}^2 + \tau_{yz}^2 + \tau_{xz}^2)}$$ **(2.17)**

$$\sigma_{eff} = \frac{1}{\sqrt{2}} \sqrt{(\sigma_1 - \sigma_2)^2 + (\sigma_2 - \sigma_3)^2 + (\sigma_3 - \sigma_1)^2}$$ **(2.18)**

The "Effective stress" (σ_{eff}) definition is important especially in plastic regime because it is the maximum stress at definite strain, strain rate and temperature.

2.2.2 Flow curve in plastic region

It has been stated that material behavior is lack of linearity when the material is in plastic region. In other words, the stress and strain is not linearly proportional anymore in this region. Beyond the yield strength, σ_0, of any metals, the metal deforms plastically.

If the material is strained up to an elastoplastic deformed state; such as point A in Figure 2.3, total strain decreases will from ε_1 to ε_2 by an amount σ/E when the applied load is removed. After the unloading, the decrease in strain $\varepsilon_1 - \varepsilon_2$ is called recoverable elastic strain [15].

9
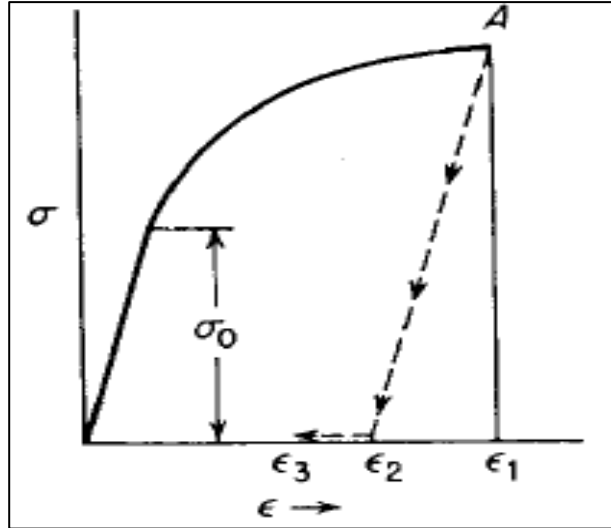
Figure 2.3 : The recovarable elastic strain [15].

After the yield point materials exhibit various stress – strain behavior. As shown in Figure 2.4, if the stress remains constant when it is strained beyond yield and elastic strain equals to zero, this type of material is called perfectly plastic. If the elastic strain is not zero and and yield strength is constant during plastic deformation, material can be modeled elastic and perfectly plastic. A more realistic way is to approximate flow stress by two straight lines corresponding to elastic and plastic regions [15].
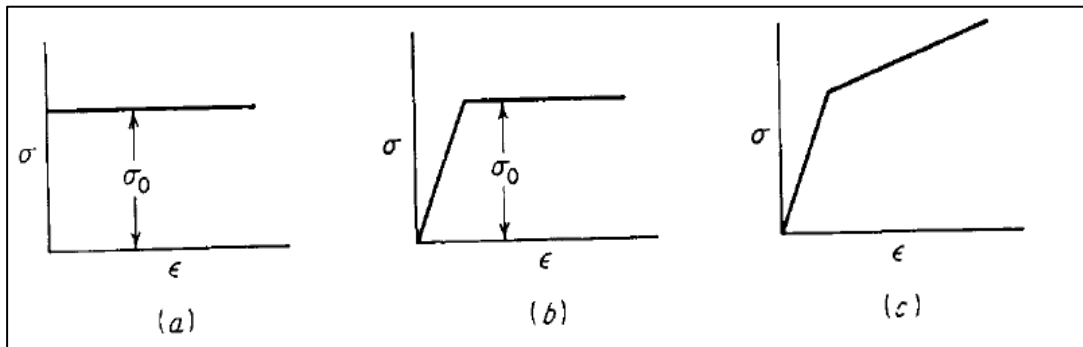
Figure 2.4 : Typical material behavior for flow curves a) Perfectly plastic material; b) Ideal plastic material with elastic region; c) Piecewise linear (strain hardening) material [15].

If the perfectly plastic material is considered, maximum stress is defined as the yield strength.

$$\sigma = \sigma_0 \tag{2.19}$$

However, it is known that the yield strength increases with plastic accumulating strain for most materials. For the stress – strain relationship in plastic region, some

empirical equations are used but it is not easy to define to describe material behavior in plastic region [16]

2.2.3 Work hardening

It is known that the increase in stress is required to accumulate further strain in the plastic region. In other words, the resistance of material increases as the material deforms in plastic region. This phenomena is called work (strain) hardening. The stress – strain relationship is defined by Ludwik as a power law given in equation **(2.20)**.

$$\sigma = K\varepsilon_p{}^n \tag{2.20}$$

where K and n are strength coefficient and strain hardening exponent respectively. Hollomon modified this power law so that it includes yield strength as following equation.

$$\sigma = \sigma_0 + B\varepsilon_p{}^n \tag{2.21}$$

where σ_0 is the yield strength at zero plastic strain, B is strain hardening coefficient and n is the strain hardening exponent.

2.2.4 Strain rate and temperature dependent constitutive models

Until now, the behavior of material is investigated by taking only strain into account. However, it has been observed in many experimental tests that the resistance of material to the deformation increases when the strain rate is increased. In other words, yield strength of material differs at different strain rates for same plastic strain value. Moreover, if the temperature of the material is increased, thermal softening occurs and yield strength decreases. As a result yield strength of a material can be described as function of strain, strain rate and temperature as,

$$\sigma_0 = f(\varepsilon, \dot{\varepsilon}, T) \tag{2.22}$$

where $\varepsilon, \dot{\varepsilon}$ and T are strain, strain rate and temperature. The behavior of materials whose properties depend on strain rate and temperature as in the form given in equation **(2.22)** can be shown in Figure 2.5.
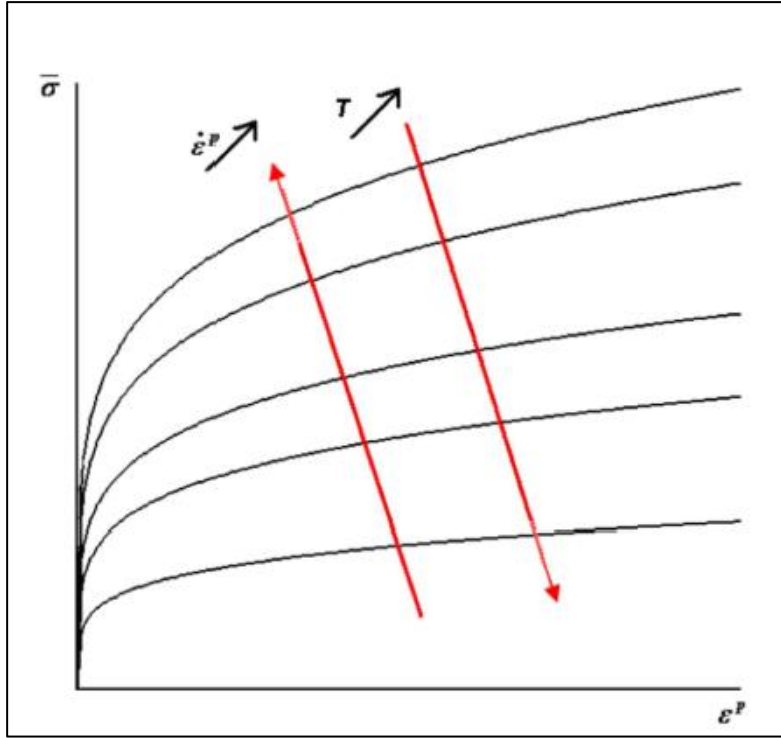
Figure 2.5 : Strain rate and temperature dependancy of effective stress [17].

In order to descibe strength of any material in terms of these parameters, many empirical relationships has been derived. These material models are called constitutive models. They are also known that strength models [17]. Most famous constitutive models for engineering materials are Johnson Cook Constitutive Model and Zerilli – Armstrong Constitutive Model. In Literature Review section, these models were introduced briefly. In this chapter, these models are explained again to emphasize the strain rate and temperature effect for material behavior in plastic region. Both of these significant strength models have some material constants which should be determined for characterizing the material behavior. To determine material constants of strength models, dynamic testing must be performed. Most known and used test is Split Hopkinson Pressure Bar test [4].

2.2.4.1 Johnson – Cook constitutive model

Johnson – Cook constitutive model is a phenomenological model which describes the stress in terms of strain, strain rate and temperature. The phenomenological definition implies that material flow stress depends on emprical observations include mathematical functions with lack of physical background that fit to experimental observations [18]. Johnson – Cook model is not a very complex mathematical model so that it consists of five material parameters. Furthermore, determination of these

material constant is not difficult due to simplicity of model. The flow stress can be calculated as a function stress, strain rate and temperature in this model as given in equations **(2.23)** and **(2.24)**.

$$\sigma = (A + B\varepsilon_p^n)(1 + C\ln\frac{\dot{\varepsilon}_p}{\dot{\varepsilon}_{0p}})(1 - T^{*m})$$

(2.23)

$$T^* = \frac{T_{inst} - T_{ref}}{T_{melt} - T_{ref}}$$

(2.24)

where ε_p is equivalent plastic strain, $\dot{\varepsilon}_p$ is plastic strain rate, $\dot{\varepsilon}_{0p}$ is the reference strain rate, T^* homologous temperature, T_{ref} is the reference temperature or room temperature at 25 $°C$, T_{inst} is instanteneous temperature, T_{melt} is melting temperature. All of temperature units are kelvin. Furthermore, A is the yield strength, B is the strain hardening coefficient, C is the strain rate coefficient, n is the strain hardening exponent and m is the thermal softening parameter. In this study, this model will be used in order to characterize material behavior.

2.2.4.2 Zerilli – Armstrong constitutive model

Zerilli – Armstrong constitutive model is a physically based emprical model [4]. The physically based definition implies that this type of constitutive model accounts for the physical aspects of material behavior grounded on the theory of thermodynamics, slip and dislocation theory. A physically based model has a lot of material constants and physical assumptions are needed for their determination [18]. Zerilli–Armstrong constitutive model has two distinct relations for face centered cubic (fcc) and body centered cubic (bcc) materials as following equations.

$$\sigma = C_0 + C_2\varepsilon_p^{1/2}\exp(-C_3T + C_4T\ln\dot{\varepsilon}_p) \qquad \text{(FCC)}$$

(2.25)

$$\sigma = C_0 + C_2\varepsilon_p^{1/2}\exp(-C_3T + C_4T\ln\dot{\varepsilon}_p) + C_5\varepsilon_p^{n} \quad \text{(BCC)}$$

(2.26)

where ε_p is the equivalent plastic strain, $\dot{\varepsilon}_p$ is the equivalent plastic strain rate, T is the temperature in kelvin and n is strain hardening exponent. Moreover, C_0 is the yield strength which can be calculated by equation **(2.27)**.

$$C_0 = \sigma_g + k_h t^{-1/2}$$

(2.27)

where σ_g is the contribution of solutes and initial dislocation density, k_h is the microstructural stress intensity and t is the average grain diameter.

3. EXPERIMENTAL METHODS

Up to now, the fundamentals of constitutive equations and elastic – plastic materials are explained. In this chapter, the testing methods for characterizing materials behavior are introduced in order to get Johnson–Cook material parameters. The experiments are generally performed at different strain rates to determine material behavior. Quasi–static tests are performed via the constant speed tensile testing machines at strain rates between $10^{-5}s^{-1} - 10^{-3}s^{-1}$. At higher strain rates ($>100s^{-1}$), there are many testing methods in order to test materials. However, the most used experimental testing device for high strain rate characterization is the Split Hopkinson Pressure Bar technique which gives stress-strain relationships correctly up to strain rates of $10^{4}s^{-1}$.

3.1 Quasi–Static Tension Tests

Since the first term of Johnson–Cook strength model includes parameters which may be obtained from quasi–static tests, many quasi–static tests are performed in the scope of this thesis. Tension tests are most widly used techniques for testing materials at quasi–static strain rates. It is a very basic test method but it provides important information about selecting materials in engineering applications. Tensile properties are evaluated during development of new materials and processes, so that different materials and processes can be compared [19].

The shape and dimensions of tensile test specimen that are shown in Figure 3.1 are specified by ASTM (American Society for Testing and Materials) standarts. In tension tests, the dogbone specimen is mounted on the grips of tensile test machine and elongated at a constant crosshead speed. Furthermore, applied load and elongation of test specimen are recorded via mechanical extensometers or camera. Finally, the recorded force and displacement data are used in order to construct stress – strain behavior of test material.
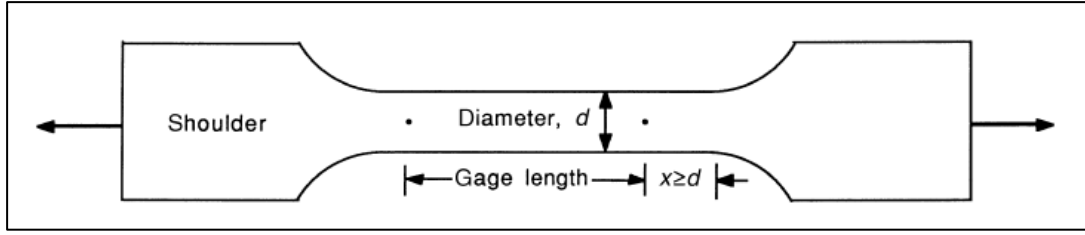
Figure 3.1 : Typical dogbone specimen [19].

3.1.1 Engineering stress – strain curves

The test specimen shown in above involves mounting of specimen in a tensile test machine and then is subjected to tension. The tensile force is recorded as a function of the increase in gage length. Moreover, these recorded values must be normalized with respect to specimen dimension in order to define material properties. Engineering stress or nominal stress, σ_{eng} , is describes as,

$$\sigma_{eng} = \frac{F}{A_0} \tag{3.1}$$

where F is (tensile) force and A_0 is the initial cross-sectional area of gage section. In addition to this, engineering strain with respect to elongation is calculated by,

$$\varepsilon_{eng} = \frac{\Delta L}{L_0} \tag{3.2}$$

where is L_0 is the initial gage length and ΔL is the change in gage length which equals to $(L - L_0)$ where L is the instaneous length of test specimen. If force – elongation data are converted into engineering stress and engineering strain and then engineering stress – strain curve can be plotted as given in Figure 3.2.
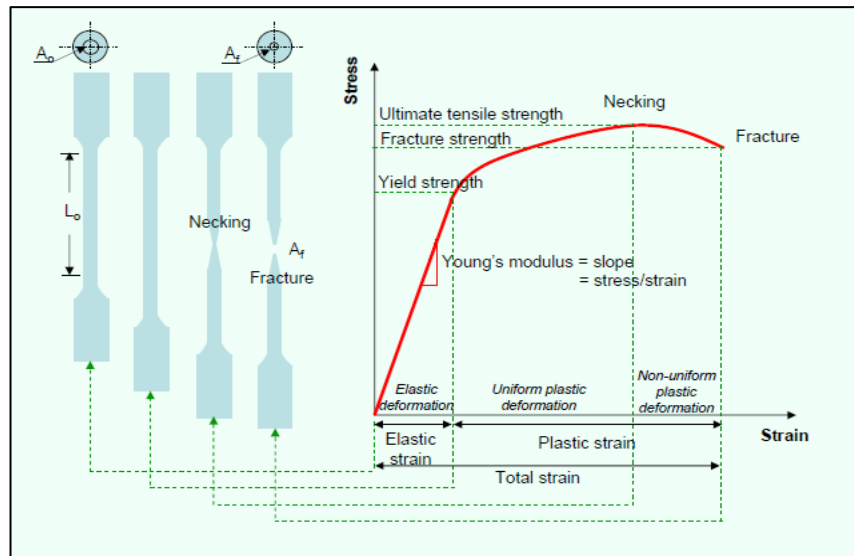
Figure 3.2 : A typical engineering stress − strain curve for a ductile material [20].

As shown in Figure 3.2, when a specimen is subjected to tensile load, the specimen deforms elastically up to a limiting point which is called yield strength. During this deformation if the force is removed, the bonds of atoms of solid material are relaxed and material turns to its original shape. This type of reversible deformation is called elastic deformation as explained in Chapter 2. Furthermore, if the material is subjected tensile loading beyond the limit value, the planes of atoms slides one over another. At that point, if the force is removed, the material can not turn into its original shape and this type of deformation is called plastic deformation. Elastic and plastic deformation of a wire is depicted in Figure 3.3.
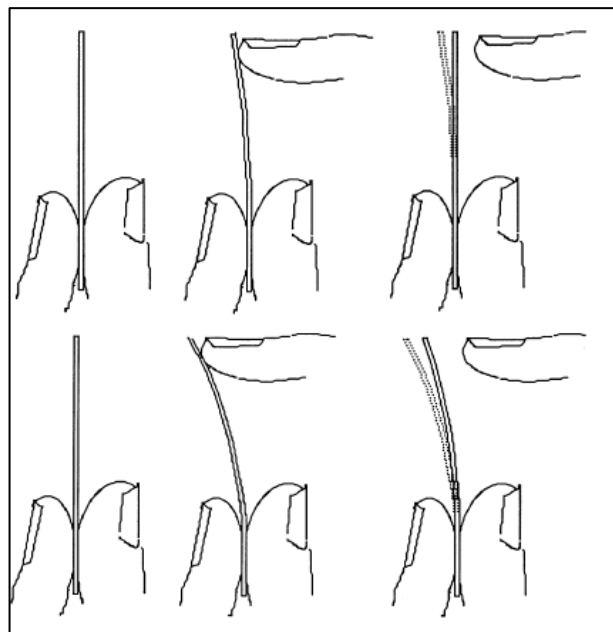
Figure 3.3 : Elastic and plastic deformations of wire with fingers [19].

3.1.2 Yielding

For most of materials, the initial portion of stress–strain curve is linear. In other words, the stress changes linearly with the strain in this elastic region. The slope of this region is called Elastic Modulus or Young's Modulus as given in equation (3.3).

$$E = \frac{\sigma_{eng}}{\varepsilon_{eng}}$$

(3.3)

After Elastic Modulus is calculated, next step is specifying yield strength of material. A value that stress–strain curve deviates from linearity is called proportional limit. However, it is not easy to determine proportional limit for some materials. In order to avoid this problem, the onset of plasticity is usually described by "offset yield strength" [19]. It can be found by constructing a straight line which is parallel to elastic portion of stress–strain curve with an offset of strain of $\varepsilon = 0.002$ or 0.2%. The yield strength is at the intersection point of offsetted straight line and stress–strain curve as presented in Figure 3.4.
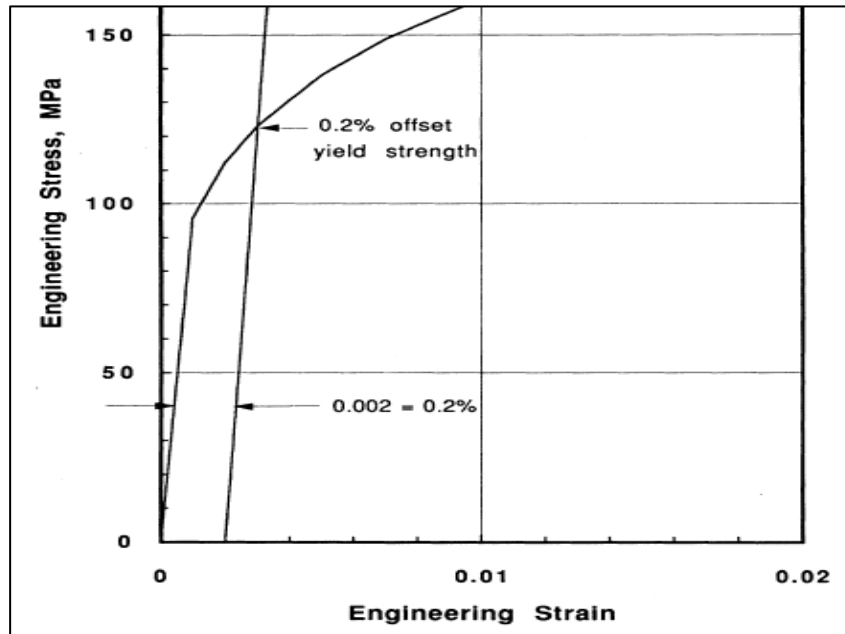
Figure 3.4 : Definition of 0.2% offset yield strength [19].

For some materials such as low carbon steel and some polymers, stress–strain curves does not resemble to Figure 3.4. For this type of materials, the stress − strain curves have initial maxima. After the initial maximum, all the deformation at any instant is occurring within a relatively small region of the specimen and continued elongations with fluctuations due to Lüder's Band occurs which shown in Figure 3.5 [19].

Lüder's Band can be explained as localized bands of plastic deformations in metals experiencing tensile stress. It can be said that defining yield strength of materials which has Luder's Band is easier than others because the yield strength fort his kind of materials is definite.
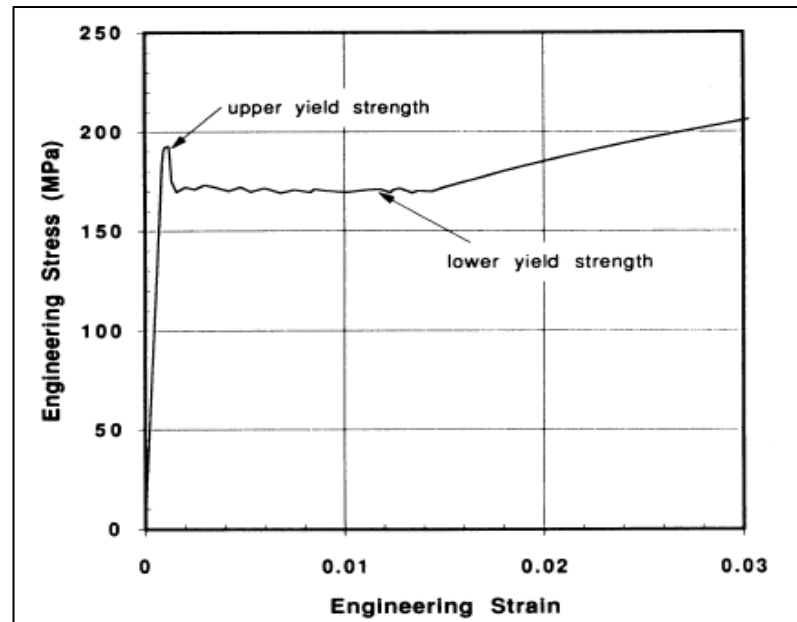
Figure 3.5 : Yielding points for low carbon steel [19].

3.1.3 True stress – true strain curves

Since the test specimen can not conserve its original shape, the engineering stress – strain curves does not give a true sense about deformation behavior of materials. Figure 3.6 shows that difference between true stress –strain curves with necking correction and engineering stress – strain curves.
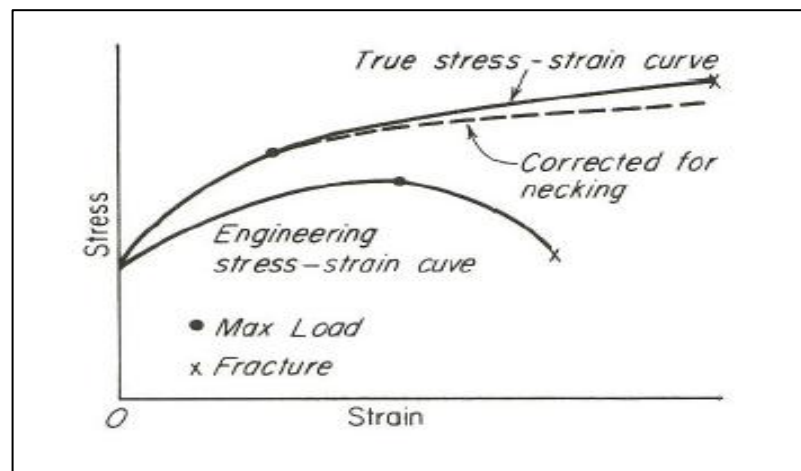
Figure 3.6 : The difference between true stress – true strain and
engineering stress – engineering strain curves [19].

19

The true stress can be calculated equation via,

$$\sigma_{tr} = \frac{F}{A_i}$$

(3.4)

where A_i is the instanteneous cross $-$ section area. The true strain is also calculated as

$$\varepsilon_{tr} = \ln(\frac{L_i}{L_0})$$

(3.5)

where L_i is the instanteneous gage length. The relationship between true stress $-$ true strain and engineering stress $-$ engineering strain can be construct by considering plastic deformation with constant volume which is explained in previous chapter as,

$$A_i L_i = A_f L_f$$

(3.6)

where subscripts i and f stand for initial and final dimension. By considering constant volume relations and engineering stress $-$ engineering strain equations true stress and true strain can be calculated in terms of engineering stress strain as presented in equation **(3.7)**.

$$\sigma_{tr} = \sigma_{eng}(1 + \varepsilon_{eng})$$
$$\varepsilon_{tr} = \ln(1 + \varepsilon_{eng})$$

(3.7)

Above equations are valid until inhomogeneous deformation, necking, starts. After onset of the necking, the recorded data does not reflect reality. The point of onset of necking can be calculated by using derivatives of stress and strain values as below.

$$\frac{d\sigma_{tr}}{d\varepsilon_{tr}} = \sigma_{tr}$$

(3.8)
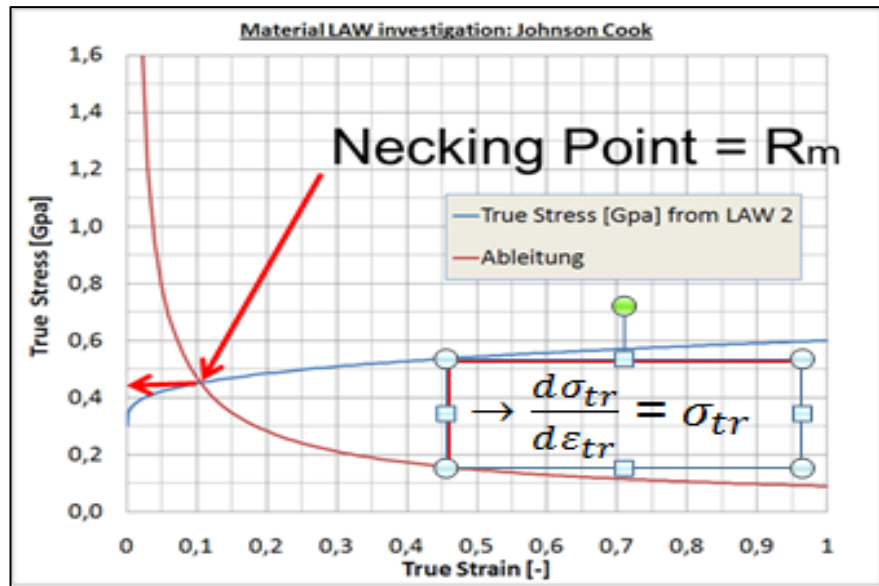
Figure 3.7 : Determination of necking point on flow curve [21].

Deviations due to necking can be corrected by using Bridgman Correction, which is out of the scope of this thesis [22].

3.2 Dynamic Tests

For material characterization at higher strain rates, most reliable and used devices are Split Hopkinson Pressure Bars. They can be classified as compression, tension and torsion bars according to loading conditions. Split Hopkinson Pressure Bars (SHPB) also known as Kolsky Bars are the most convenient characterization tools for the mechanical response of materials at strain rates $(10^2 - 10^4 s^{-1})$ [22]. This section gives information about background, working principles and equations for construction stress–strain diagrams for its compression type.

3.2.1 Split Hopkinson Pressure Bar: Background

The design of stuctures depends on tabulated material data that consist of stress–strain diagrams. Moreover, material properties such as yield strength, ultimate tensile strength defined in material handbooks are obtained from quasi–static tests which are presented previous section. However, it is known that yield strength of materials is sensitive to strain rate changes. In order to provide product reliability under impact conditions such as vehicle collision, military bullet penetration, bird impact to aircraft and so on, the mechanical responses of materials under similar loading conditions must be characterized accurately [22].

The first attempt in order to characterize material response at higher strains came from Bertram Hopkinson. He invented a pressure bar to measure the pressure produced by high explosives and or high speed impact of bullets in 1914 [22]. Hopkinson used pendulums with a pencil and paper to record the movements of cylinders in order to obtain a pressure – time curve produced by detonation of the gun cotton was obtained as shown in Figure 3.8.
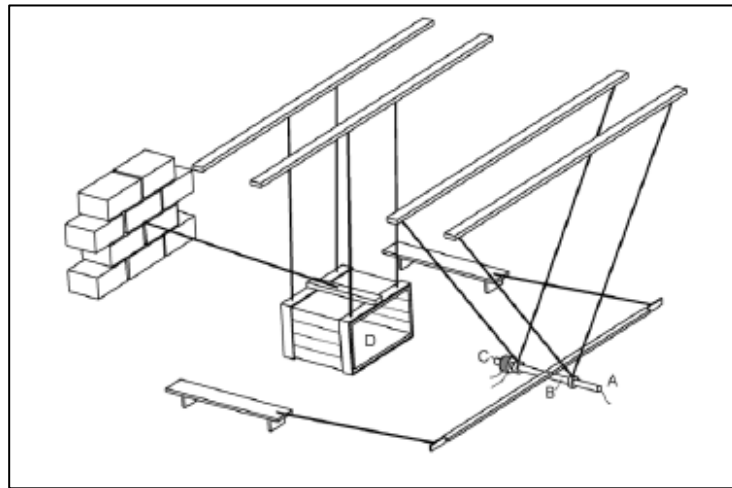
Figure 3.8 : The Hopkinson Experiment [22].

In 1948, Davis conducted a critical study by using parallel plate and cylindrical condenser microphones to electrically measure the axial and radial movements of the bar loaded by detonation as in Figure 3.9. The output from the condenser is proportional to the displacement – time relations assuming that the pressures in the bars are under the elastic limit of the material [23]. Davis also studied the dispersion of the stress waves' propogating in a long rod.
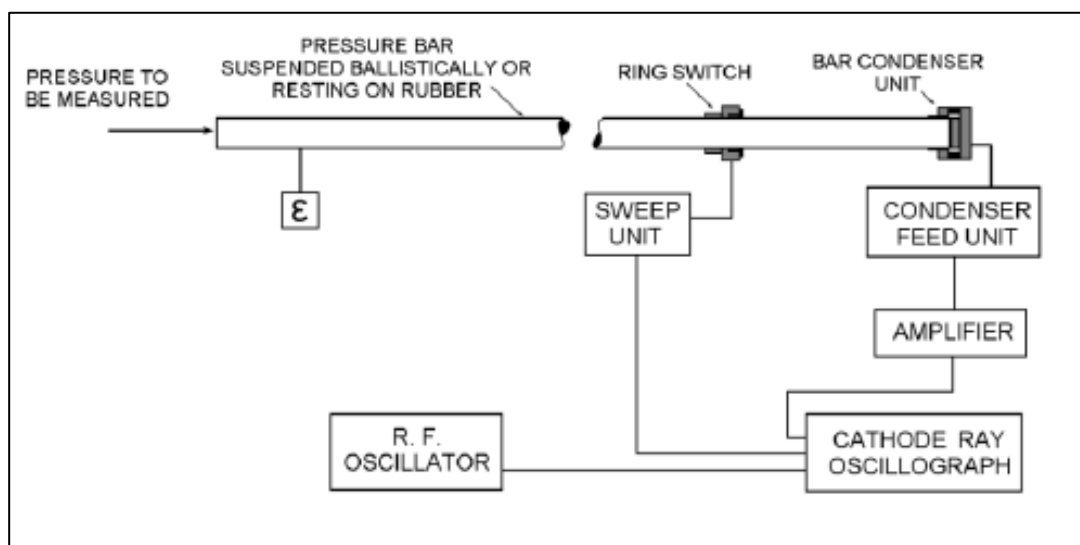
Figure 3.9 : Davis Experiment [22].

Kolsky added a second pressure bar to Hopkinson's device and extended the technique to measure stress – strain response of materials under impact loading conditions in 1949. The difference between Kolsky bar and Davis' apparatus is that Kolsky used two bars where a specimen was sandwiched in between as shown in Figure 3.10.
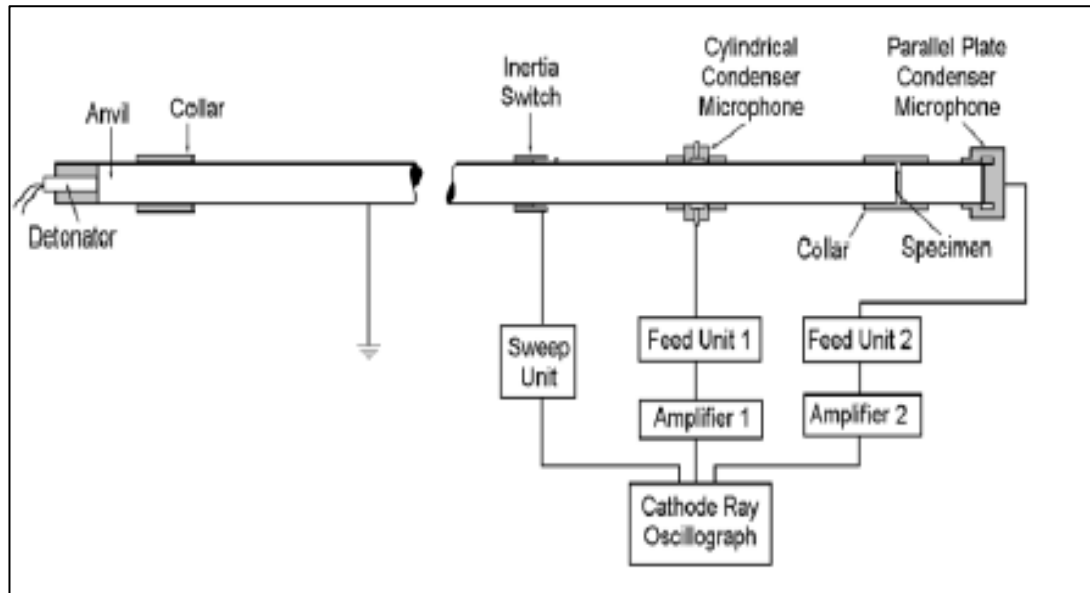
Figure 3.10 : The Kolsky Bar [22].

Kolsky also presented expressions to calculate material properties based on strain data in the bars. The technique of Kolsky is also called Split Hopkinson Bar in the memory of Bertram Hopkinson.

In 1954, Krafft firstly mounted strain gages to measure the strains in the two bars of SHPB instead of condenser microphones [23]. He also used a gun to launch a projectile, a striker bar, to impact on the incident bar. The advantage of using a striker is obtaining trapezoidal shaped pulse which have been recognized ideal for Kolsky bar experiments.

In 1964, Lindholm introduced an updated version of the SHPB and presented as a valid dynamic characterization tool. This apparatus became a popular among laboratories among world. Nowadays, new improvements have been occurred with recent technological devices in SHPB. The Kolsky bar techniques have extended for tension and torsion tests for different materials.

3.2.2 Split Hopkinson Pressure Bar Apparatus

A general Split Hopkinson Pressure (Kolsky) Bar consists of three major components such as a loading device, incident and transmitted bars and data acquisition system as shown in Figure 3.11.
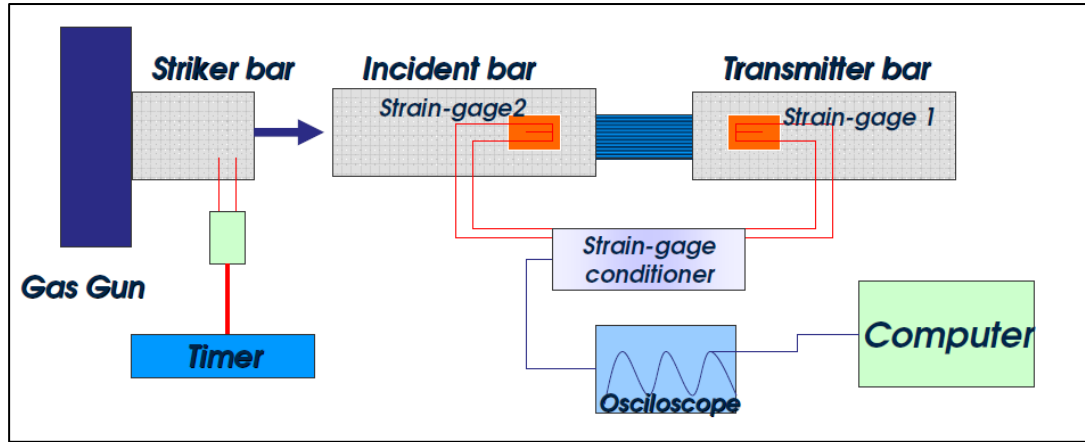
Figure 3.11 : The schematic view of SHPB [24].

In SHPB experiments, the loading should be controllable. The most common method for dynamic loading is to launch a striker impacting on the incident bar. For this purpose, gas guns and pressure vessels are generally used. The striker is launched by a sudden release of the compressed air in a pressure vessel and then accelerates through a long gun tube to impact on the end of the incident bar. When the striker bar impacts to the end of the incident bar with initial impact velocity (v_0), it forms a compressive wave in incident bar. The amplitude of this compressive wave is directly proportional with initial impact velocity. The impact velocity can be measured optically or magnetically at onset of impact. When the compressive wave propogates through the incident bar, it comes to the interface between incident bar and sandwiched specimen. At this location, a portion of compressive wave is reflected back into the incident bar while the rest is transmitted into specimen. Incident and transmitted strains are measured by strain gages on pressure bars via a data acquisition system. For this purpose, two strain gages are attached on the surface of the incident and transmitted bars. In order to record signal and monitor strain data, amplifier and oscilloscope should have high frequency response because voltage outputs from the strain gages are small amplititude [25]. The minimum frequency response of all components in the data acquisition system should be 100 KHz [25].

3.2.3 Split Hopkinson Pressure Bar Theory

Up to now, the equations which are needed to calculate stress and strain are not discussed. In this section, the theory behind this experiment is introduced. Initially, elastic waves in cylindrical bars are explained in order to constitute equation of motion. After that, the equations will be derived in order to calculate strain rate, strain and stress.

3.2.3.1 Elastic waves in a cylindrical bar

The fundamental elements of Split Hopkinson Pressure Bar are incident and transmitted bars as shown in Figure 3.11. Both bars should be fabricated from same materials. The bar material is desired to be linearly elastic during all tests with a high yield strength. The pressure bars have cross–section area A_0, elastic modulus E, and density ρ. Typically, the length to diameter ratio of pressure bars should be greater than 10 to ensure uniaxial and homogeneous elastic deformation in bars [25]. Many books explained the calculation of velocity of propogation in a thin bar. The derivation starts from a differential element of a bar. Figure 3.12 depicts that the striker bar impacting a long cylindrical bar with initial impact velocity v_0 and differential element before and after impact.
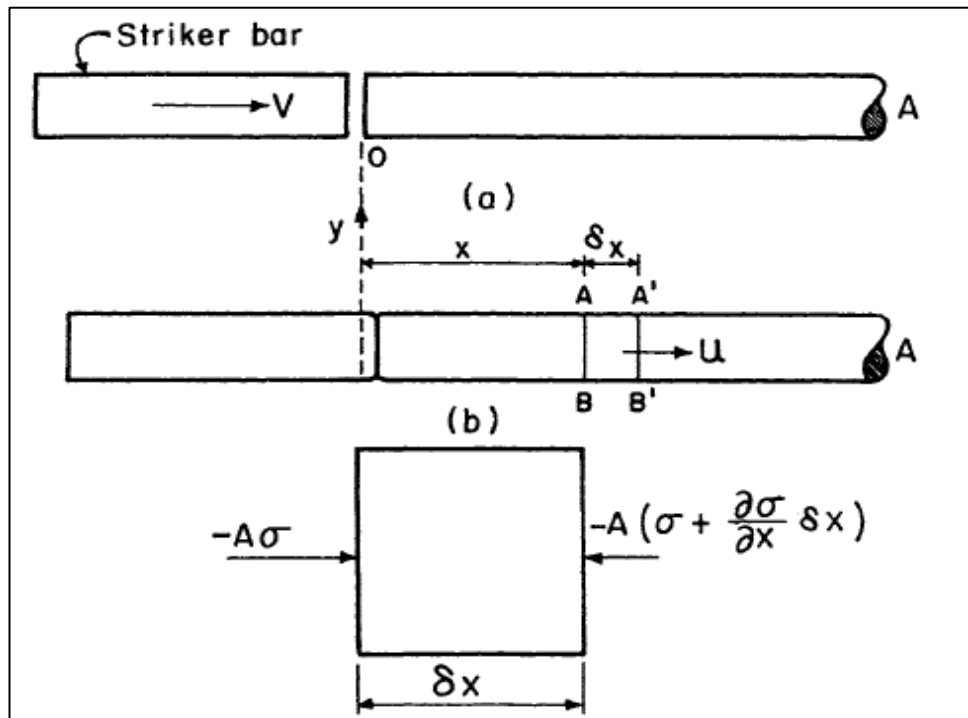
Figure 3.12 : Propogation of a compression wave in a cylindrical bar [26].

The forces in differential element shown in Figure 3.12 (b) are related to the stress on the cross–section of this element. The strains in the element can be expressed in terms of displacement of differential element in x-direction. By applying Newton's Second Law to the cross section $AA'B'B$ as;

$$F = m_e a = m_e \frac{\partial^2 u}{\partial t^2}$$

$$-[A_0 \sigma - A_0 (\sigma + \frac{\partial \sigma}{\partial x} \delta x) = A_0 \rho \delta x \tag{3.9}$$

$$\frac{\partial \sigma}{\partial x} = \rho \frac{\partial^2 u}{\partial t^2}$$

is obtained, where m_e is the mass of differential element, u is the displacement in x-direction and t is time. Since the deformation is elastic, stress can be defined as in equation **(2.1)**.

$$\frac{\sigma}{\varepsilon} = E \tag{3.10}$$

where ε is the strain can be defined as $\partial u / \partial x$. By combining stress and strain definition and inserting into (3.9), the equation of motion of wave is obtained as given in equation **(3.11)**.

$$\frac{\partial}{\partial x}[E \frac{\partial u}{\partial x}] = \rho \frac{\partial^2 u}{\partial t^2} \tag{3.11}$$

and it can be simplified as,

$$\frac{E}{\rho} \frac{\partial^2 u}{\partial x^2} = \frac{\partial^2 u}{\partial t^2} \tag{3.12}$$

In addition to these, if the wave velocity C_0 is taken into account as below equation **(3.13)** and then inserted into equation **(3.2)**.

$$C_0 = \sqrt{\frac{E}{\rho}}$$

$$C_0^2 \frac{\partial^2 u}{\partial x^2} = \frac{\partial^2 u}{\partial t^2}$$

(3.13)

This differential equation is known as one-dimensional wave equation. This equation of motion has no practical use in Split Hopkinson Pressure Bar analysis. However, it can be used for calculating strain rate, strain and stress.

3.2.3.2 Strain rate, strain and stress calculation for SHPB

In this section, basic equations that provide strain rate, strain and stress will be introduced from the strain gage recordings. The testing section and recordings strains are shown in Figure 3.13.
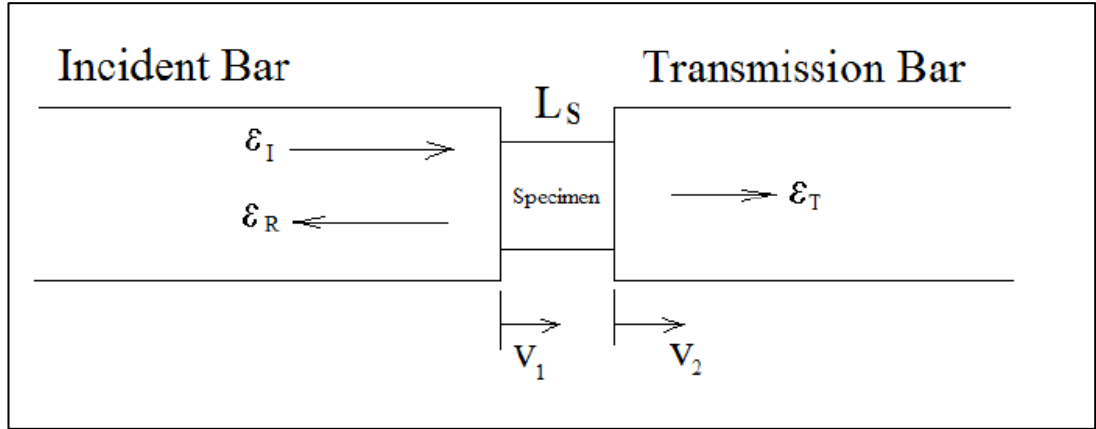
Figure 3.13 : Testing region of SHPB [22].

The incident and reflected pulses are measured by strain gages on the incident bar while the transmitted is measured by on the transmission bar. These strains can be described ε_I, ε_R, ε_T. Moreover, L_s is the length of specimen and v_1 and v_2 are the interface velocities at the ends of specimen. The interface velocities can be calculated by equations **(3.14)**.

$$v_1 = C_0(\varepsilon_I - \varepsilon_R)$$

$$v_2 = C_0\varepsilon_T$$

(3.14)

where C_0 is the wave velocity of bars. The average engineering strain rate and strain of specimen can be calculated as,

$$\frac{d\varepsilon_s}{dt} = \frac{v_1 - v_2}{L_s} = \frac{C_0}{L_s}(\varepsilon_I - \varepsilon_R - \varepsilon_T) \tag{3.15}$$

The strain is found by integrating strain rate in equation **(3.15)** from 0 to t as;

$$\varepsilon_s = \frac{C_0}{L_s}\int_0^t (\varepsilon_I - \varepsilon_R - \varepsilon_T)dt \tag{3.16}$$

where ε_s is the average strain of specimen. The stresses at the both ends of specimen can be calculated as;

$$\sigma_{s1} = \frac{A_b}{A_s}E_b(\varepsilon_I + \varepsilon_R)$$
$$\sigma_{s2} = \frac{A_b}{A_s}E_b\varepsilon_T \tag{3.17}$$

where σ_{s1} and σ_{s2} are the stress at first and second end of specimen respectively. Furthermore, it is assumed that the specimen deforms uniformly and is to be stress equilibrated [22]. If this stress equlibirium is considered and inserted into equation **(3.17)** related specimen stress,

$$\sigma_{s1} = \sigma_{s2}$$
$$\varepsilon_I + \varepsilon_R = \varepsilon_T \tag{3.18}$$

are obtained. Finally, equations **(3.16)** and **(3.17)** can be simplified as below equations.

$$\frac{d\varepsilon_s}{dt} = -2\frac{C_b}{L_s}\varepsilon_R$$
$$\varepsilon_s = -2\frac{C_b}{L_s}\int_0^t \varepsilon_R dt \tag{3.19}$$
$$\sigma_s = \frac{A_b}{A_s}\varepsilon_T$$

These equations are necessary to produce dynamic stress – strain curves. However, it is the fact that these equations are affected by testing condition remarkably [23]. The main assumption for the validity of these equations is that the specimen deforms

uniformly. Furthermore, the stress equilibrium should be ensured. For these purposes, lubrication between specimen and bar ends is used and dimensions of specimen are chosen properly. If these considerations taken into account, equation **(3.16)** is effective for constituting dynamic stress − strain curves of many materials.

3.2.3.3 High temperature testing

In order to find thermal softening coefficient (m) of Johnson − Cook constitutive model, high temperature testing of materials is needed. It is known that the high temperature testing should be performed at high strain rates [27]. However, SHPB at ITU BIOMECHANICS AND STRENGTH OF MATERIALS LAB has not such a kind of modeification. Therefore, the high temperature tests will be performed at quasi−static strain rates.

4. EXPERIMENTAL RESULTS

In order to simulate the structural response of material, a crucial point is to determine flow stress of this material as a function. In this chapter, the procedure to obtain five material parameters of Johnson – Cook from experimental results for three materials will be introduced. Moreover, how the quasi–static tension, quasi–static tension at high temperature and dynamic compression tests are performed will be explained elaborately.

4.1 Quasi–Static Tensile Testing Procedure

The fundamental aim of the quasi–static tensile tests is obtaining the true stress – true strain curve of AISI 1040, AISI 1045(cold – rolled) and AISI 4140 (Cr42Mo4) materials. From obtained true stress – true strain curves, first part of Johnson–Cook equation which includes A, B and n parameters can be found. For testing of three materials, MTS Tensile Testing Machine and MTS extensometer are used.

4.1.1 Tensile test specimens

The tensile test specimen was presented in previous chapter with Figure 3.1. For AISI 1040 steel, diameter is 6.5 mm and gage length which extensometer is mounted is 20 mm. For AISI 1045 and AISI 4140 steels, the diameter is 5.1 mm and gage length is 20 mm respectively. Figure 4.1 and Figure 4.2 depict AISI 1040 and AISI 1045 specimens respectively.

Figure 4.1 : AISI 1040 tensile test specimen.

Figure 4.2 : AISI 1045 and AISI 4140 tensile test specimens.

4.1.2 Testing

Quasi-static tension tests were performed using the MTS test machine in Figure 4.3 with a strain rate $10^{-3} s^{-1}$. Five succesive quasi–static tests for each material are performed in order to constitute true stress – true strain curves as shown. Table 4.1 shows the dimensions of specimens for AISI 1040.

Table 4.1 : The dimension and strain rates for AISI 1040 tests.

1. Test No	2. Diameter [mm]	3. Gage Length [mm]	4. Strain Rate [1/s]
1	6.5	20	0.001
2	6.5	20	0.001
3	6.5	20	0.001
4	6.5	20	0.001
5	6.5	20	0.001

For AISI 1045 and AISI 4140, tests were repeated four times and diameter of specimen is 5.1 mm differently from AISI 1040 specimens. Engineering stress–strain curves can be provided after tests shown in Figure 4.3.


Figure 4.3 : Tensile test machine and MTS extensometer.

The force and displacement signals come from crosshead sensors and extensometer are recorded via the controllable data acquisition system of MTS. After that, force – displacement data are converted to true stress – true strain data by using equations from **(3.1)** to **(3.7)**.

$$
\begin{aligned}
\sigma_{tr} &= \sigma_{eng}(1 + \varepsilon_{eng}) \\
\varepsilon_{tr} &= \ln(1 + \varepsilon_{eng})
\end{aligned}
\tag{4.1}
$$

It can be said that two curves slightly differ with each after yield strength as can be seen in Figure 4.4
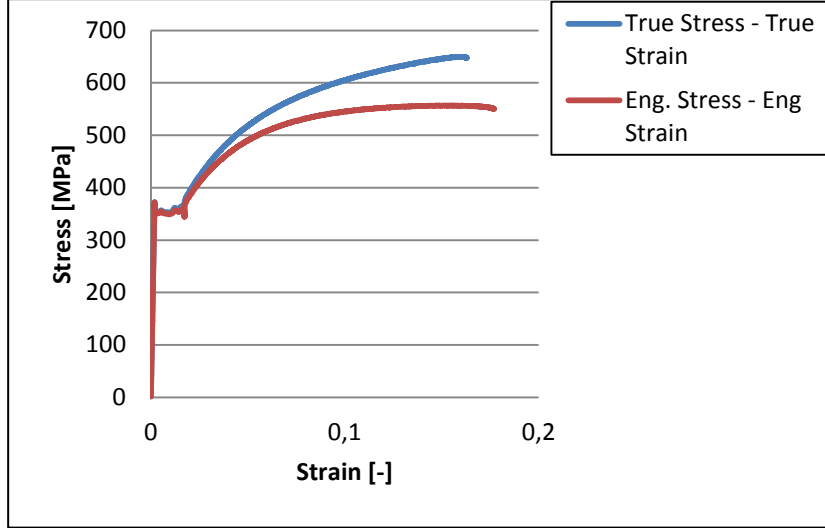
Figure 4.4 : Engineering and true stress – strain curve for tension test of AISI 1040.

If the first term of Johnson–Cook constitutive model shown in equation **(2.28)** is considered, it can be easily seen that the plastic strain is needed as presented in equation **(4.2)**.

$$\sigma = A + B\varepsilon_p{}^n \tag{4.2}$$

This equation is modified version of Johnson–Cook constitutive model at quasi-static strain tensile tests. To make clear, it is the fact that there is no significant temperature change in quasi–static tensile tests. In addition to this, test is performed at low strain rates so strain rate effect also does not occur. To sum up, Johnson–Cook constitutive equation **(2.24)** rolls-down to equation **(4.2)** at quasi–static tensile tests.

According to equation **(4.2)**, the plastic strain calculation is required for determining flow stress. In Chapter 2, it is explained that total strain consists of elastic and plastic strains as shown in Figure 3.2. Moreover, strain in elastic region can be calculated by Hooke's Law from equation **(3.3)**. According to this results, the true plastic strain and true plastic strain rate is calculated by using following relations.

$$\varepsilon_p = \varepsilon_t - \frac{\sigma}{E}$$

$$\dot{\varepsilon}_p = \frac{d\varepsilon_p}{dt} \tag{4.3}$$

where ε_t is total true strain. In order to determine A, B and n parameters, true stress–true plastic strain curve of material is plotted as shown in Figure 4.5.

34
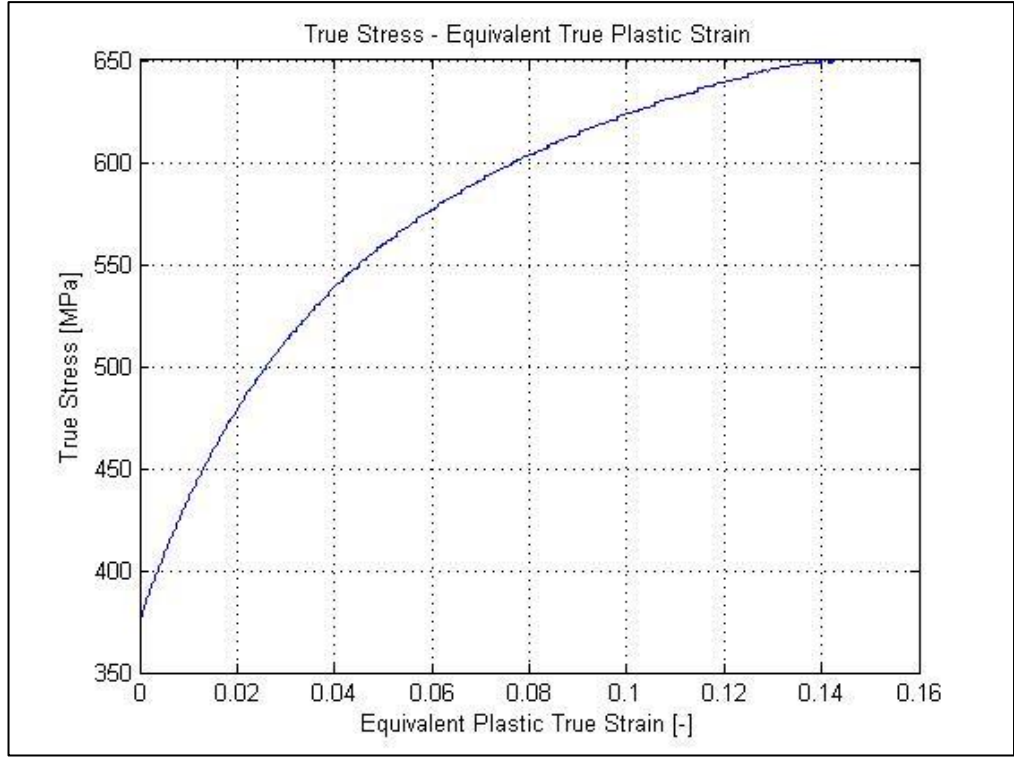
Figure 4.5 : True stress – Equiv. true plastic strain graph example for AISI 1040.

After the true stress – equivalent true plastic strain curve is plotted, logarithm of stress and strain value are taken to find A, B and n parameters easily. For this purpose, equation **(4.2)** should be modified as;

$$
\begin{aligned}
\sigma &= A + B\varepsilon_p^{\,n} \\
\sigma - A &= B\varepsilon_p^{\,n} \\
\ln(\sigma - A) &= \ln(B\varepsilon_p^{\,n}) \\
\ln(\sigma - A) &= \ln B + n\ln(\varepsilon_p)
\end{aligned}
\tag{4.4}
$$

where equation **(4.4)** is a linear function $\ln(\varepsilon_p)$ and $\ln(\sigma - A)$, where ε_p and σ are equivalent true plastic strain and stress respectively. Moreover, A is the yield strength of material. In order to find B and n parameters, a first order polynomial is used. This approach is called direct fitting. The direct fitting of stress – strain data in Figure 4.5 according to equation **(4.4)** is presented in Figure 4.6.
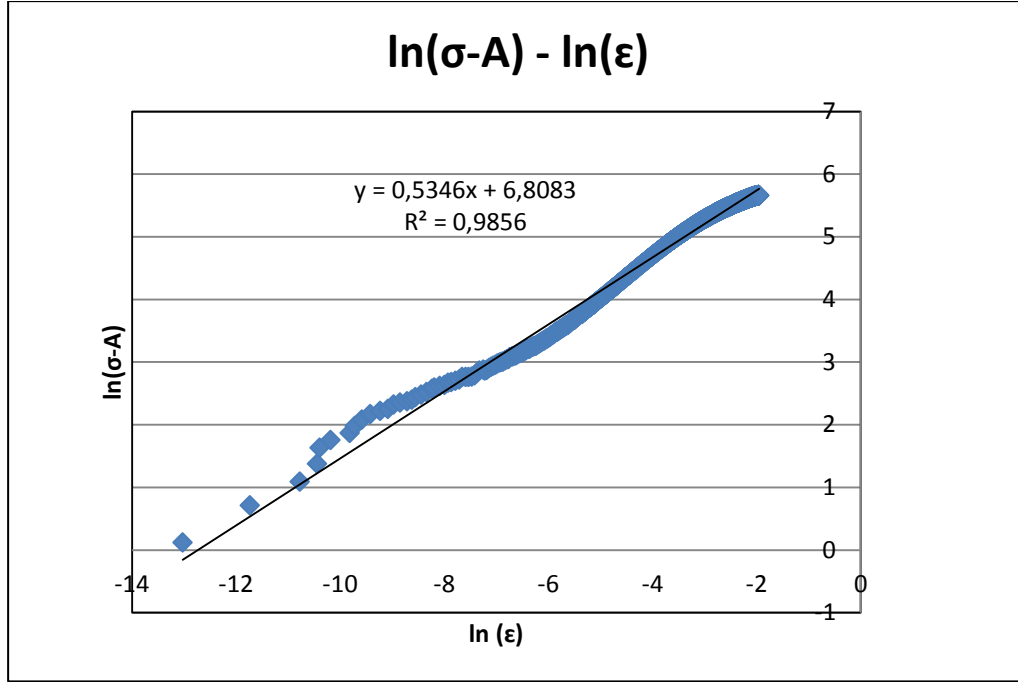
Figure 4.6 : Ln-Ln graph of flow curve for AISI 1040.

From Figure 4.6, strain hardening exponent (n) equals to 0.5346 and B equals to $e^{6.8083} = 905$ MPa. This procedure effective and simple but it may be sometimes problematic. Moreover, it has proved to be inconvenient to choose the parameter A as the yield strength because the power law curve might deviate substantially from the stress – strain graph to be represented, such that the representation become inaccurate [28]. Therefore, an alternative approach, regression analysis, will be used for parameter identification during this thesis. Thanks to regression analysis, yield strength A can be determined with B and n parameters by the regression algorithm. Regression algorithm depends on minimizing the square of the difference between experimental stress and stress found from constitutive model as shown in equation **(4.5)**.

$$\sum_{i=1}^{k}(\sigma_{exp} - \sigma_{model})^{2} = \min \tag{4.5}$$

where σ_{exp} and σ_{model} are experimental stress and stress calculated by Johnson – Cook constitutive model. Moreover, k is the total number of data points. This procedure will be used after this section in order to obtain Johnson – Cook constitutive model parameters.
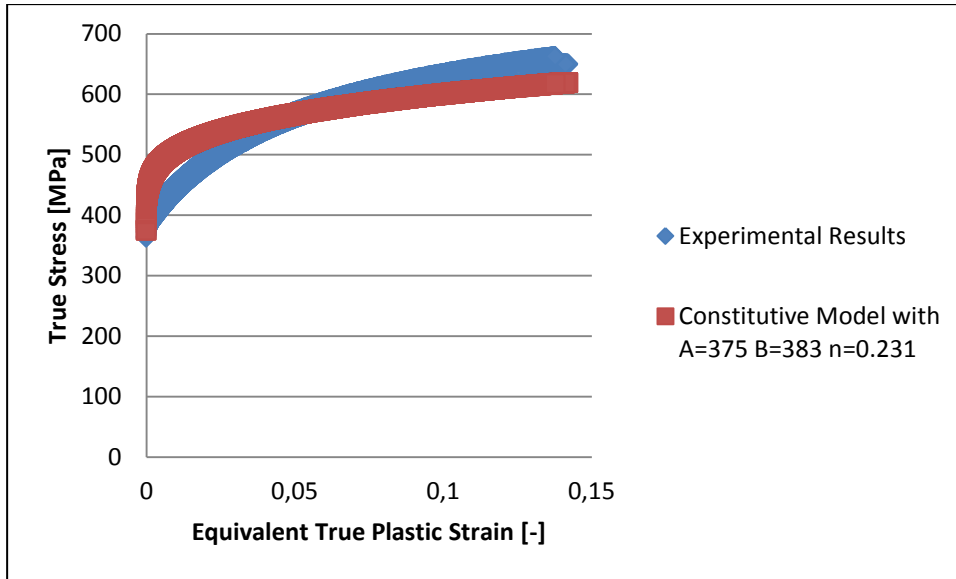
4.1.3 AISI 1040 results

For AISI 1040 steel, five successive tensile tests performed. Since AISI 1040 show yield phenomena, it is not difficult determine yield strength of material. In addition to this, it can be accepted that yield strength of a material can be differently with each other up to 10% at tensile tests. Figure 4.7 depicts that five different test results for true stress–true strain curves.
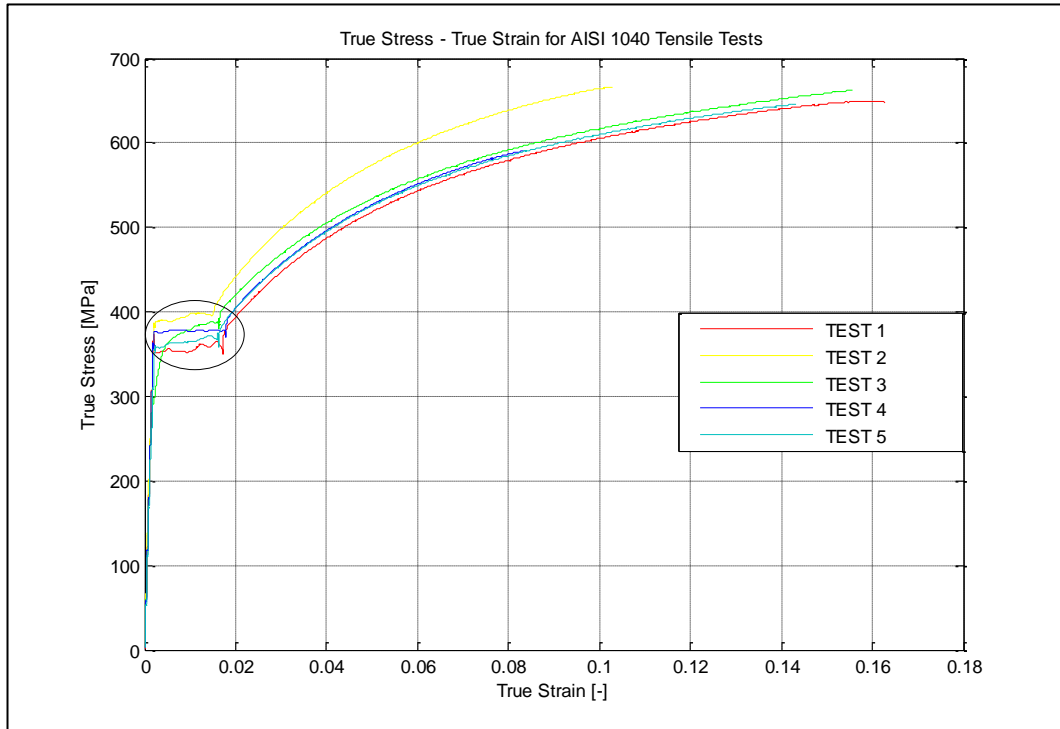
Figure 4.7 : True Stress – True Strain Curves for AISI 1040.

The yield phenomenon during tests is shown with black ellipse in Figure 4.7. It is clear that yield strength values are not same for all tests. Instead of finding A , B and n parameters for each test, a unique curve is fitted to all of data points by taking average yield strength value. In order to minimize error between experimental stress results and calculated stress from constitutive model, regression analysis presented in equation **(4.6)** was used. Microsoft Excel software is highly effective in finding parameters by using regression analysis with Microsoft Excel Solver. As a result, the average yield strength of five tests are calculated and then strain hardening coefficient B and strain hardening exponent n can be found easily via Microsoft Excel Solver as shown in Figure 4.8.

Figure 4.8 : Curve Fitting of Experimental Test Results for AISI 1040.

According to regression analysis and curve fitting, yield strength of material A is found as 375 MPa, strain-hardening coefficient B is found as 383 MPa and strain hardening exponent n is found as 0.23. The constitiutive fitting of each tests can be seen in Appendix A. Finally, the first term of Johnson – Cook constitutive model became as equation **(4.6)** for AISI 1040.

$$\sigma = (375 + 383\varepsilon_p^{0.23})$$ **(4.6)**

4.1.4 AISI 1045 results

The same procedure for AISI 1040 steel is also used for AISI 1045 steel. The only difference is that AISI 1045 steel specimens do not show yield points. Therefore, 0.2% yield strength which is also called proof stress should be found. At the end of the test, one of the AISI 1045 is shown in Figure 4.9.

Figure 4.9 : The fracture of AISI 1045 specimen.

In order to find 0.2 % yield strength of material, the linear portion of true stress − true strain curve is plotted and its slope is found. This slope represents the Young Modulus E of material. An example of this procedure is shown in Figure 4.10.
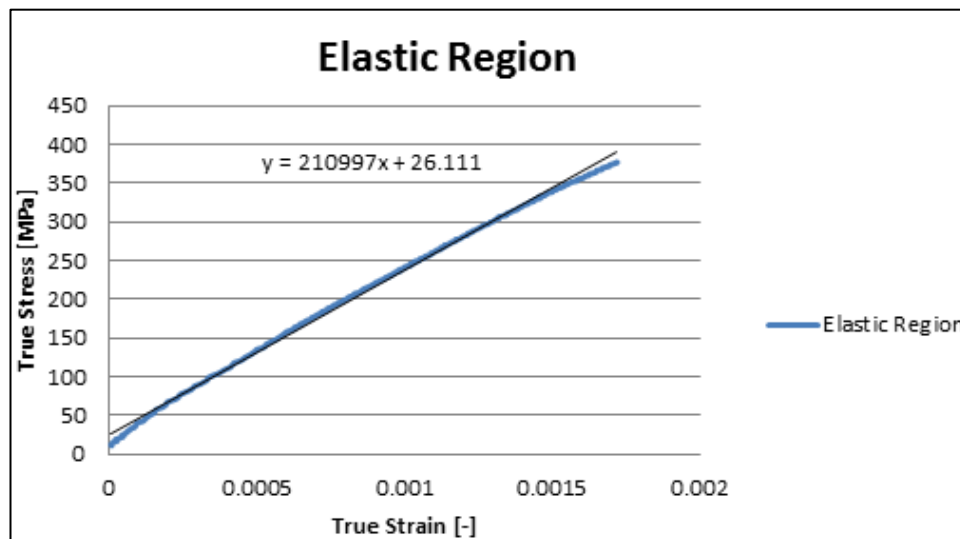
Figure 4.10 : Elastic portion of true stress − true strain curve.

From Figure 4.10, it can be seen that the slope of elastic portion of true stress − true strain curve is equal to 210997 MPa. It is known that Elastic Modulus of many steels 210000 MPa and Elastic Modulus found from experiment is consistent with literature data. Four tensile tests were performed for AISI 1045 and true stress − true strain curves are shown in Figure 4.11.
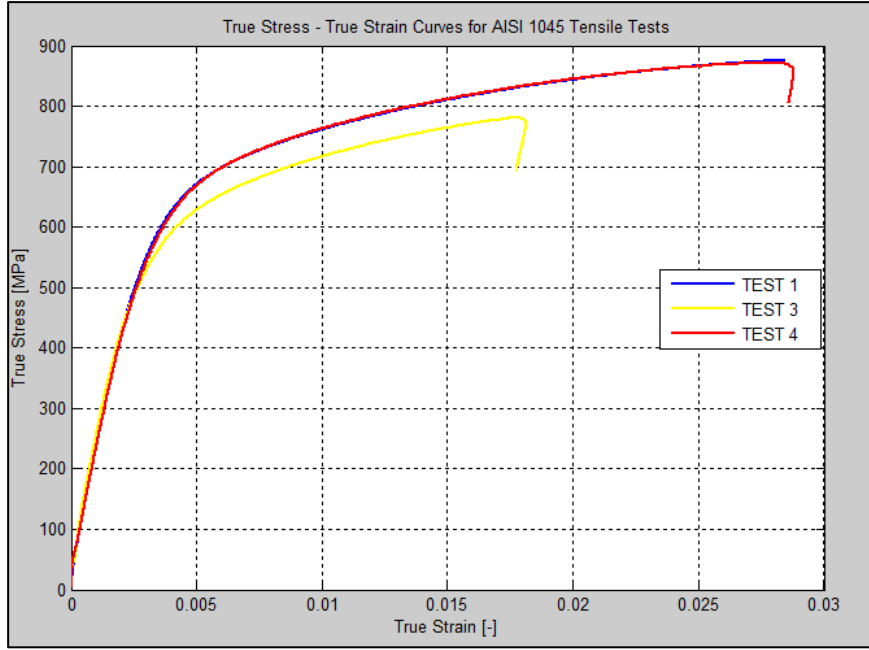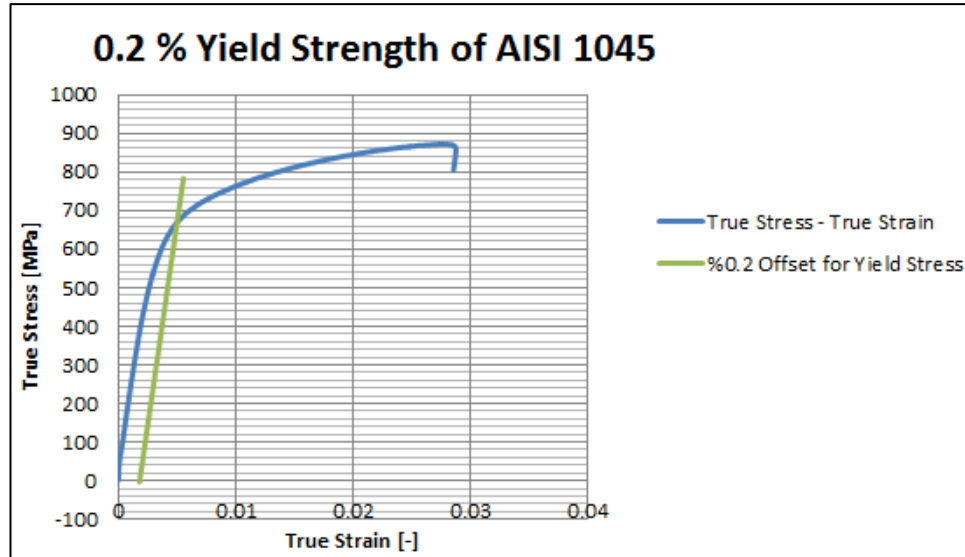
Figure 4.11 : True stress − true strain curves for AISI 1045 tensile tests.

Unfortunately, the result of Test 2 is meaningless. Therefore, the constitutive fitting is performed for other three tests. After the stress − strain curves are obtained, a key point is to determine the yield strength. For this purpose, the offset curve should be plotted. Initially, equations of linear curve were found for each test and then the offset curve is plotted by equation **(4.7)**.

$$\sigma_{offset} = a(\varepsilon_{tr} - 0.002) + b \tag{4.7}$$

where σ_{offset} is calculated stress for offset curve, a is the slope of linear curve and b is the constant. After the offset curve is plotted, 0.2% offset yield strength can be found at point which intersects with true stress − true strain curve as shown in Figure 4.12.

Figure 4.12 : 0.2 % yield strength of AISI 1045 (TEST 4).

After determining the proof stress for each test, the equivalent plastic strain values are found according to equation **(4.3)** and then true stress–equivalent plastic strain curves are plotted. In order to determining B and n parameters, regression analysis, which is presented previos section, is used. Finally, a unique curve is fitted to all tests as given in Figure 4.13.
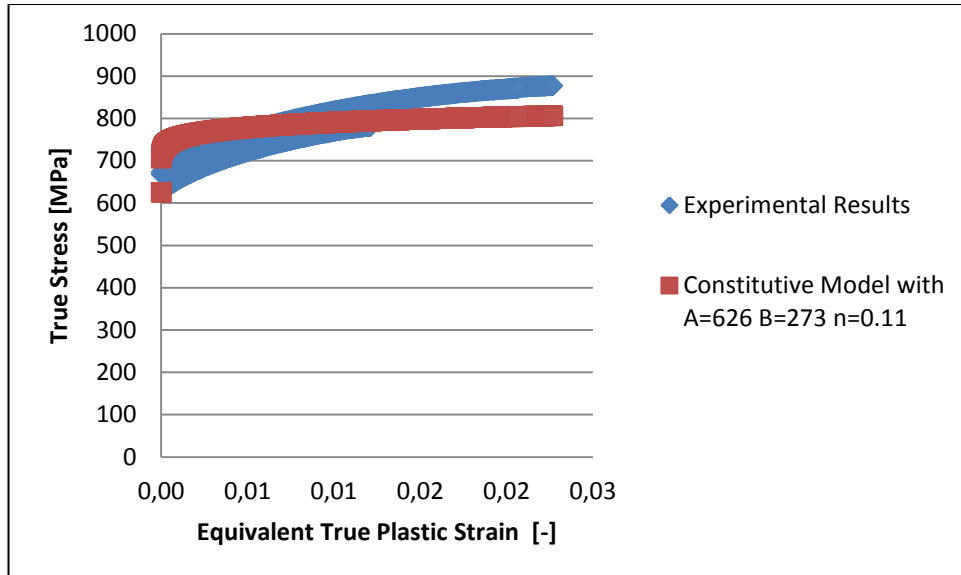

Figure 4.13 : Curve fitting of experimental test results for AISI 1045.

According to regression analysis and curve fitting, yield strength of material A is found as 625 MPa, strain-hardening coefficient B is found as 273 MPa and strain hardening exponent n is found as 0.11. It should be remembered that work hardening is applied to AISI 1045 (Cold Drawn) steel. It is known that the yield strength of material increases when ductility of material decreases if the cold drawn process is

applied to any material. In addition to this, the test does not show a necking behavior so the slope is then also too high. A. Finally, the first term of Johnson–Cook constitutive model became as equation **(4.8)** for AISI 1045.

$$\sigma = (625 + 273\varepsilon_p^{0.11})$$

(4.8)

4.1.5 AISI 4140 (Cr42Mo4) results

Four tests are performed for AISI 4140 specimens. True stress–True strain curves are presented in Figure 4.14.
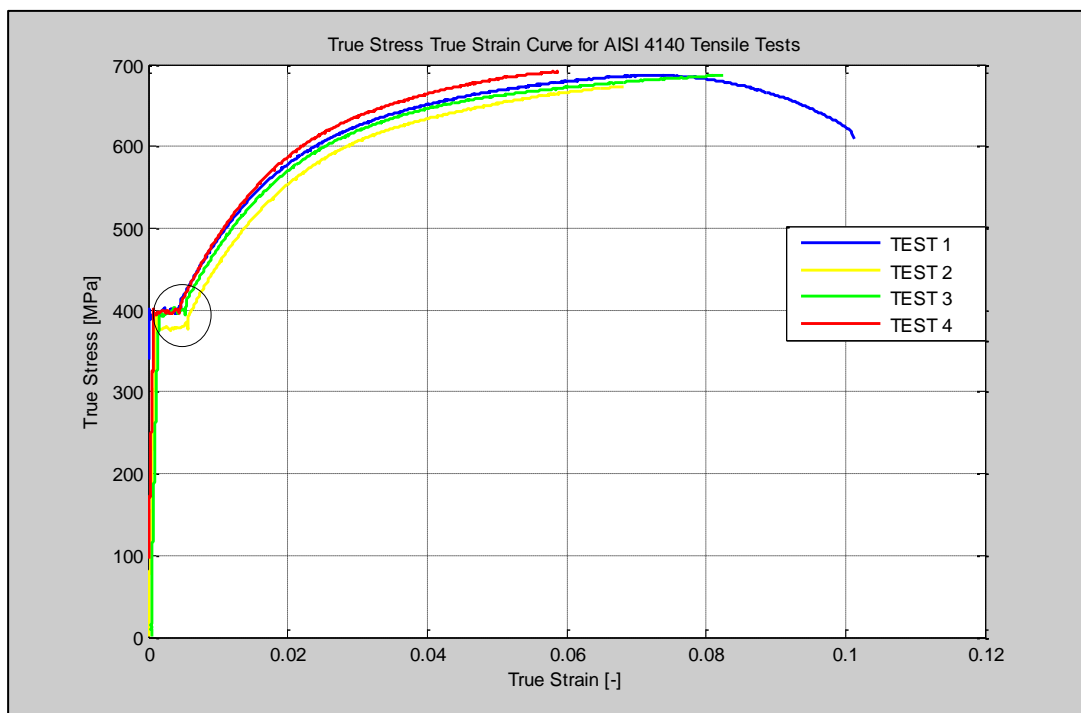
Figure 4.14 : True stress – true strain curves for AISI 4140.

From Figure 4.14, it can be understood that yielding point phenomena occurs for AISI 4140 steel. The average yield strength is assumed 395 MPa according to Figure 4.14. After this assumption was made, the unique curve is fitted to all data points includes four tests with respect regression analysis procedure that presented in previous sections.
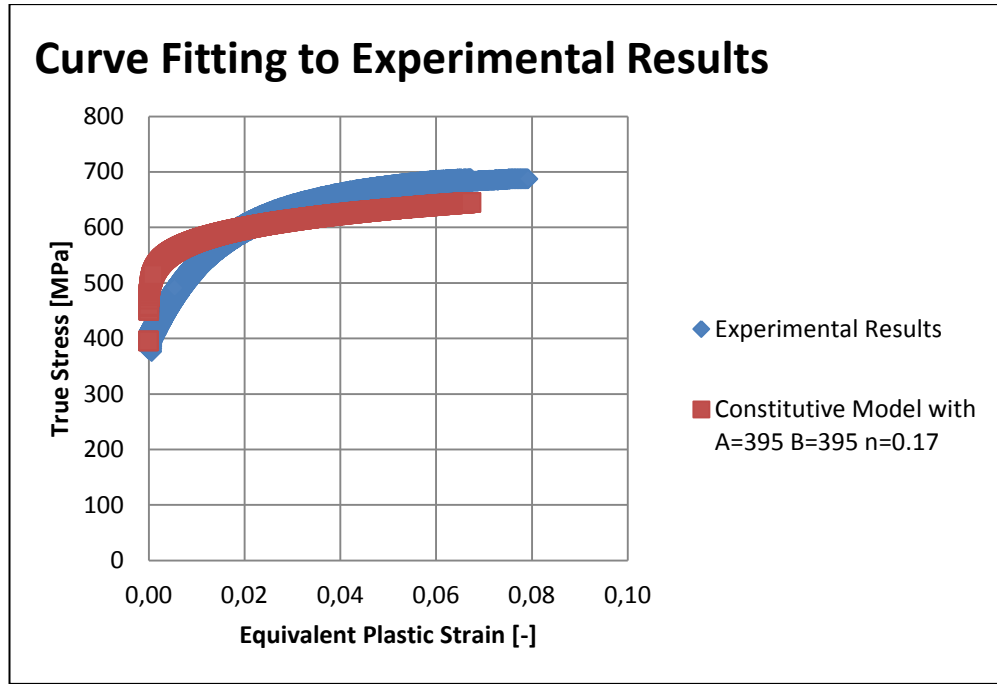
Figure 4.15 : Curve fitting of experimental test results for AISI 4140.

Figure 4.15 shows the curve fitting of all data points of four tests. In addition to this, AISI 4140 is supposed to heat treatment and cold working process. Therefore, the mechanical properties such as yield strength remarkably changes. According to regression analysis and curve fitting, yield strength of material *A* is found as 395 MPa, strain-hardening coefficient *B* is found as 395 MPa and strain hardening exponent *n* is found as 0.17. The constitiutive fitting of each tests can be seen in Appendix A. Finally, the first term of Johnson – Cook constitutive model became as equation **(4.9)** for AISI 4140.

$$\sigma = (395 + 395\varepsilon_p^{0.17})$$

(4.9)

Curve fitting of AISI 4140 is worst among all curve fittings. The reason of this reality is not known clearly. In addition to this, if yield strength *A* is changed, better curve fittings with less error can be obtained. However, the author choose to determine yield strength as average of yield strength values of all tests during this study. For instance, there is a better fit for AISI 4140 steel specimens with yield strength *A* as choosen 315 MPa. However, it is clear that yield strength of any test results is not equal to 315 MPa. Therefore, parameter *A* is chosen as an average value which equals to 395 MPa. To sum up, the calculated stress with respect to true strain values from the determined parameters as presented in Table 4.2.

Table 4.2 : Quasi – Static Johnson – Cook Parameters.

Material	A [MPa]	B [MPa]	n
AISI 1040	375	383	0.25
AISI 1045	625	273	0.11
AISI 4140	395	395	0.17

4.2 Quasi–Static Tensile Tests at High Temperature

The third term of Johnson–Cook constitutive model represents thermal softening effect. For this purpose, quasi–static test are performed at 80 $°C$ and $260°C$. It is observed strain rate dependency of temperature and supposed that high temperature test should be performed at high strain rates for more accurate results [27]. Unfortunately, there is no experimental set up so that the high temperature tests are performed with Split Hopkinson Pressure Bar. Instead of this technique, quasi-static tests at high temperatures were performed in order to see thermal softening effect. Moreover, some difficulties are faced during high temperature quasi–static tests. First of all, the extensometer gives accurate strain values up to $150°C$. Therefore, the correct strain values are taken for only 80 $°C$ with extensometer. The force–elongation curve for tensile tests at $260°C$ are obtained without using extensometer. In this case, the test machine remarkably extends during the tests. In other words, most of the displacement comes from the crosshead motion of machine due to test machine stiffness. In order to overcome this problem, the author tried to compare all tensile test results without extensometers but the meaningful results cannot be obtained. In addition to this, the tensile test results are not adequate for determining thermal softening parameter m. In order to understand the effect of the temperature effect, tests should be performed at higher temperatures up to 1000 $°C$. Johnson and Cook determined that m is equal to 1 for most of metals especially steels studied in this thesis. Through this section, thermal softening parameter m determination is attempted. However, if any meaningful value cannot be obtained, a unit value for m will be used.

4.2.1 High temperature testing procedure

The main goal of quasi–static tests at high temperature is determining thermal softening effect m which appears in third term in Johnson – Cook constitutive equation.

$$\sigma = (A + B\varepsilon_p^n)(1 + C\ln\frac{\dot{\varepsilon}^p}{\dot{\varepsilon}_0^p})(1 - T^{*m})$$

(4.10)

where T^* can be expressed as homologous temperature as shown in following relation.

$$T^* = \frac{T_{inst} - T_{ref}}{T_{melt} - T_{ref}}$$

(4.11)

If the tensile tests are performed at quasi–static strain rates, the second term of Johnson–Cook constitutive equation became negligible and equation (4.11) diminishes to equation (4.12).

$$\sigma = (A + B\varepsilon_p^n)(1 - T^{*m})$$

(4.12)

Equation 4.12 can be used for especially determining yield strength of materials. Moreover, the average of m values are taken into account for determining this parameter. In order to perform high temperature tests, MTS tensile testing machine with an environmental chamber (furnace) for this kind of tests is used as shown in Figure 4.16. After the position of environmental chamber is adjusted for test, the desired temperature is given via the controllable data acquisition system. The test specimens after quasi–static tensile tests can be seen as presented in Figure 4.17

Figure 4.16 : Environmental chamber and data acquisition system.

Figure 4.17 : AISI 1040 specimens after high temperature tests.

4.2.2 AISI 1040 results for high temperature testing

For AISI 1040 specimens, five successive tests were performed at 80 $^\circ C$ and 260 $^\circ C$ respectively. The measurement difference sourced by using extensometers was explained. In Figure 4.17, it can be seen that difference between true stress − true strain curves of tests with extensometers and without extensometers.
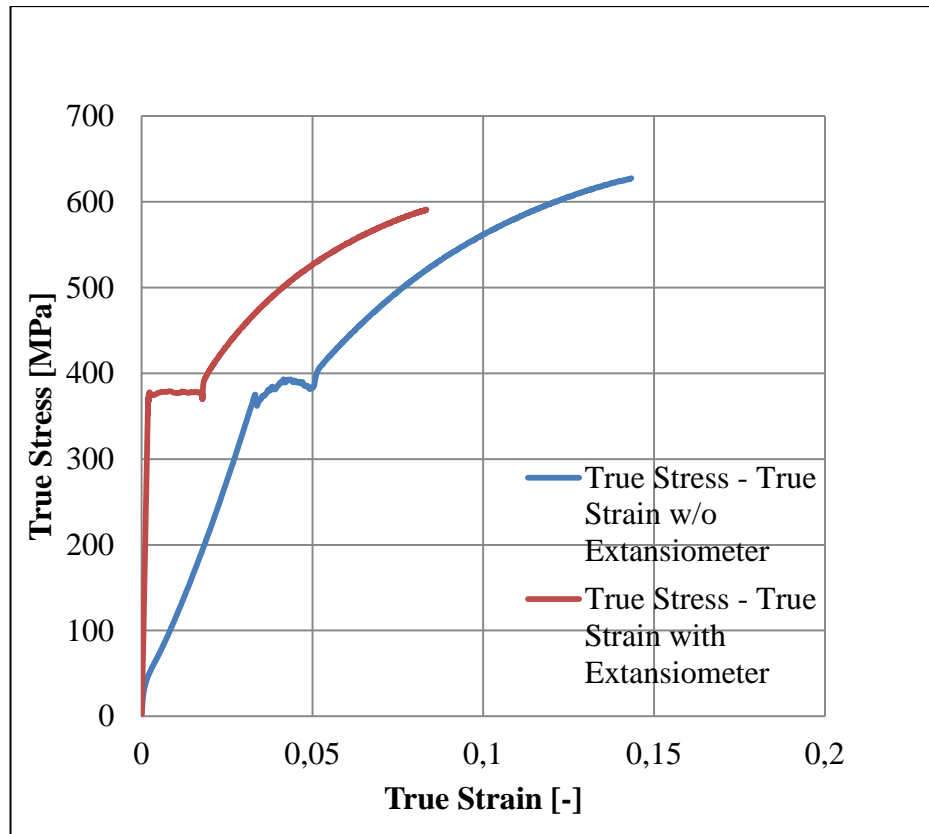
Figure 4.18 : The effect of extensometer usage on flow curves.

Figure 4.18 depicts that strain values significantly changes if the extensometer which used to measure changes in length of specimen. For tests at 80 $^{\circ}C$ extonsemeter is used but its specification is not suitable for $260\,^{\circ}C$. For overcoming this problem, two different approaches were tried. One of these approaches is preparing very rigid tensile specimen which its diameter is relatively high so that it does not elongate so much. By this way, the elongation value are recorded that are related only to machine stiffness. After the force-displacement curve is obtained for machine rigidity., the stiffness of the machine can be found. Figure 4.19 shows a rigidity model of the tensile test – machine specimen system.
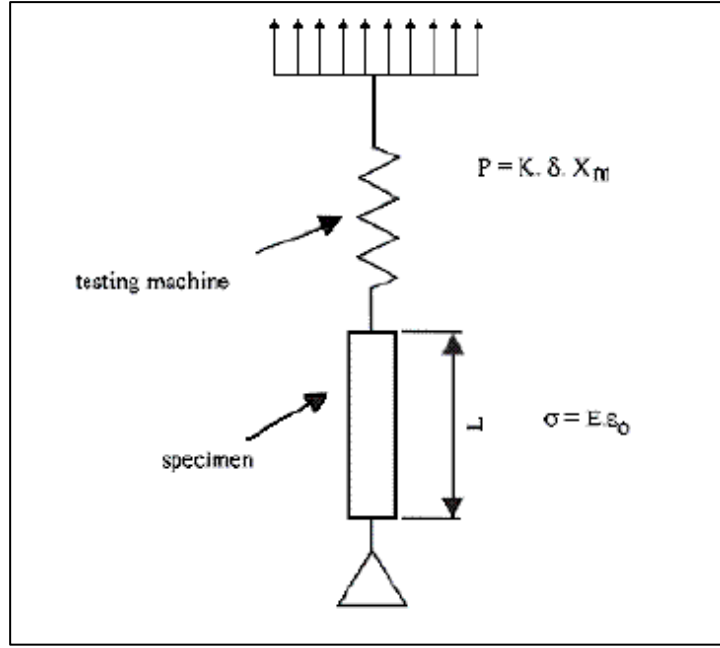
Figure 4.19 : Tensile test – machine specimen rigidity model [29].

Equation **(4.13)** gives the system machine – specimen stiffness, K_{sys}.

$$\frac{1}{K_{sys}} = \frac{1}{K_m} + \frac{1}{K_{specimen}}$$

(4.13)

where $K_{specimen}$ is the specimen linear stiffness and K_m is the machine linear stiffness. In Figure 4.20, two curves are shown which are elastic regions of curves in Figure 4.18. To obtain the specimen stiffness, the contribution of low part of the machine should be subtracted [29].
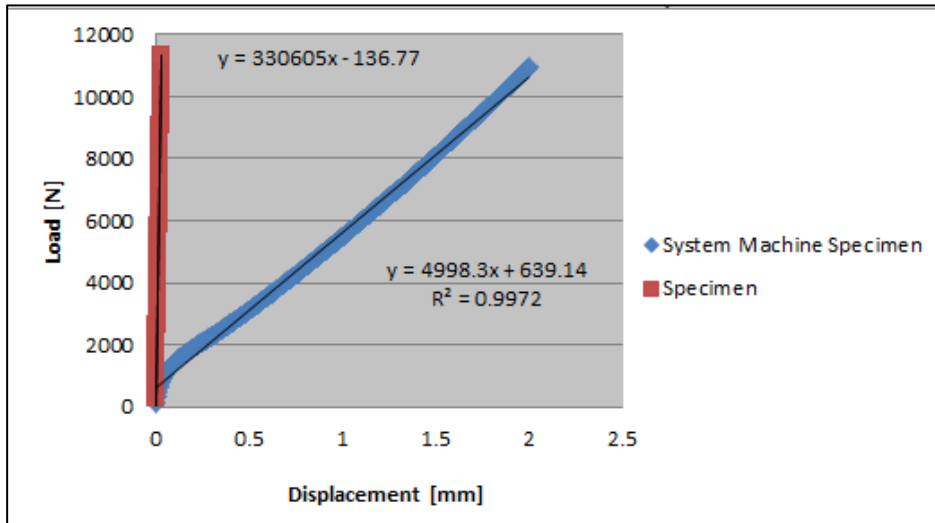
Figure 4.20 : Linear stiffness curves of the specimen and of the system machine – specimen.

48

From Figure 4.20, it can be shown that linear stiffnesses of two measurement systems are slightly different with each other. In Figure 4.21, the setup of test for determining machine rigidity can be shown.

Figure 4.21 : Machine rigidity test.

After the machine rigidity test was performed, displacement – force curve was plotted and a high order polynomial is fitted to this curve for strain correction as shown in Figure 4.22.
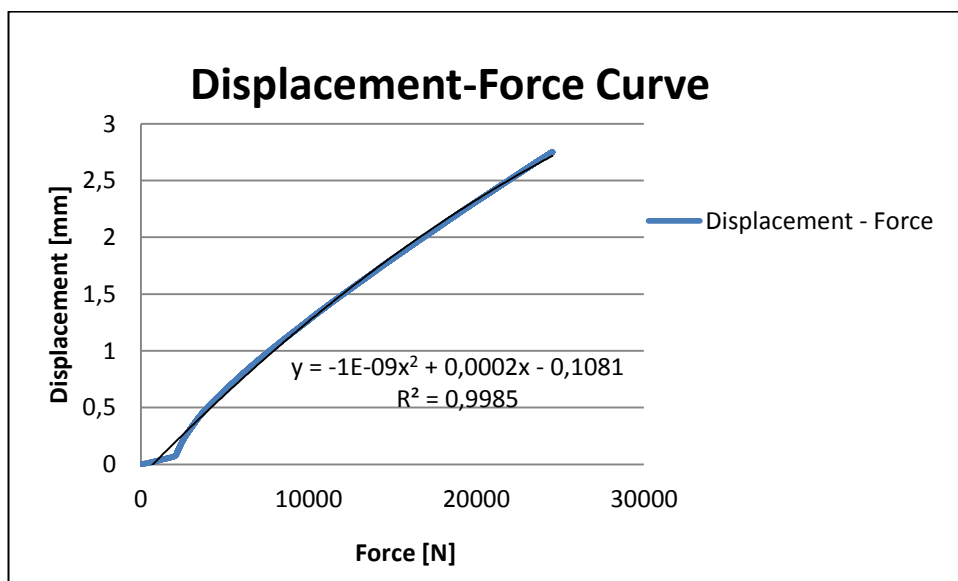
Figure 4.22 : Displacement–Force curve of machine rigidity test.

The equation obtained from displacement – force curve is used for correcting the strain data. One of the example of this correction is shown in Figure 4.23.
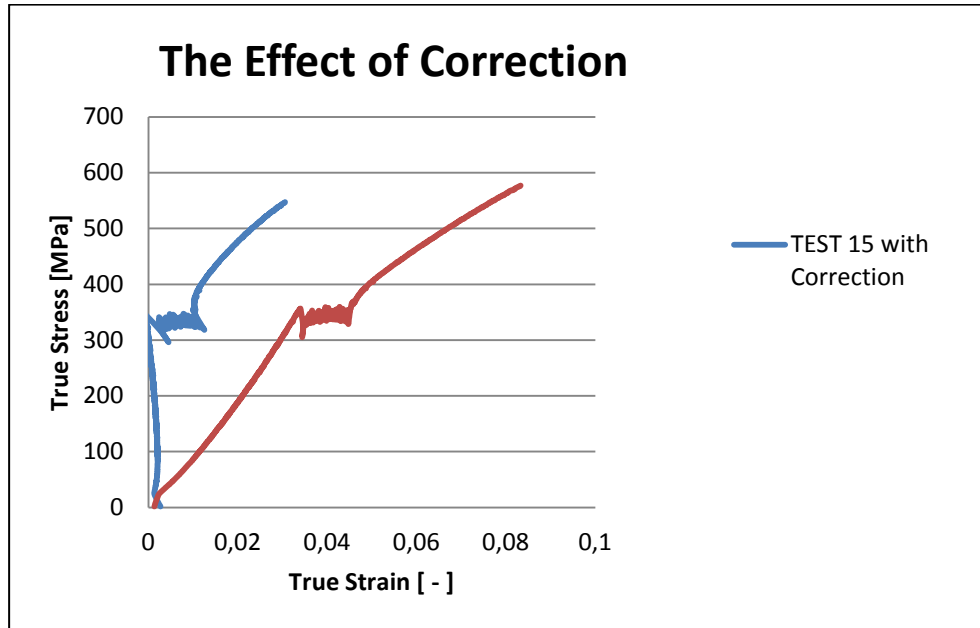
Figure 4.23 : The effect of correction for AISI 1040 (TEST 15 at 260 $°C$).

It can be said that the high order polynomial corrected flow curve. However, it is observed that the correction is not effective for lower stresses. Therefore, another approach is attempted to find thermal softening effect. For this purpose, test results at $80°C$ will be compared with test results at $25°C$ according to results obtained by extensometer. Moreover, test results at $260°C$ will be compared test results at $25°C$ obtained without extensometer. In order to clarify, the high temperature results are evaluated according to reference temperature ($25°C$). Due to the fact that extensometer gives accurate results up to $80°C$, it cannot be used for tests performed at $260°C$. Therefore, the decrease at yield strength at $260°C$ should be compared with test results at $25°C$. Both elongation values acquired by machine and extensometer are available for $25°C$ and $80°C$. The author expects that, the trendline does not change, although strain values are not true for results obtained without extensometer. Finally, quasi–static parameters of Johnson–Cook constitutive equation are taken into account and thermal softening parameter m for each test at high temperatures. A general decrease in yield strength of AISI 1040 can be shown in Figure 4.24.
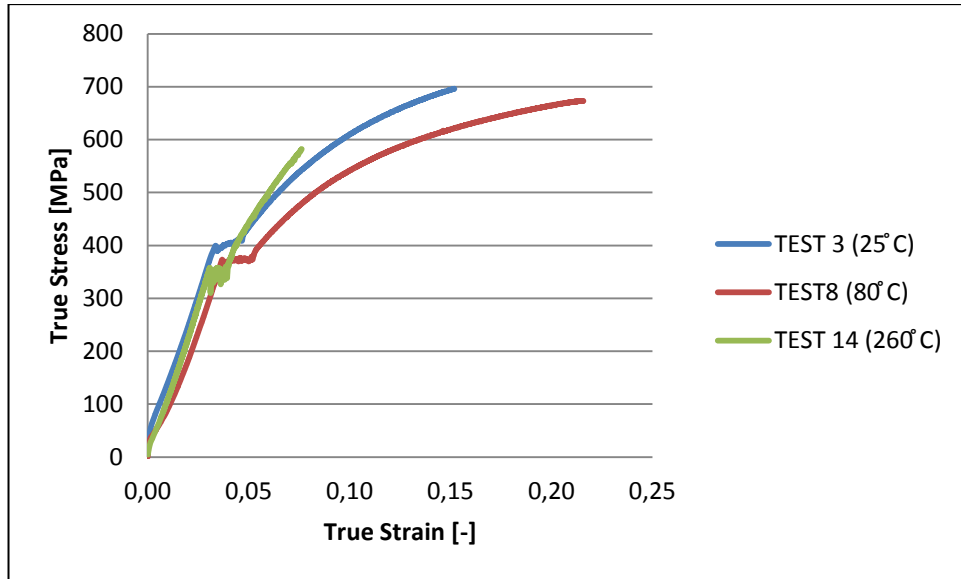
Figure 4.24 : Thermal softening effect on yield strength of AISI 1040.

From Figure 4.24, it can be said that the yield strength of material decreases with temperature rise. The hardening behavior of test results for 25 $^{\circ}C$ and 80 $^{\circ}C$ resemble with each other. However, the test results at 260 $^{\circ}C$ show a different hardening behavior from results at other two temperatures. Since the normalization process is not applied to materials the hardening curve behaves differently. Figure 4.22 also depicts that, different stress values are experimentally obtained for same true strain values. If equation **(4.12)** is applied for test results at $80\,^{\circ}C$, the average of thermal softening parameter m is found as 0.98. For this purpose, the constitutive equation is fitted to all data points for $80\,^{\circ}C$ and the error between experimental results and constitutive equation with given equation **(4.12)** is minimized by using least − squares technique as given in equation **(4.5)**. Figure 4.25 depicts that regression fitting of experimental results with determined thermal softening parameter m. The determined parameter is logical because the temperature difference ($55\,^{\circ}C$) is found to be satisfactory relatively low when it is compared to melting temperature of steel which is $1521\,^{\circ}C$. In addition to this best fit is obtained for Test 7, which is shown in Figure 4.26. Other fits are presented in Appendix B.
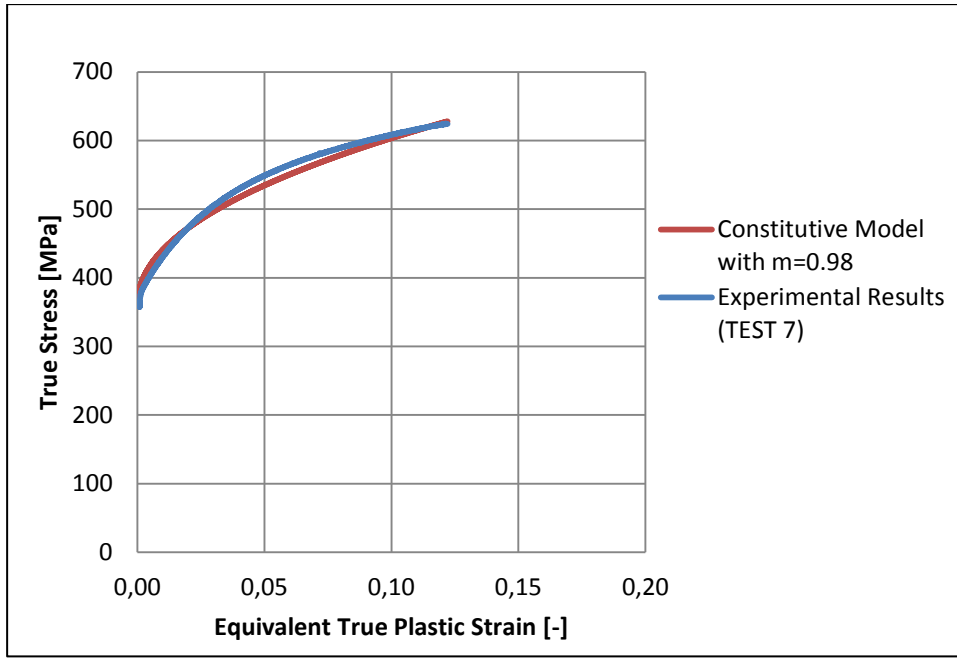
Figure 4.25 : Curve fitting to experimental results for TEST 7 at $80\,^{\circ}C$ with m=0.98.

As stated before, thermal softening parameter for most metals can be accepted as 1. Unfortunately, curve fitting results for $260\,^{\circ}C$ are not successful as test results at $80\,^{\circ}C$. The curve fitting of all data points according to equation **(4.12)** as presented in Figure 4.27.
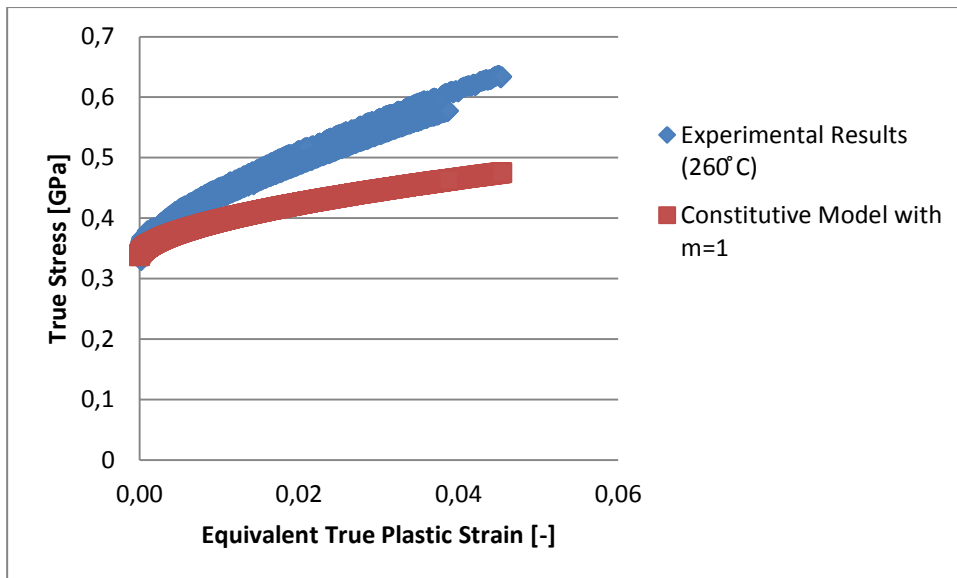
Figure 4.26 : Curve fitting to experimental results of AISI 1040 at $260\,^{\circ}C$ with m=1.0.

One reason of unrealistic fitting result in Figure 4.27 may be taking data without extensometer. In addition to this, it is the fact that the model predicts stresses that are

crucially higher than stresses obtained from experimental tests. Finally, the thermal softening parameter m is an average value of $80\,^{\circ}C$ and $260\,^{\circ}C$ tests (0.99) and equation 4.12 becomes for AISI 1040.

$$\sigma = (375 + 383\varepsilon_p^{\,0.23})(1 - T^{*0.99})$$

(4.14)

4.2.3 AISI 1045 results for high temperature testing

In previous sections, it is explained that AISI 1045 specimen does not show yield point phenomena so its yield strength can be determined by using 0.2 % offset proof stress. This situation makes more difficult specifying yield strength for results obtained without extensometers because the elastic curve is not true. In addition to this, AISI 1045 specimens provided by steel manufacturer is manufactured for military purposes and special heat treatment and cold – working process is applied to material and no normalizing was applied before tests. Therefore, the hardening and thermal softening characteristics of AISI 1045 may be different than literature values for normalized materials.

The same procedure for AISI 1040 is used to determine thermal softening parameter m for AISI 1045. Figure 4.27 depicts that thermal softening effect for a test performed at $80\,^{\circ}C$ with extensometer. Figure 4.28 also shows the same effect for a test performed at $260\,^{\circ}C$ without extensometer.
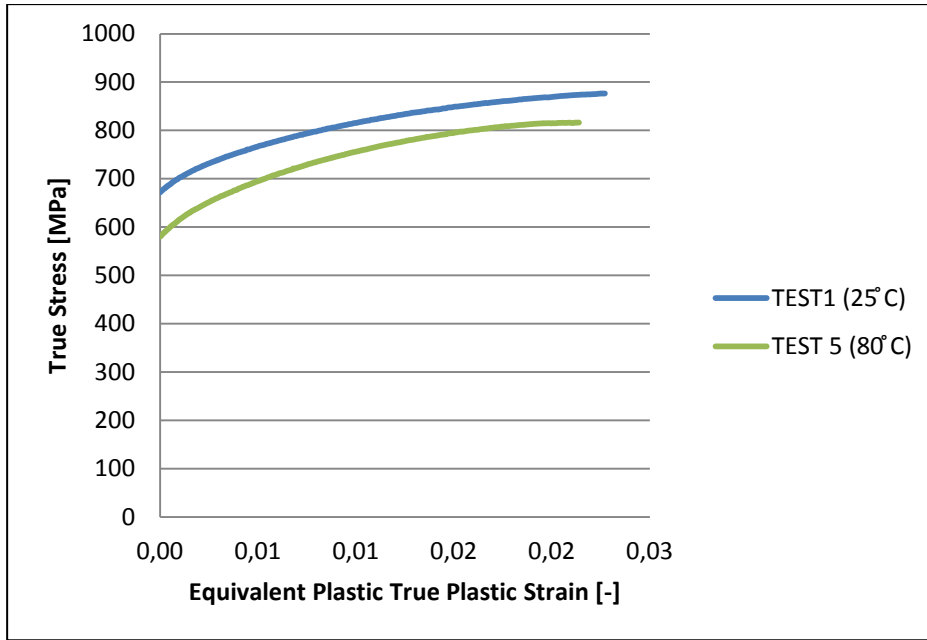
Figure 4.27 : Thermal softening effect on yield strength of AISI 1045 for $80°C$.
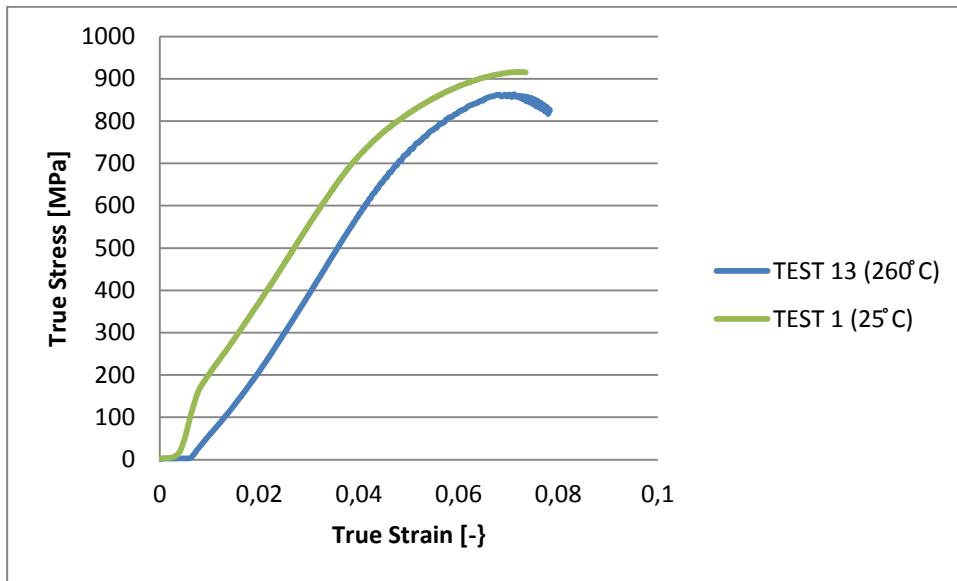
Figure 4.28 : Thermal softening effect on yield strength of AISI 1045 for $260°C$.

It can be said that finding 0.2% proof stress is difficult from Figure 4.28. For $80°C$ results, a unique curve is fitted to all data points which are performed for three tests at this temperature as shown in Figure 4.29.
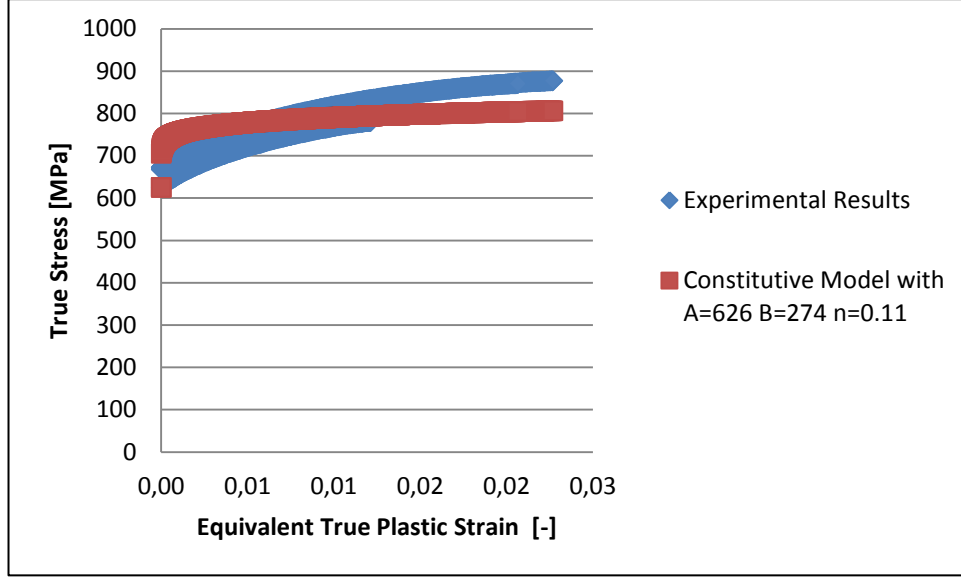
Figure 4.29 : Curve fitting to experimental results of AISI 1045 at 80°C with m=0.69.

A best fit is obtained with $m=0.69$ and curve fitting for each test will be given in Appendix B. Nevertheless a good fit is not obtained for tests performed at 260°C. However, the two tests were chosen so that the thermal softening effect can be clearly observed as given 4.29 and thermal softening parameter is attempted to predict. Finally, best fit is again obtained for $m=0.69$. Finally, equation **(4.12)** becomes for AISI 1045 as presented in

$$\sigma = (625 + 273\varepsilon_p^{0.11})(1 - T^{*0.69})$$

(4.15)

4.2.4 AISI 4140 results for high temperature testing

For AISI 4140 test specimens, high temperature tests are only performed at 260°C due to experimental reasons. Therefore, resulst must be compared for data recorded without extensometer. Thermal softening effect can be seen in Figure 4.30.
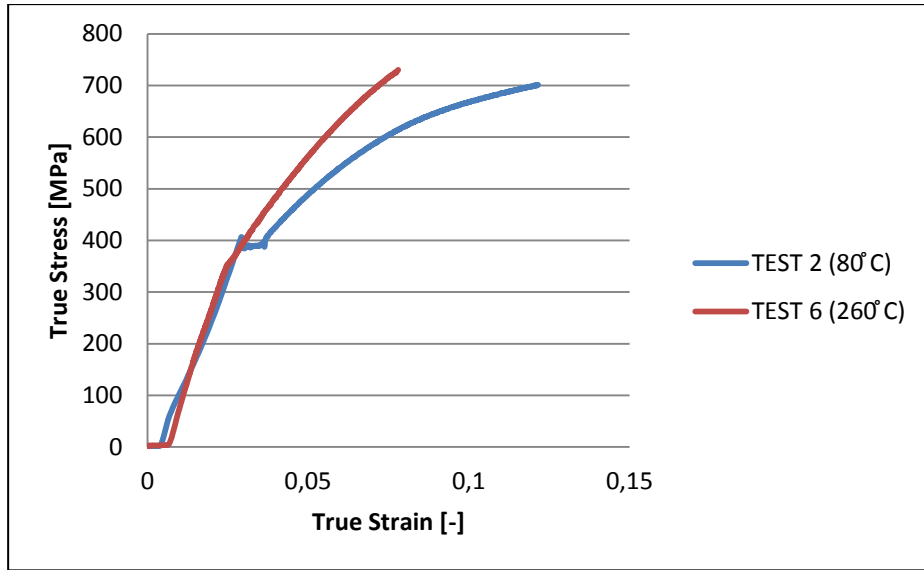
Figure 4.30 : Thermal softening effect on yield strength of AISI 4140 for $260\,^{\circ}C$.

The same problem with other specimens due to measurement without extensometer is faced again according to Figure 4.30. The hardening curve's behavior is not obtained correctly. Since the melting temperature of steel is nearly 1500 K, the temperature change does not affect the results. Therefore, the thermal softening parameter m is chosen as 1.0. Finally, equation **(4.12)** becomes as equation **(4.13)**.

$$\sigma = (395 + 395\varepsilon_p^{\,0.17})(1 - T^{*1.0}) \tag{4.16}$$

4.3 High Strain Rate Testing Results

In order to determine all parameters of Johnson–Cook parameters, final task is determining strain rate coefficient parameter C. The device consists of a striker and two pressure bars made of maraging steel, two strain gages on the surface of incident and transmission bars, a data acquisition sytem which has 400 kHz frequency response and pressure vessel. For this purpose, SHPB at ITU BIOMECHANICS AND STRENGTH OF MATERIALS LAB as shown in Figure 4.31 is used. The fifteen tests were performed for each material for different length- diameter ratios. The strain rate coefficient can be calculated by fitting most suitable curves to data points for each strain rate. Initially, a simple curve is fitted to all points then the least square methods is used in order to determine the strain rate coefficient. A lubricant is used between specimen and pressure bars' interfaces in order to prevent high stress values due to friction during tests.

4.3.1 AISI 1040 results for high strain rate results

The strain rate coefficient parameter (C) is determined for AISI 1040 steel. The fifteen succesive tests were performed for different length-diameter ratios as in Table 4.3.

Table 4.3 : Specimen dimensions and pressure for AISI 1040.

L [mm]	D [mm]	Pressure [Bar]	Number of Tests
15	9	6	3
12	9	4	3
6	9	4	4
9	9	4	5

Figure 4.31 : ITU split hopkinson pressure bar.

Figure 4.32 : Strain gage on the incident bar.

Figure 4.33 : AISI 1040 specimen for high strain rate testing.

For this purpose, the strain recordings from the strain gages on the bars are plotted as Figure 4.34.
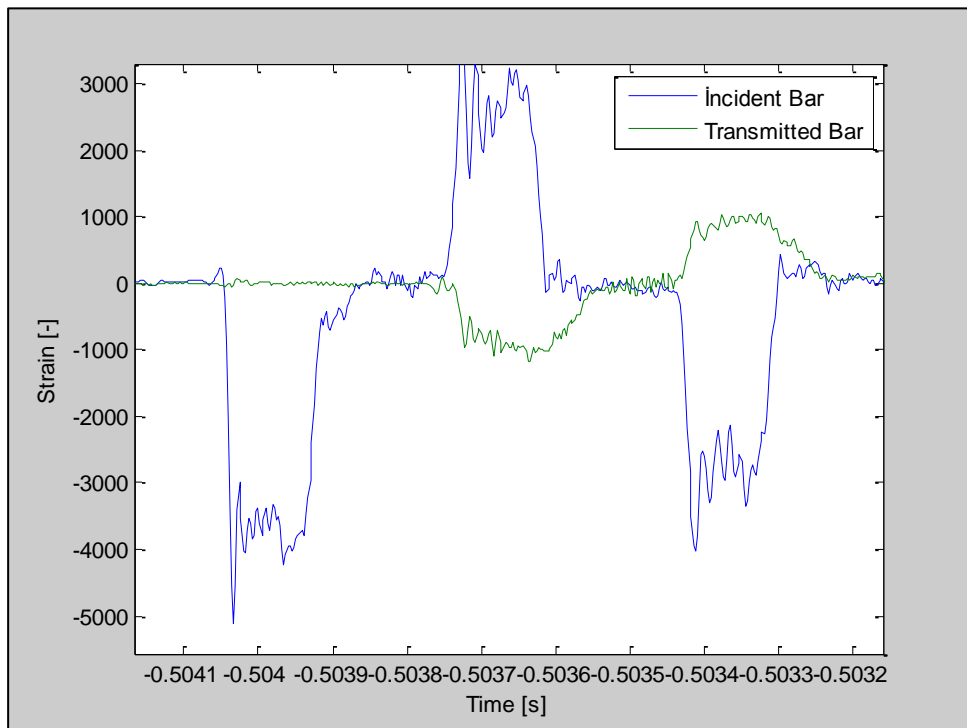
Figure 4.34 : Strain gage signals from the pressure bars.

The first negative blue wave is the incident wave on the incident bar, the second blue wave, which is the positive reflected wave and it is used in order to calculate strain

58

rate and strain according to equation **(3.18)**. If the wave speed is taken $C_B = 4857 m/s$,diameter of pressure bars equals to 22.7 mm and diameter of specimen is taken 9 mm and it is considered that the the sample rate of data acquisition system is 400 kHz, the strain rate, strain and stress are plotted as below figures.
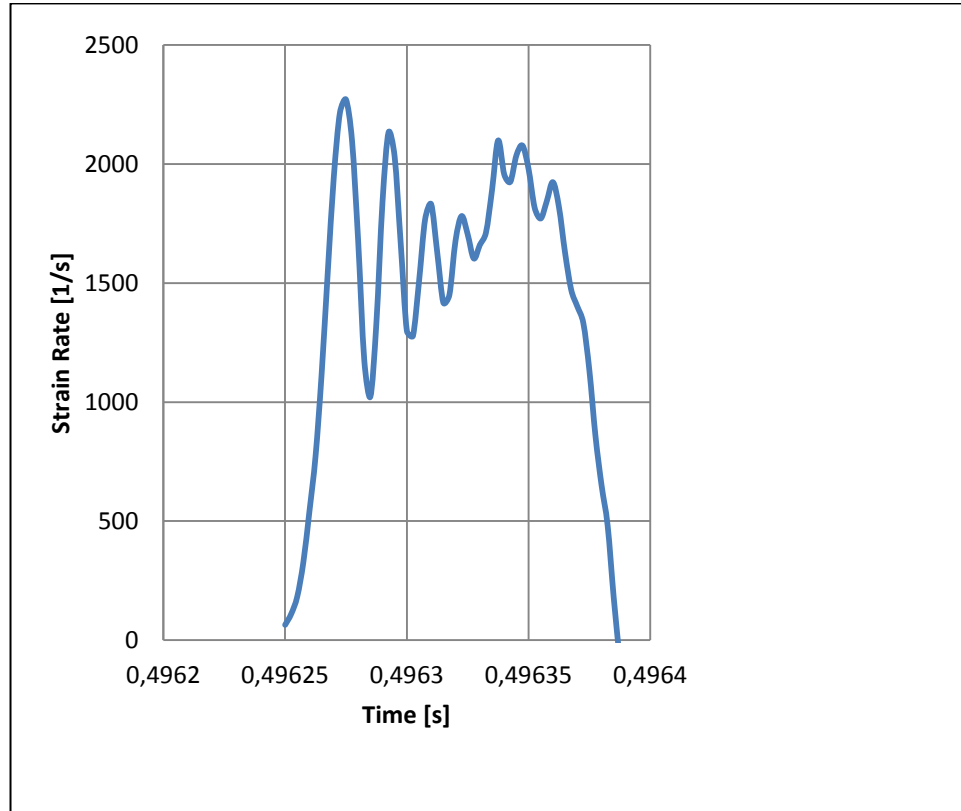
Figure 4.35 : Strain rate – time curve of test1 for AISI 1040.
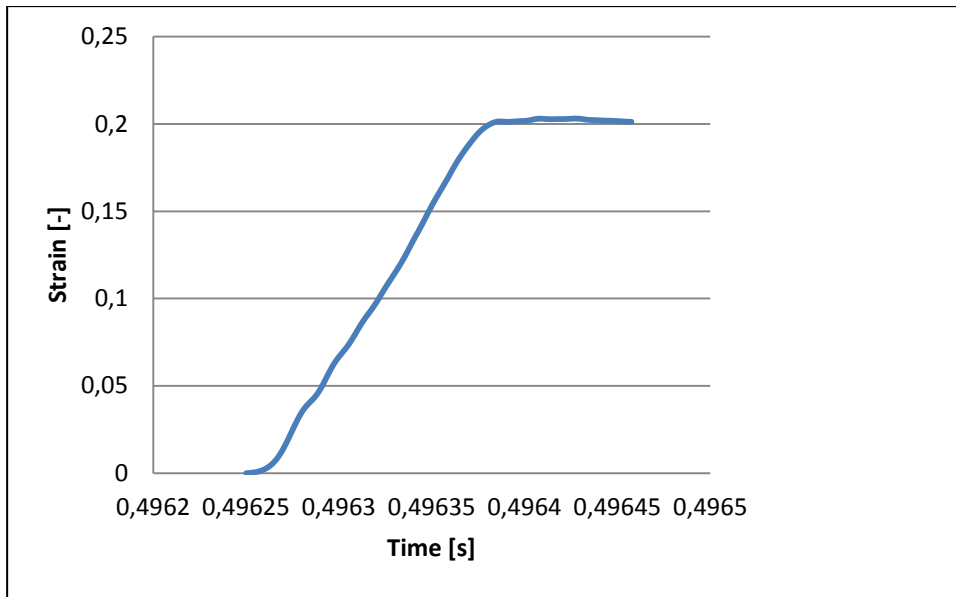
Figure 4.36 : Strain – time curve of test1 for AISI 1040.
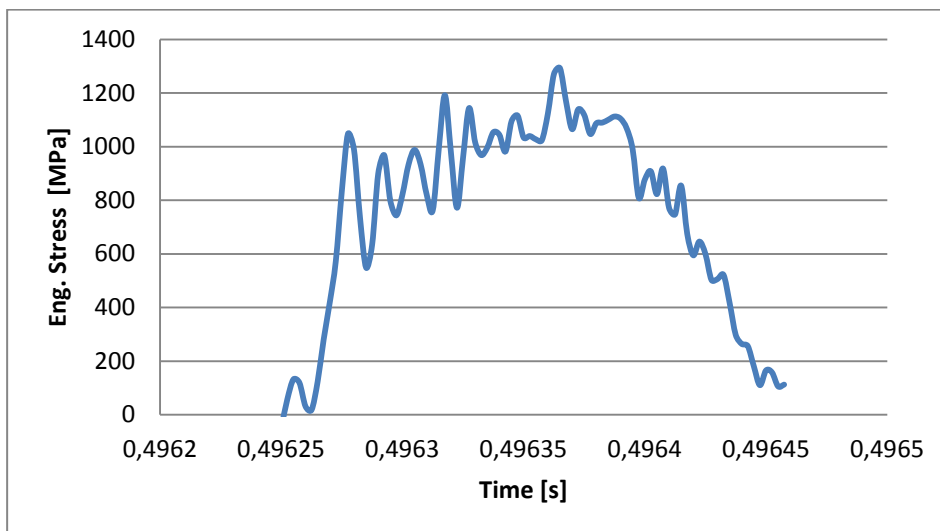
Figure 4.37 : Engineering Stress–time curve of test1 for AISI 1040.
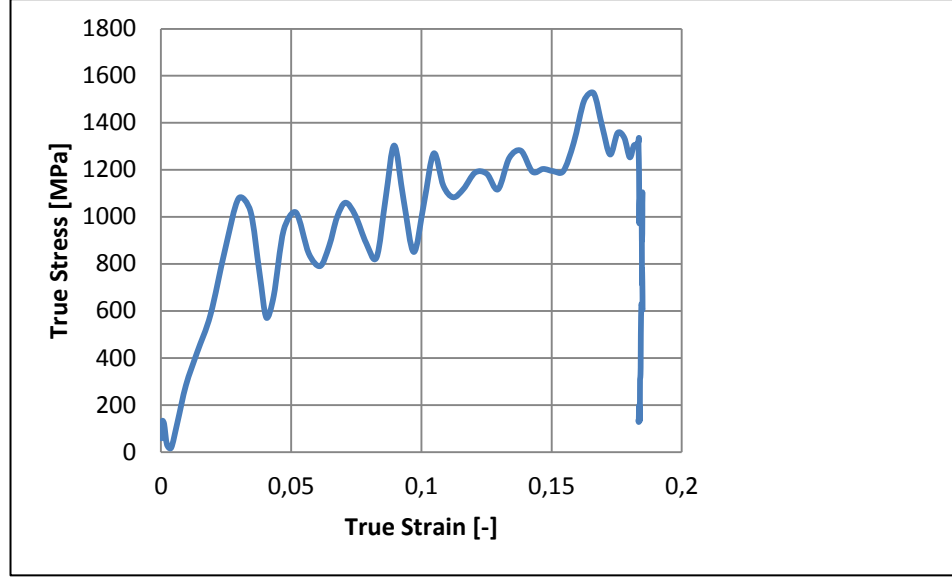
Figure 4.38 : True stress – time curve of test1 for AISI 1040.

It can be seen that the average strain rate can be found as approximately 1700 s^{-1} from Figure 4.35. Engineering strain and stress data with respect to time are also presented in Figure 4.36 and 4.37. Finally, true stress–true strain curve can be obtained as presented in Figure 4.38. In order to determine the strain rate coefficient parameter C, Johnson–Cook constitutive equation should be modified as given in.

$$C = [\frac{\sigma}{(A+B\varepsilon_p{}^n)(1-T^{*m})}]\frac{1}{\ln\frac{\dot{\varepsilon}_p}{\dot{\varepsilon}_0}}$$

(4.17)

Finally, the strain rate coefficient C is determined 0.04 for TEST 1. The constitutive fit can be shown in Figure 4.39.
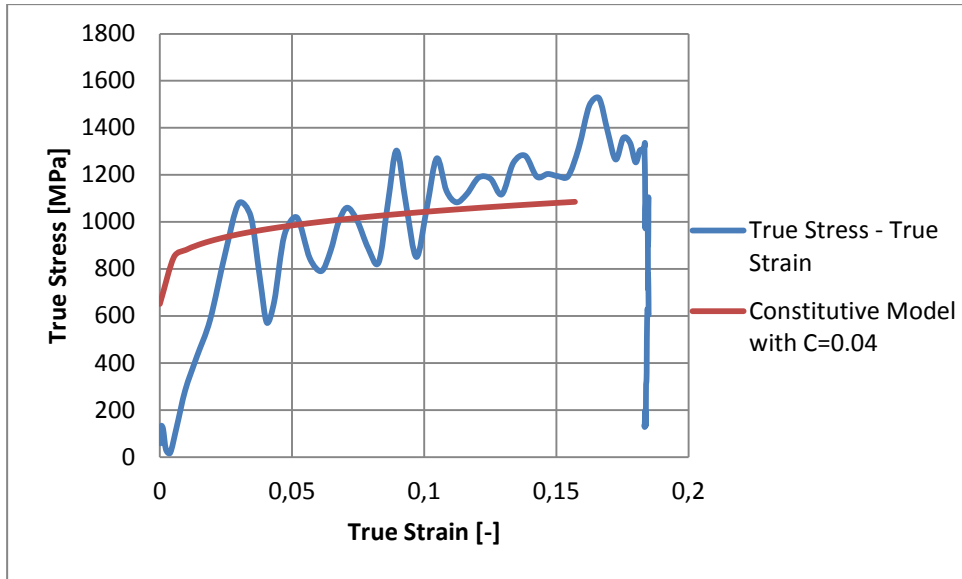
Figure 4.39 : Constitutive fit with C=0.04.

Moreover, the increase in stress response due to the strain rate effect is given as Figure 4.40.
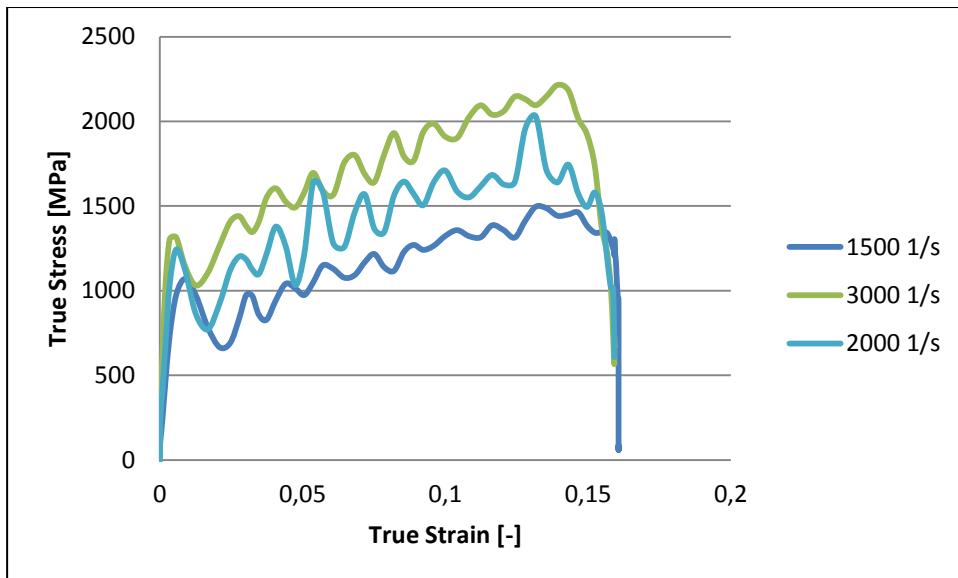

Figure 4.40 : True Stress vs. True Strain for AISI 1040 at strain rates of $1500\,s^{-1}$, $2000\,s^{-1}$ and $3000\,s^{-1}$.

From Figure 4.40, it can be said that stress values increases proportional to strain rate increase. In addition to this, Luder's bands dominate the response of the specimen at higher strain rates. The yield strength of AISI 1040 specimen increases from 400 MPa to 1000 MPa with respect to strain rate effect. It can be said that the strain rate coefficient (C) changes in the range between 0.04 and 0.1. On the other hand, it can be seen that the good fit cannot be obtained with the strain hardening parameters B

and n. These values. are used because of the necking behavior can be provided only with these values. On the other hand, the values for strain hardening parameters, which results better fit to test data, are also used and true stress- true strain graphs are plotted in Appendix C. Finally, Johnson-Cook parameters are obtaines as given in Table 4.4.

Table 4.4 : Johnson-Cook parameters for AISI 1040.

Material	A [MPa]	B [MPa]	n	C	m
AISI 1040	375	383	0.23	0.07	0.99

4.3.2 AISI 1045 results for high strain rate results

The fourteen successive tests were performed for AISI 1045 high strain rate tests as given in Table 4.5.

Table 4.5 : Specimen dimensions and pressure for AISI 1045.

L [mm]	D [mm]	Pressure [Bar]	Number of Tests
6	9	4	6
9	9	3	3
9	9	6	1
12	9	3	2
12	9	6	1
12	9	7	1

Two different parameter sets are used in order to fit curve to all data points. These curves will be presented in Appendix C. AISI 1045 specimens for high strain rate tests before and after experiments are shown as Figure 4.41 and Figure 4.42 respectively.

Figure 4.41 : AISI 1045 test specimens.

Figure 4.42: AISI 1045 test specimen after SHPB experiments.

The same procedure was used to obtain data. Moreover, the strain rate, strain and stress with respect to time are plotted as below,
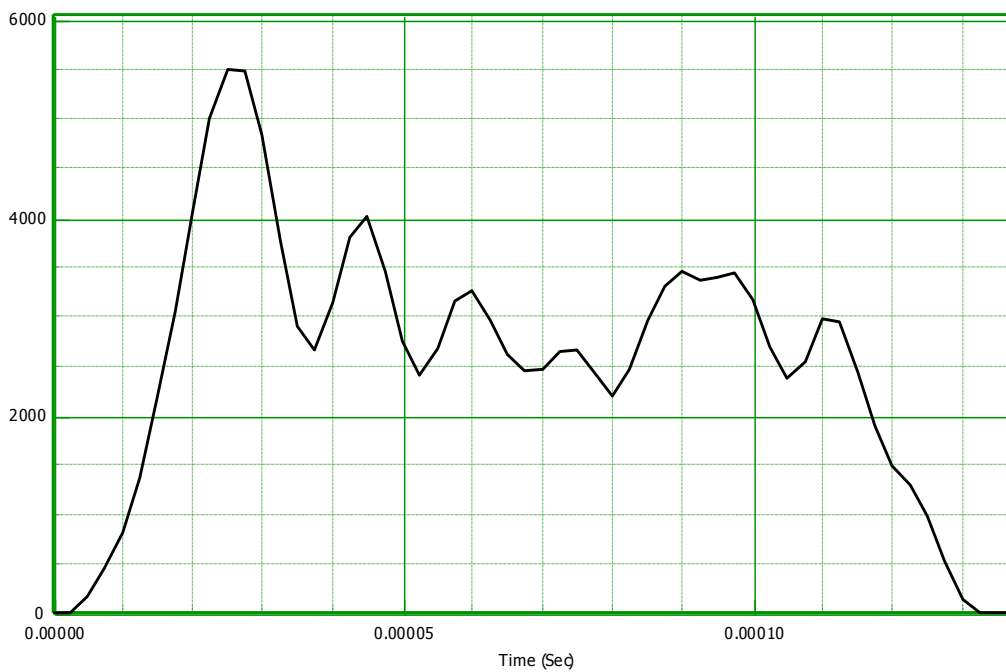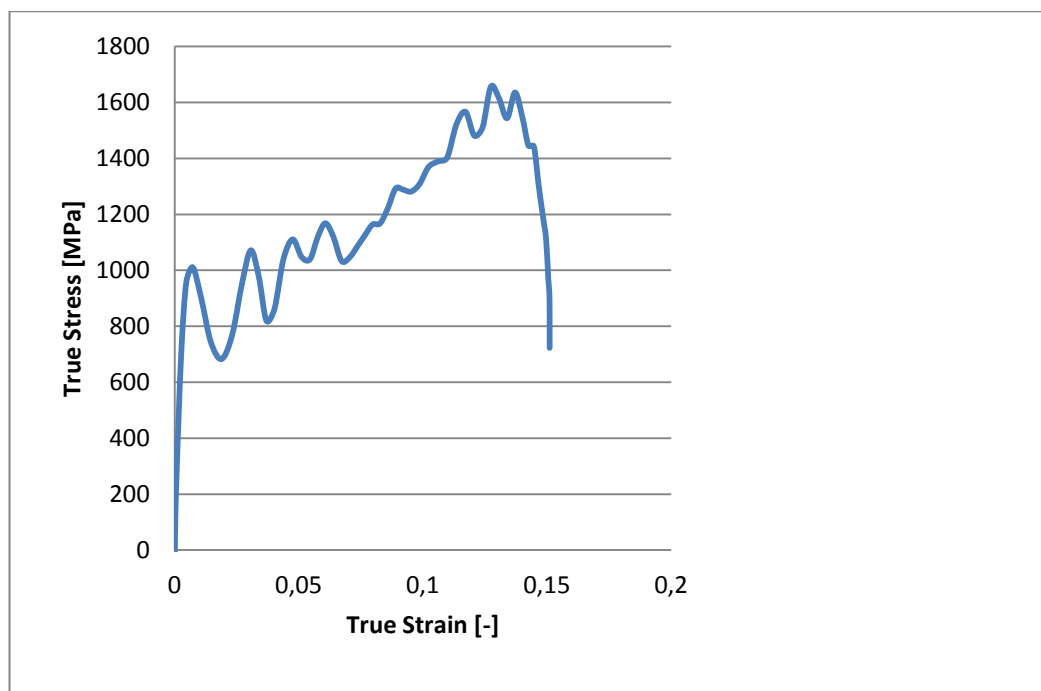

Figure 4.43 : Strain rate – time curve of test1 for AISI 1045.
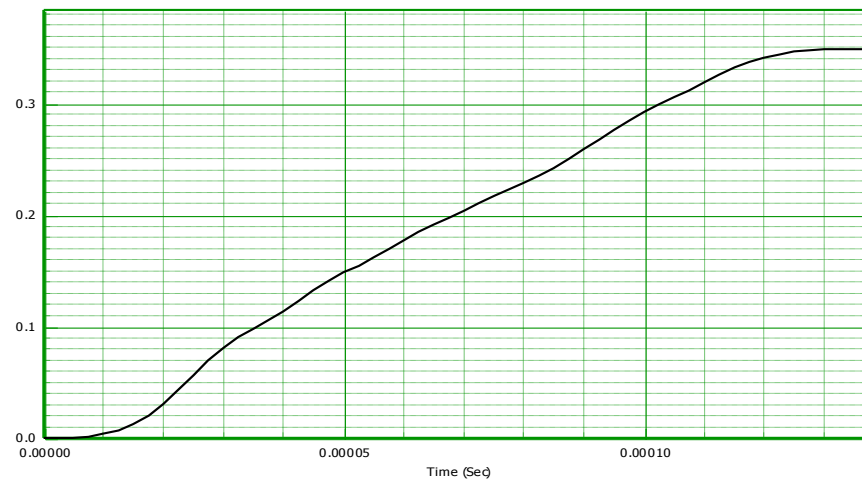
**Figure 4.44 :** Strain–time curve of test1 for AISI 1045.
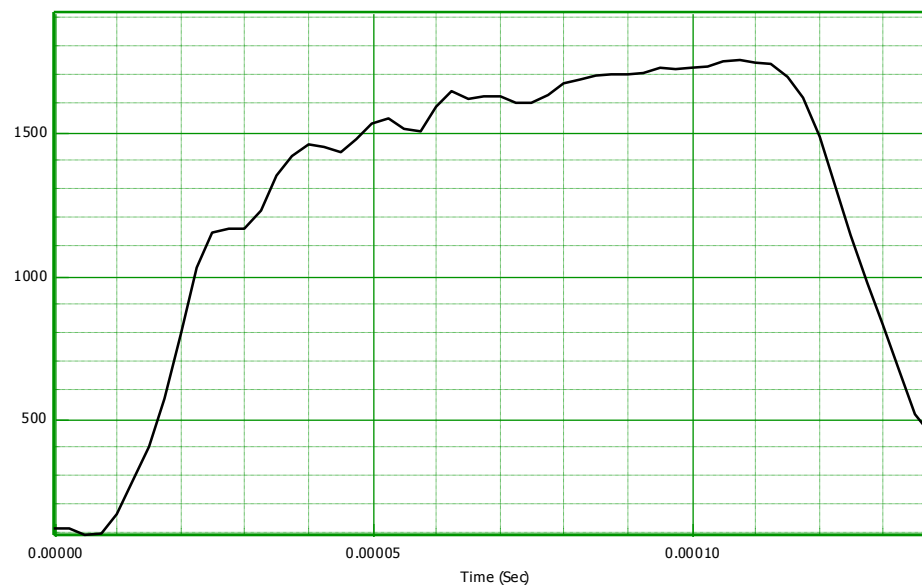
**Figure 4.45 :** Engineering Stress – time curve of test1 for AISI 1045.
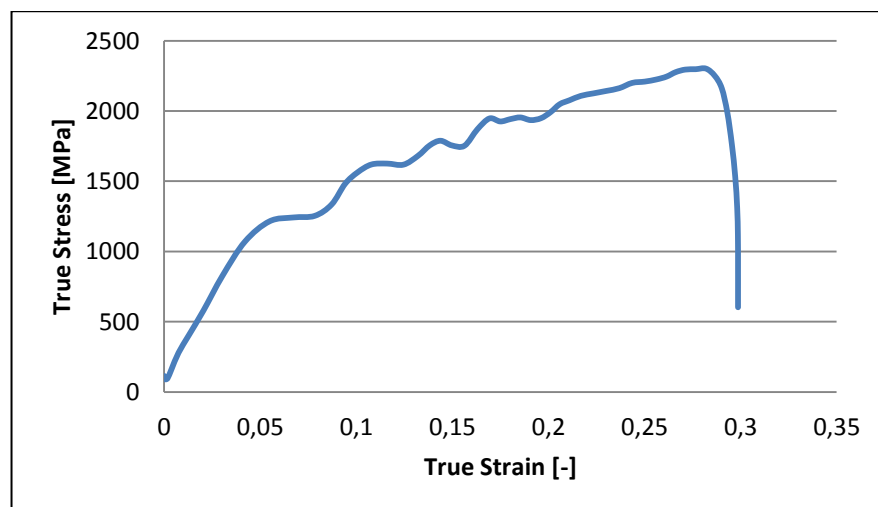
Figure 4.46 : True Stress – True Strain curve of test1 for AISI 1045.

The strain rate effect on stress response can be seen as given in Figure 4.46.
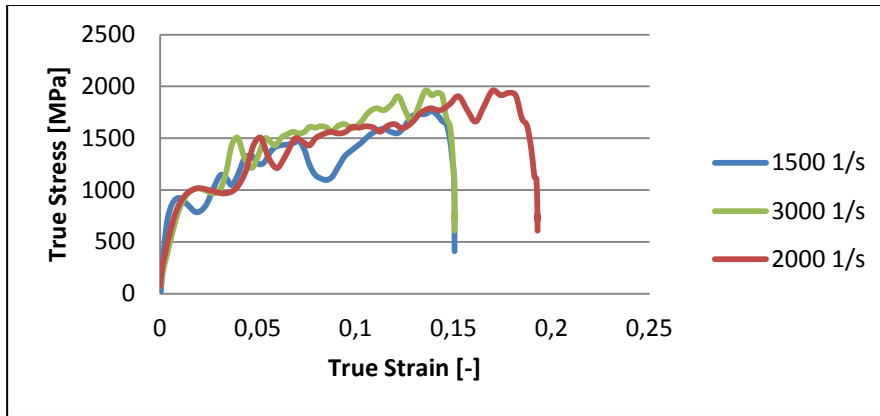
Figure 4.47 : True Stress vs. True Strain for AISI 1040 at strain rates of $1500\,s^{-1}$, $2000\,s^{-1}$ and $3000\,s^{-1}$.

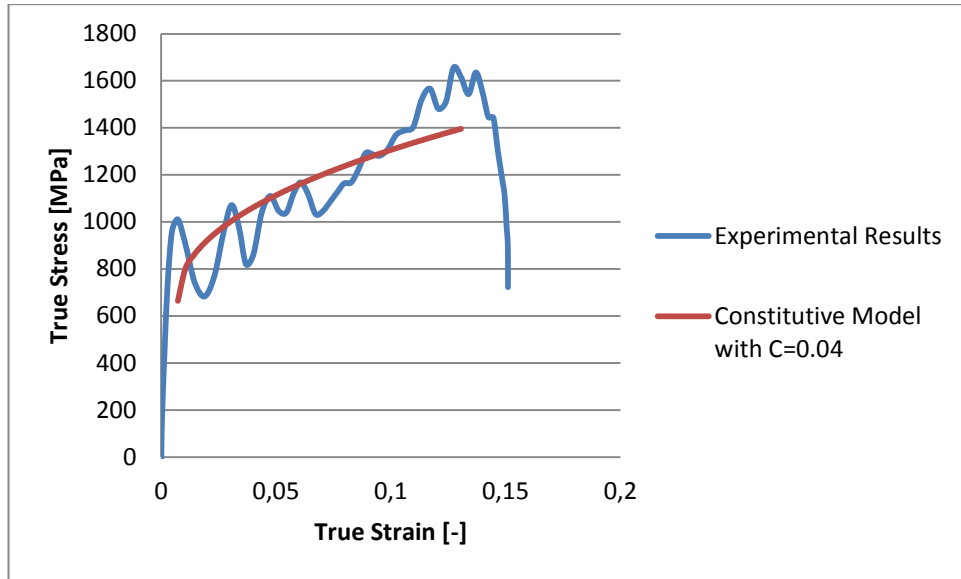Finally, the strain rate coefficient parameter (C) changes between the range 0.06 and 0.08 with respect to strain rate. Johnson-Cook fit with $c = 0.08$ can be seen in Figure 4.47 for $3000\,s^{-1}$.
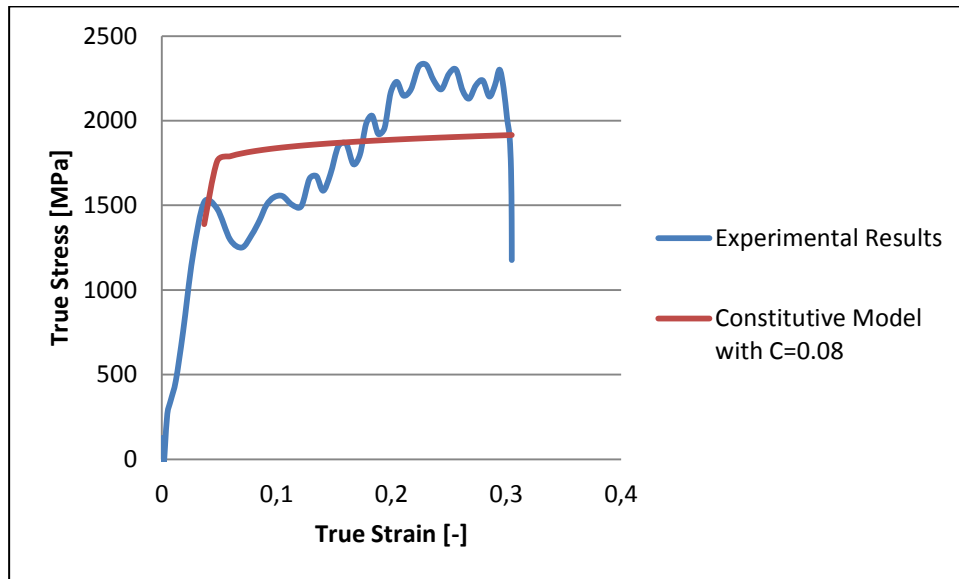
Figure 4.48 : Constitutive fit with C=0.08.

The constitutive model does not provide a good fit to experimental results. The strain hardening parameters may be reason of these results. In order to clarify this explanation, a different model with $B = 1647 MPa$ and $n = 0.49$ is tried to fit data points as given in Figure 4.48.
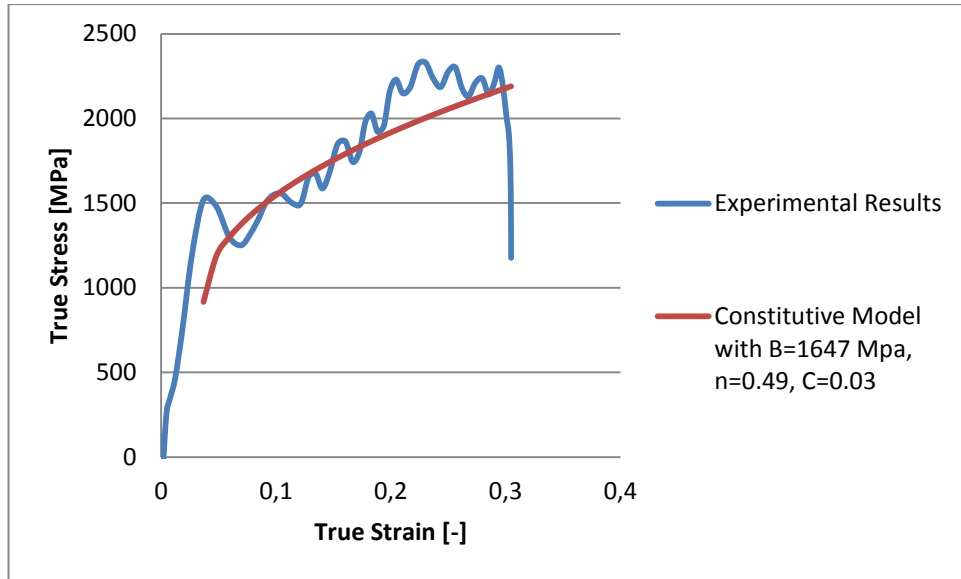
Figure 4.49 : Constitutive fit with different parameters for AISI 1045.

It can be seen that better fit is obtained with parameters shown in Figure 4.48. All of these curve fits with different parameters are given in Appendix C. Furthermore, the strain rate coefficient (C) is taken as 0.08, an average of calculated values between 0.06 and 0.11, and Johnson-Cook parameters for AISI 1045 is given as,

Table 4.6 : Johnson-Cook parameters for AISI 1045.

Material	A [MPa]	B [MPa]	n	C	m
AISI 1045	625	274	0.11	0.08	0.69

4.3.3 AISI 4140 results for high strain rate results

The fourteen successive tests were performed to determine the strain rate coefficient (C) at high strain rates for different length-diameter ratio as given in Table 4.7.

Table 4.7 : Specimen dimensions and pressure for AISI 4140.

L [mm]	D [mm]	Pressure [Bar]	Number of Tests
12	9	3	2
12	9	4	3
9	9	3	2
9	9	4	2
9	9	6	3

The strain rates, strain and stress recordings with respect to time for Test 1 can be shown in below figures.
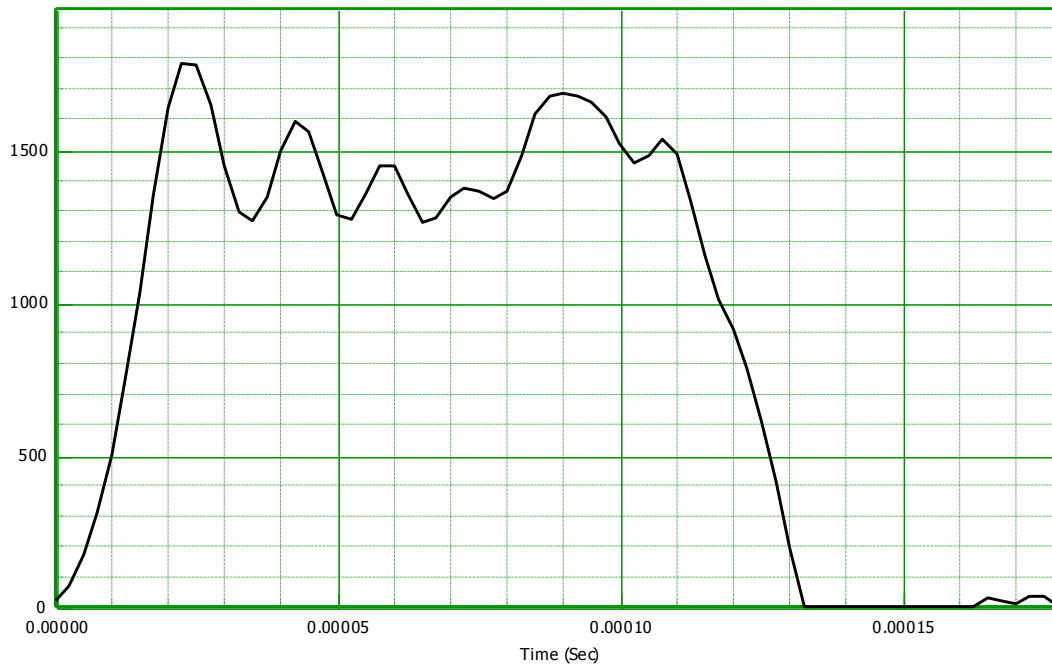
Figure 4.50 : Strain rate – time curve of test1 for AISI 4140.
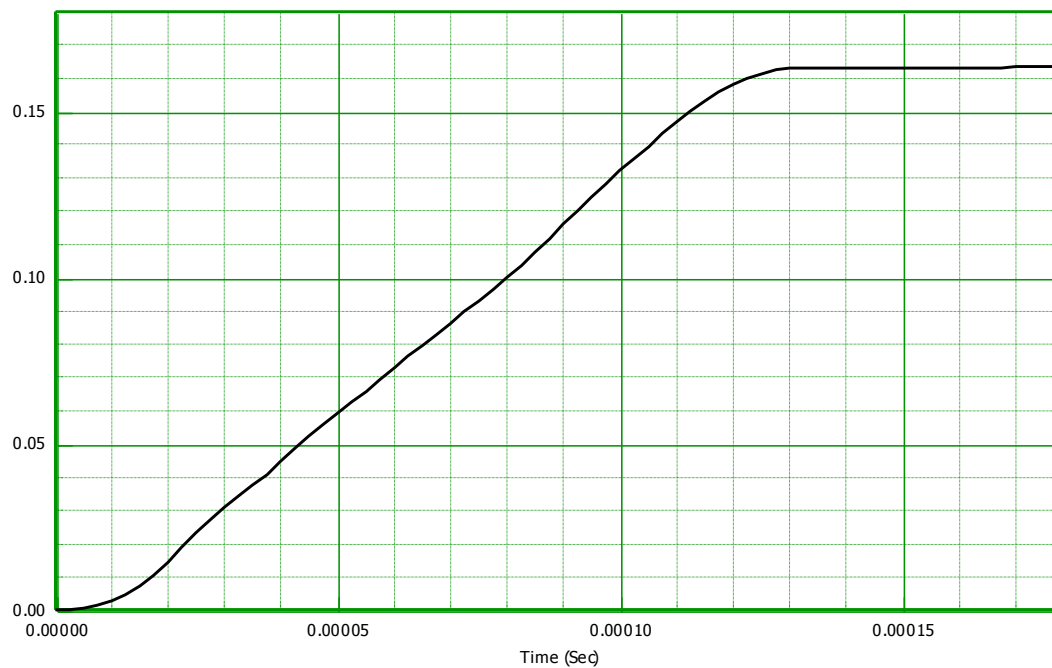
Figure 4.51 : Strain–time curve of test1 for AISI 4140.
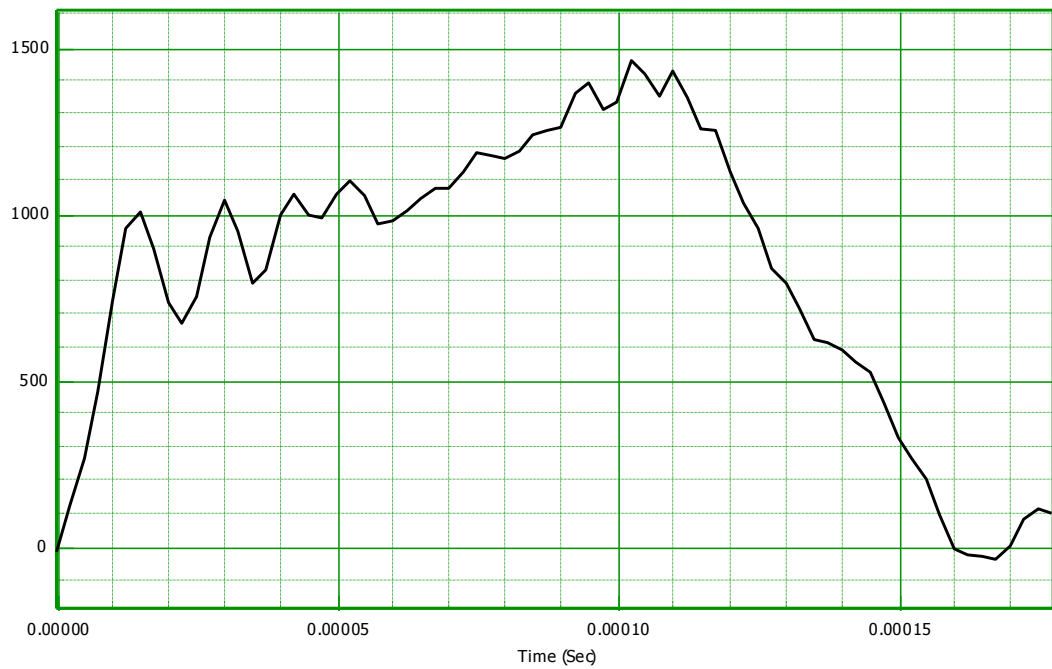
Figure 4.52 : Engineering stress-time curve of test 1 for AISI 4140.

Figure 4.53 : True stress-time curve of test 1 for AISI 4140.

It can be seen that the average strain rate can be found as approximately 1500 s^{-1} from Figure 4.49. Engineering strain and stress data with respect to time are also presented in Figure 4.50 and 4.51. Finally, true stress–true strain curve can be obtained as presented in Figure 4.52. The strain rate effect on stress response is depicted as in Figure 4.53.
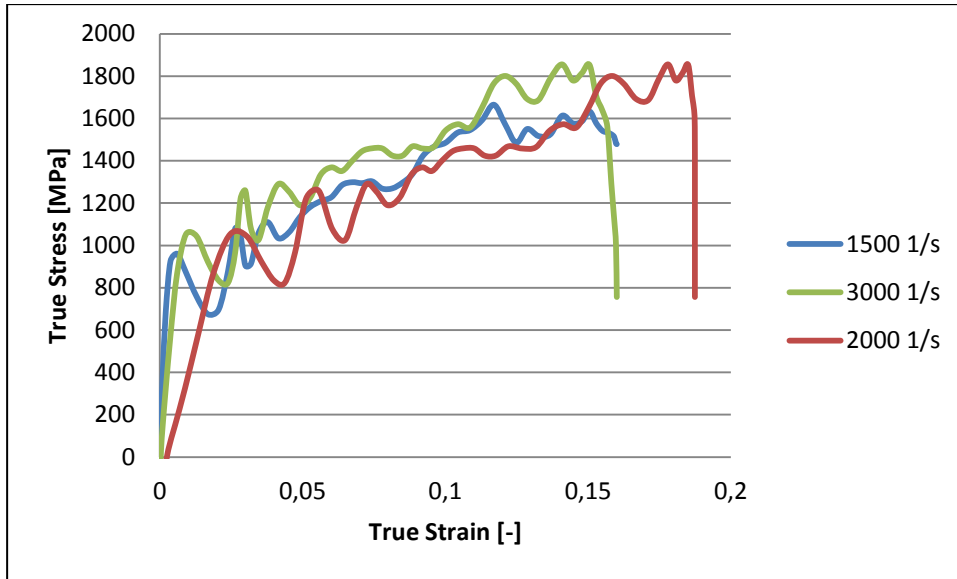
Figure 4.54 : True Stress vs. True Strain for AISI 1040 at strain rates of $1500\,s^{-1}$, $2000\,s^{-1}$ and $3000\,s^{-1}$ **.**

From Figure 4.53, it can be understood that stress values increases with respect to strain rate increase. Finally, the constitutive model fit to experimental data is obtained as Figure 4.54.
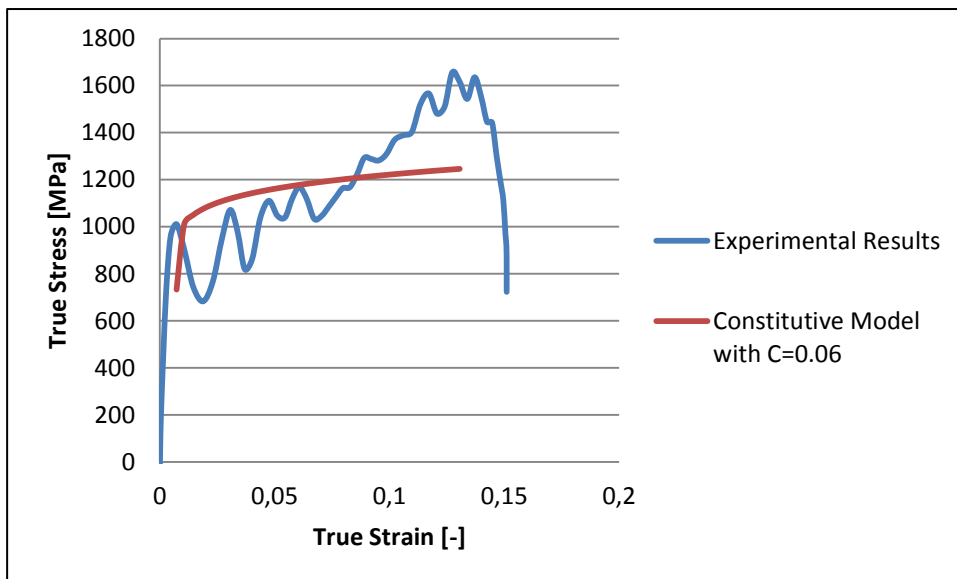
Figure 4.55 : Constitutive fit with C=0.06.

From Figure 4.54, it can be said that the constitutive model does not approximate to experimental data points. For obtaining better constitutive fit, the parameters related with strain hardening parameters B and n are chosen as 1142 MPa and 0.46 respectively. The constitutive fit with these parameters is given as;

Figure 4.56 : Constitutive fit with different parameters for AISI 4140.

It can be seen that better fit is obtained with parameters shown in Figure 4.55. Furthermore, the strain rate coefficient (C) is taken as 0.07, an average of calculated values between 0.06 and 0.08, and Johnson-Cook parameters for AISI 4140 is given as,

Table 4.8 : Johnson-Cook parameters for AISI 4140.

Material	A [MPa]	B [MPa]	n	C	m
AISI 4140	395	395	0.17	0.07	1.0

Finally, Johnson-Cook constitutive model parameters for all materials in this study are tabuleted as;

Table 4.9 : Johnson-Cook constitutive model parameters for all materials.

Material	A [MPa]	B [MPa]	n	C	m
AISI 1040	375	383	0.23	0.07	0.99
AISI 1045	625	274	0.11	0.08	0.69
AISI 4140	395	395	0.17	0.07	1.0

In this thesis, another parameter set for obtaining better fitting is used. The second parameter set for Johnson-Cook constitutive model is given as;

Table 4.10 : Johnson-Cook constitutive model parameters for all materials for a better fit.

Material	A [MPa]	B [MPa]	n	C	m
AISI 1040	375	765	0.48	0.07	0.99
AISI 1045	625	1647	0.49	0.03	0.69
AISI 4140	395	1142	0.46	0.05	1.0

5. CONCLUSIONS AND RECOMMENDATIONS

In the present study, Johnson–Cook strength model parameters of three materials were determined. For this purpose, the material behavior in elastic and plastic regime is introduced initially. Moreover, experimental methods for material characterization are detailed explained. The Johnson–Cook parameters were determined through quasi–static ($10^{-3}s^{-1}$) and quasi–static tests with higher temperatures at $80°C$ and $260°C$ are performed. In addition to this, high strain rate tests were performed by using compression SHPB apparatus. The following results are obtained based on experiments.

1. The hardening behaviors are obtained for AISI 1040 steels correctly but the results found AISI 1045 and AISI 4140 specimens are suspicious. The heat treatment and cold–drawn processes were possibly applied to this material and they do not show necking behavior.

2. High temperature quasi–static tests depict that flow stress decreases with temperature increase. It can be said that the use of extensiometer of high temperature are crucial for determining thermal softening parameter m.

3. The flow stresses of all tested materials were found to increase with strain rate increasing. This depicts that all of materials are strain rate sensitive.

4. The determined Johnson–Cook parameters for AISI 1040 is consistent with literature. However, the other materials parameters are different. The brittleness of these materials may be a reason of this result. The cold drawing and heat treatment processes also effects the yield strength and hardening behavior significantly.

5. Two different parameter sets were obtained. One of them shows necking behavior in true stress-true strain curve but it does not

provide a good fit for experimental tests. Vice versa, the second parameter set does not show necking behavior in true stress-true strain curve but it provides a good fit for experimental tests. This is a questionable issue that what data set should be chosen. Therefore, the results for two sets were given in Appendix part.

In conclusion, the constitutive model proposed by Johnson–Cook does not allow an easy parameters determination. In order to obtain tese parameters correctly, both of tension and compression quasi–static tests are needed. It is also recommended that performing high temperature tests incorpareted with high strain rates in order to obtain correct stress values. Finally, for the determination of constitutive model parameters a lot of tests should be performed for commenting results statistically.

REFERENCES

[1] **Reichert, B.** (2010). Cost − Benefit Conflict in Material Modeling. (faurecia)

[2] **Elgün, H.** (2009). Development of a reliability assessment method for brake caliper under application of specific conditions. MS Thesis; University of Stuttgart

[3] **Runesson, K.** (2005). CONSTITUTIVE MODELING OF ENGINEERING MATERIALS, The Primer. Lecture Notes; University of Goteborg

[4] **Johnson, G.R., Cook, W.H.** (1983), A constitutive model and data for metals subjected to large strains, high temperatures. In Proceedings of the seventh International Symposiumon Ballistic; The Netherlands, The Hague, pp. 541-547

[5] **Zerilli, F.J and Armstrong, R.W. (**1987), Dislocation − Mechanics Based Constitutive Relations a for Material Dynamics Calculation, Journal of Applied Physics, Vol. 61

[6] **Johnson, G.R., Holmquist, T.J.** (1988), Evaluation of Cylinder Impact Data for Impact Data for Constitutive Model Constants, J. Appl. Phys., 64 (8).

[7] **Noble, J.P., Harding, J.** (1994), An evaluation of constitutive relations of high rate material behaviour using the tensile Hopkinson Bar. l de Physique IV (C8) 477- 482.

[8] **Dowling, A.R., Harding, J., Campbell, J.D.** (1970), The dynamic punching of metals. J. Inst. Met. 98, 217-224.

[9] **Demirkol, M.** (2001), Malzemelerin Mekanik Davranışı, Ders Notları.

[10] **Wilkins, M.L**. (1999), Computer Simulation of Dynamic Phenomena, Springer.

[11] **Hill, R.** (1950), The Mathematical Theory of Plasticity, Oxford Classical Texts in Physical Sciences.

[12] **Url-1** < http://geologyclass.org/Structures%20Concepts.html >, date retrieved 01.15.2013.

[13] **Ugural A.C, Fenster S.K.** (1994), Advanced Strength and Applied Elasticity, Prentice Hall PTR.

[14] **Url-2** < http://mscsoftware.com/training%MultiaxialFatigue.html >, date retrieved 01.15.2013.

[15] **Dieter C.E**. (1988), Mechanical Metallurgy, McGraw-Hill Book Company.

[16] **Dunne F., Petrinic N.** (2005), Introduction to Computational Plasticity, Oxford University Press.

[17] **Konokman H.E.** (2008), Development of Lagrangian Hydrocode for High Speed Impact Analysis and Its Experimental Verification, MS Thesis, Middle East Technical University.

[18] **Polyzois I.** (2010) , Finite Element Modeling of the Behavior of Armor Materials under High Strain Rates and Large Strains, MS Thesis, University of Manitoba.

[19] **Davis J.R.,** (2004), Tensile Testing Second Edition, Davis & Associates.

[20] **Udomphol T.** (2007), Tension Test Lecture Notes, Suranaree University of Technology.

[21] **Bulla M.** (2012), Radioss Materials Lecture Notes.

[22] **Chen W., Song B.** (2011), Split Hopkinson (Kolsky) Bar Design, Testing and Applications, Springer Science.

[23] **Kaiser M.A.** (1998), Advancements in the Split Hopkinson Bar, MS Thesis, Virginia Polytechnic Institute.

[24**] Kiranli E.** (2009), Determination of Material Constitutive Equation of a Biomedical Grade Ti6Al4V Alloy for Cross – Wedge Rolling, MS Thesis, Izmir Institute of Technology.

[25] **Tasneem N.** (2002), Study of Wave Shaping Techniques of Split Hopkinson Pressure Bar Using Finite Element Analysis, MS Thesis, Wichita State University.

[26] **Meyers M.A.** (1994), Dynamic Behavior of Materials, John Wiley & Sons Inc.

[27] **Lesuer D.** (2000), Experimental Investigation of Material Models for Ti - 6Al – 4V and 2024 – T3, FAA Report DOT/FAA/AR-00/25.

[28] **Liessem A., Knauf G., Zimmermann S.** (2007), Strain Based Design, What the Contribution of a Pipe Manufacture Can Be.

[29] **Jutras M.** (2008), Improvement of the Characterisation Method of the Johnson – Cook Model, MS Thesis, Quebec University.

APPENDICES

APPENDIX A: Quasi-Static Test Results
APPENDIX B: High Strain Rates Testing Results

APPENDIX A

Since various tests are performed, all of these tests cannot presented in previous chapters. In this part all quasi-static test results will be given for two different parameter sets for Johnson-Cook consititutive model.

APPENDIX A.1 Quasi-Static Test Results for Parameter Set 1

In Conclusion part, it was discussed that two parameter sets are used for curve fitting. The initial parameter set which was given in Table 4.9 was chosen so that the results shows necking behavior. The quasi-static test results by using this parameter set is given as below figures.
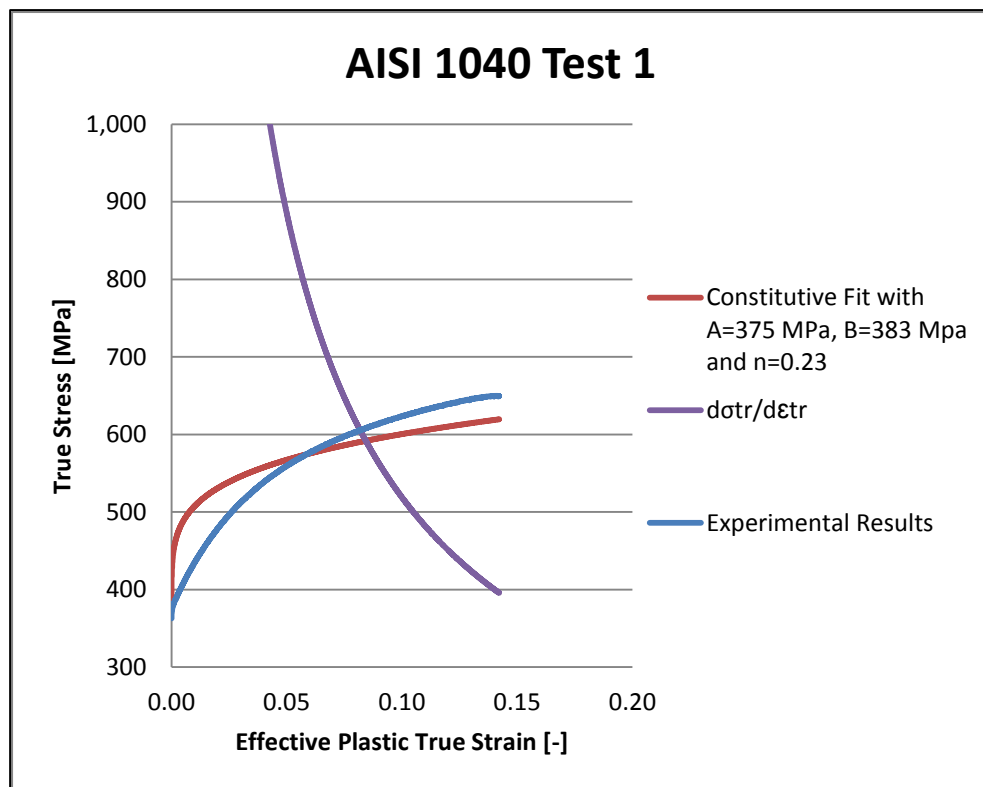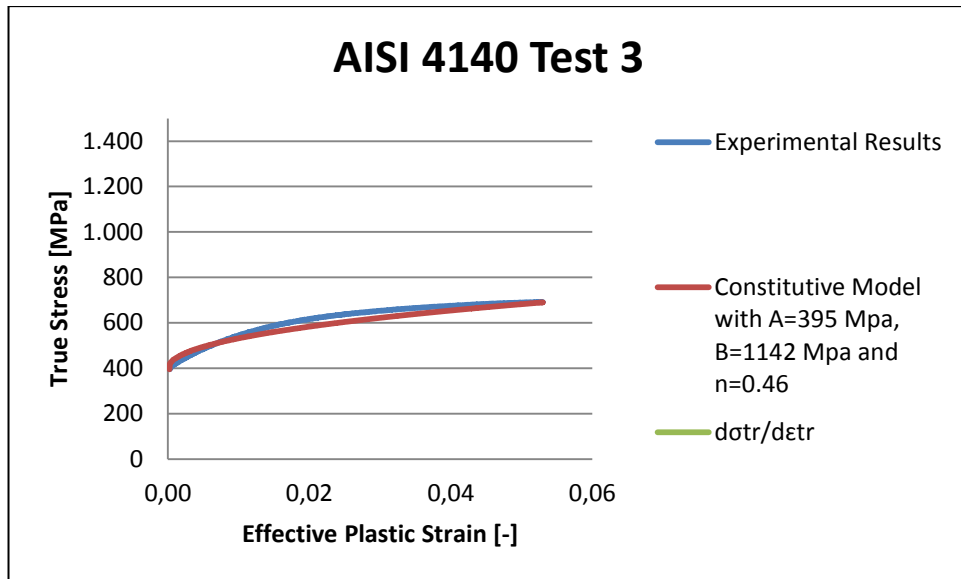

Figure A.1 : Constitutive fitting for AISI 1040 test 1.
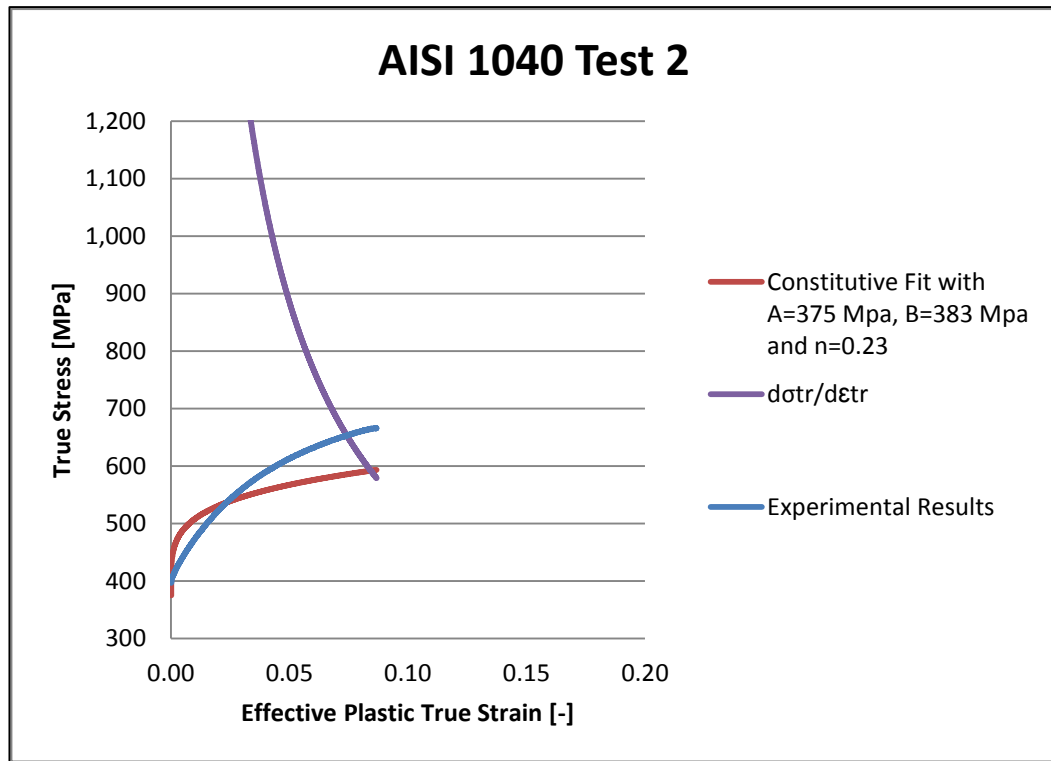
Figure A.2 : Constitutive fitting for AISI 1040 test 2.
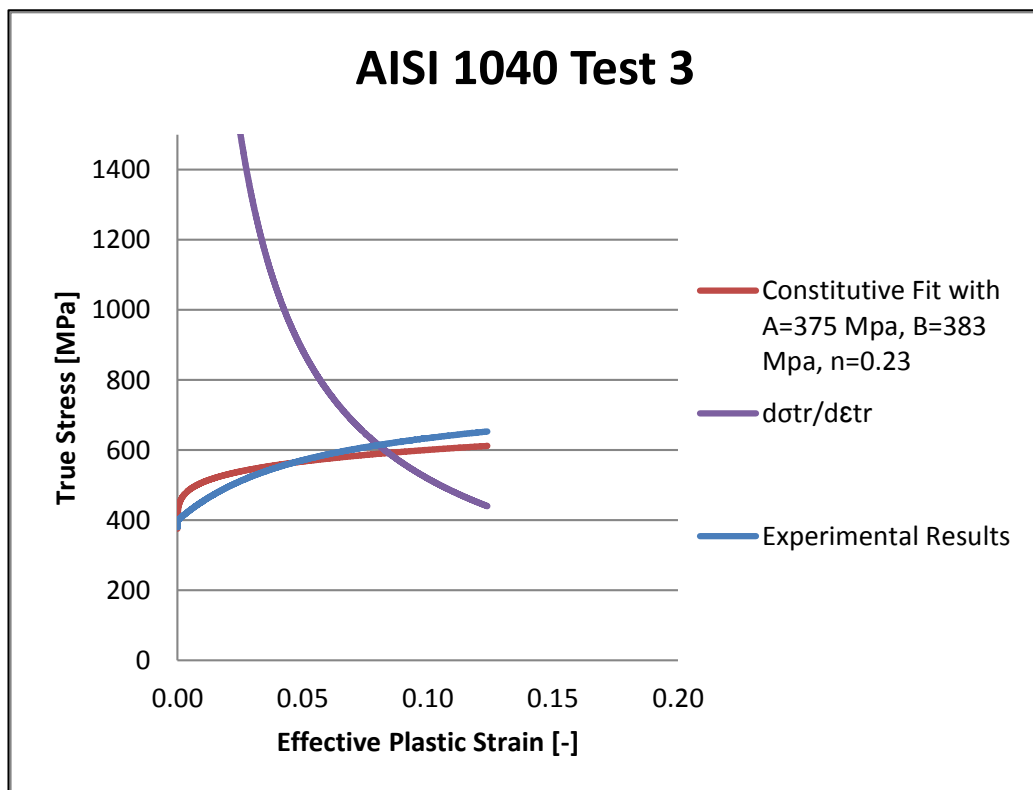
Figure A.3 : Constitutive fitting for AISI 1040 test 3.
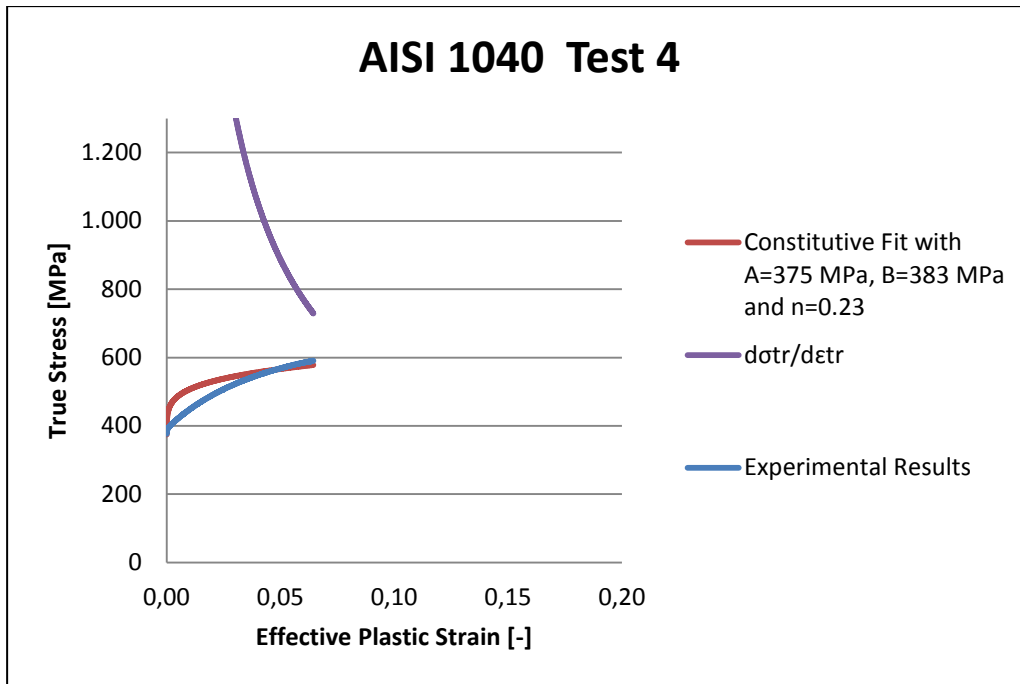
Figure A.4 : Constitutive fitting for AISI 1040 test 4.
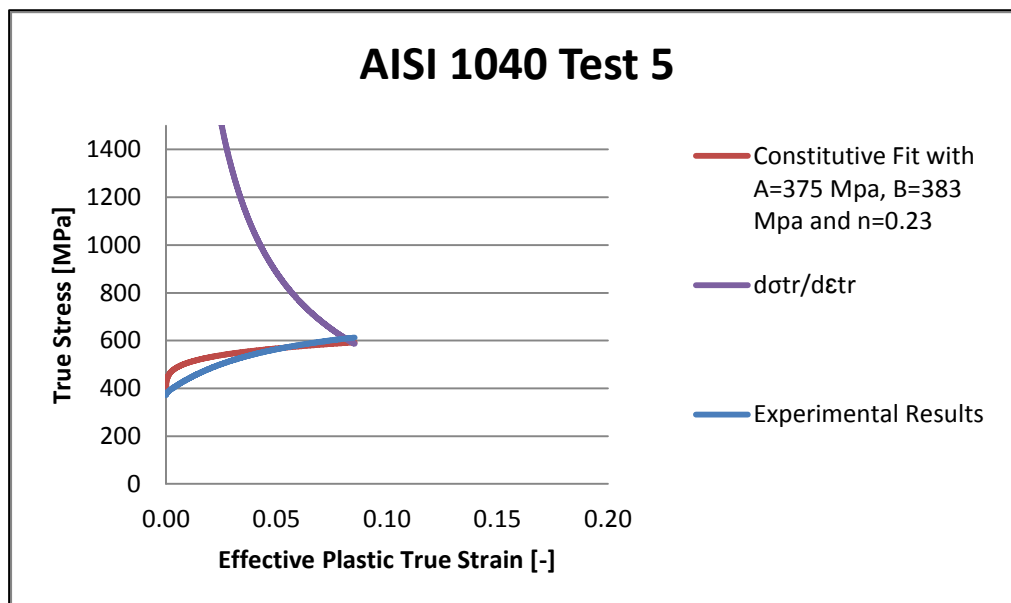
Figure A.5 : Constitutive fitting for AISI 1040 test 5.
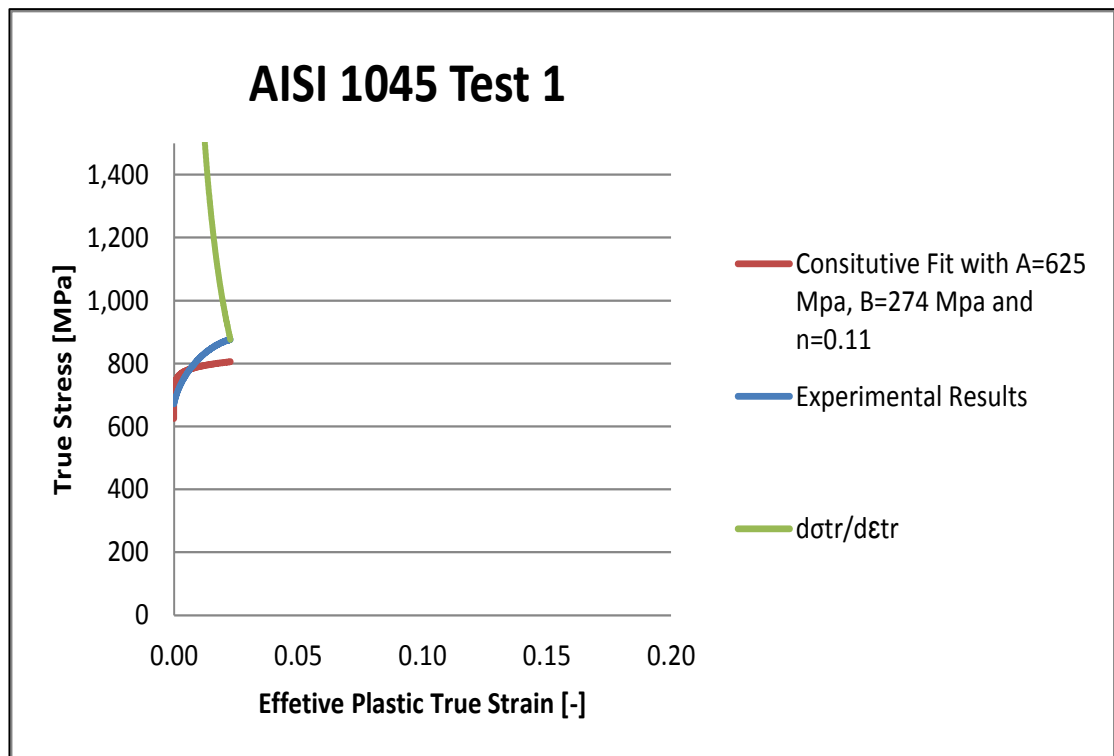
Figure A.6 : Constitutive fitting for AISI 1045 test 1.
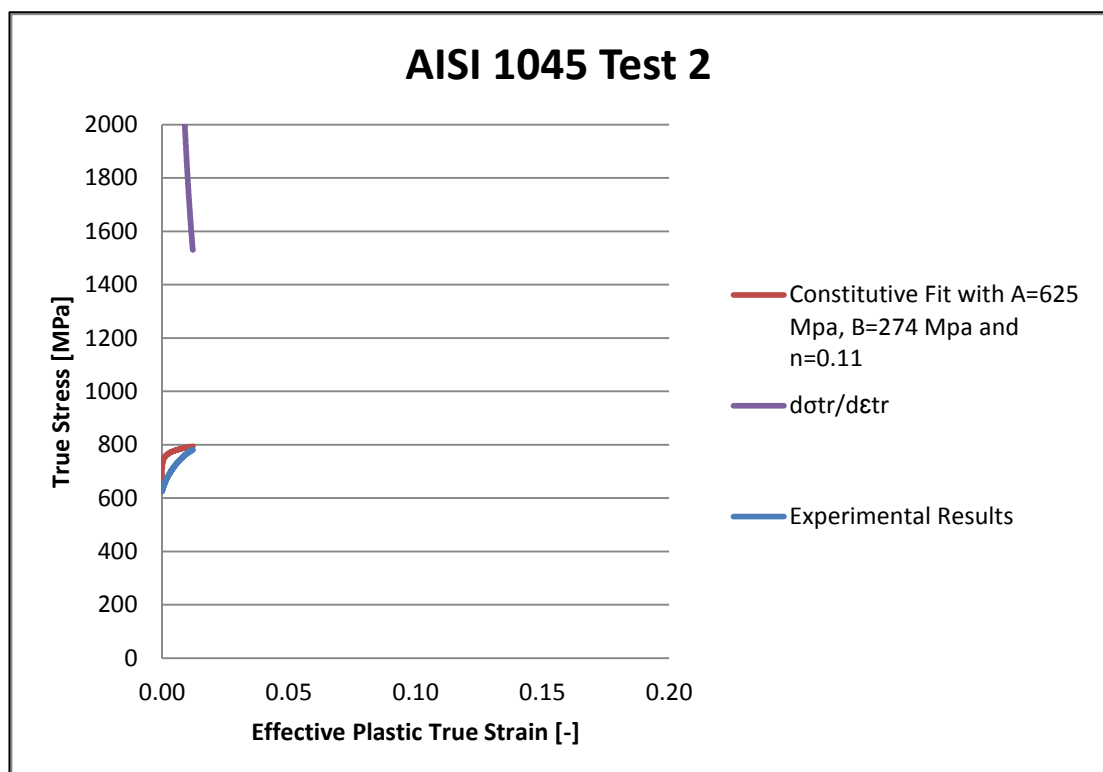
Figure A.7 : Constitutive fitting for AISI 1045 test 2.
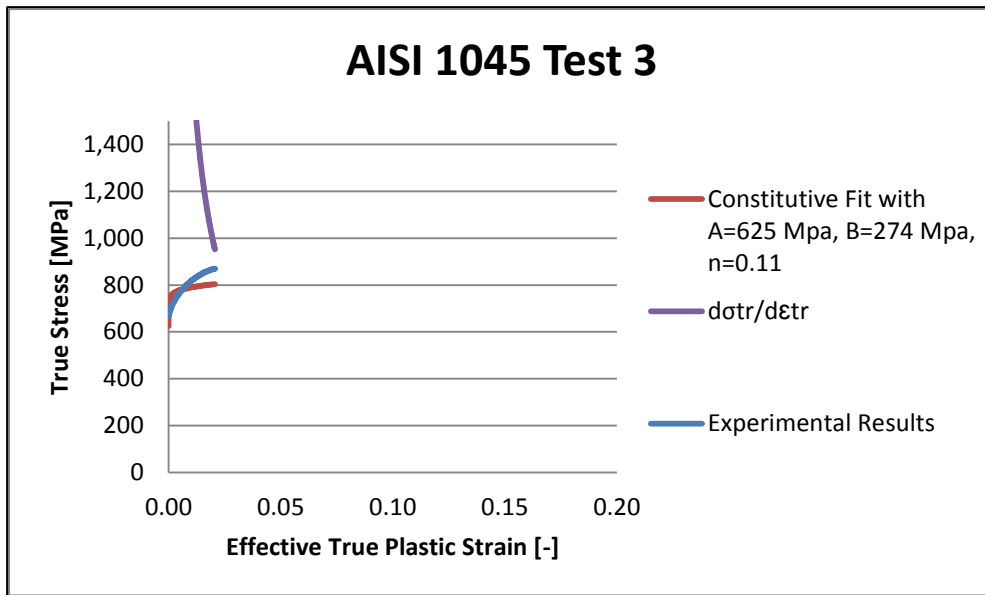
Figure A.8 : Constitutive fitting for AISI 1045 test 3.
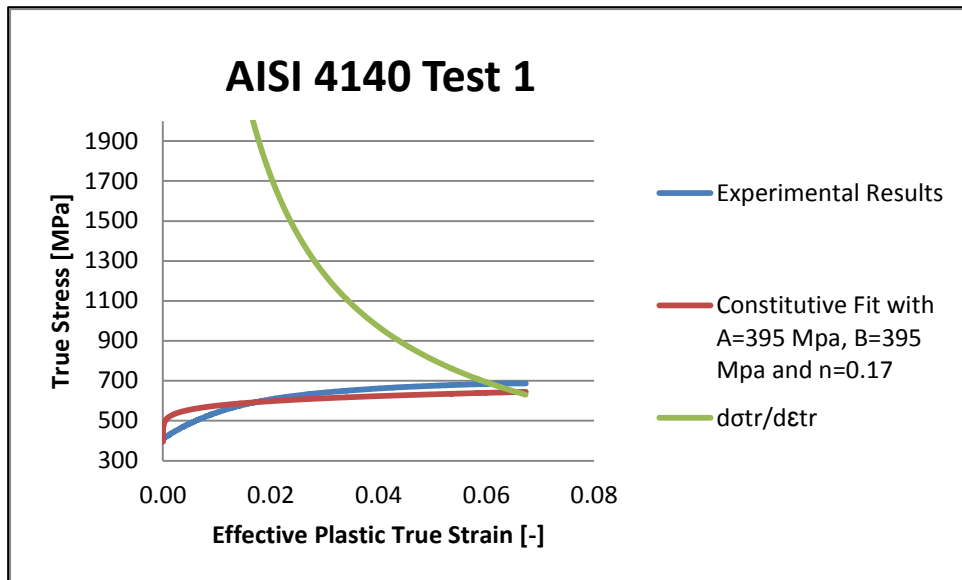
Figure A.9 : Constitutive fitting for AISI 4140 test 1.
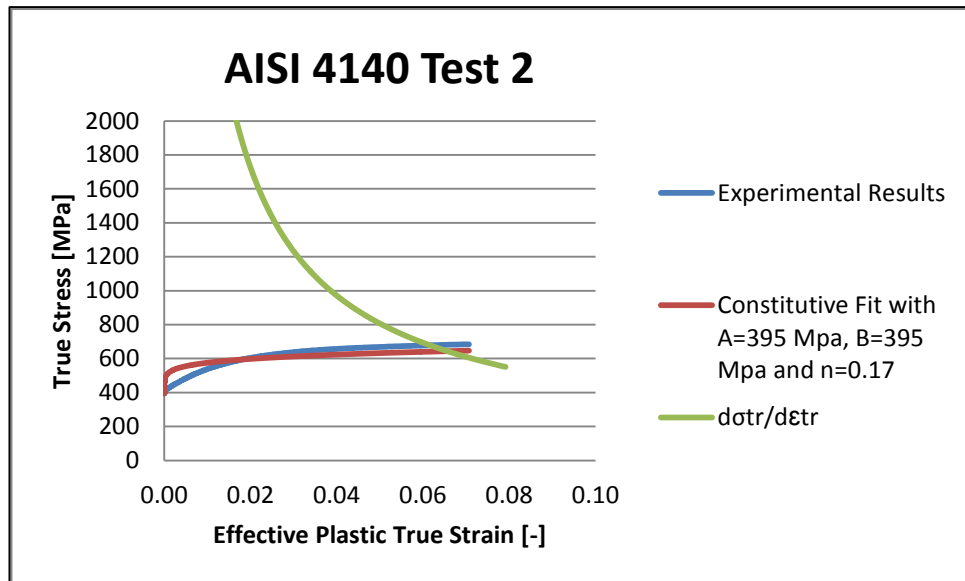
Figure A.10 : Constitutive fitting for AISI 4140 test 2.
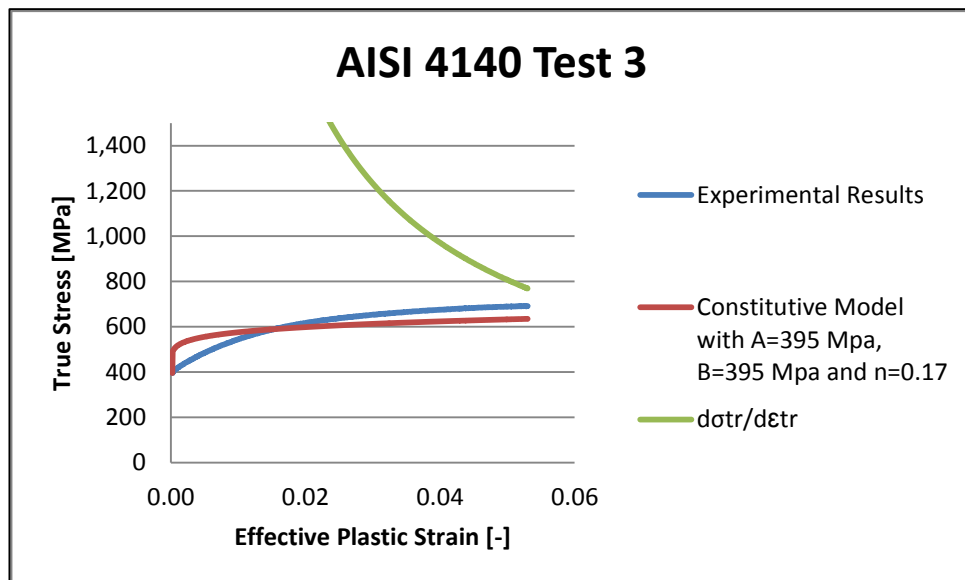
Figure A.11 : Constitutive fitting for AISI 4140 test 3.

APPENDIX A.2 Quasi-Static Test Results for Parameter Set 2

The second parameter set for Johnson-Cook constitutive model provides better fit to data points but it does not show necking behavior in true stress- true strain curves. The quasi-static test results by using this parameter set is given as below figures.
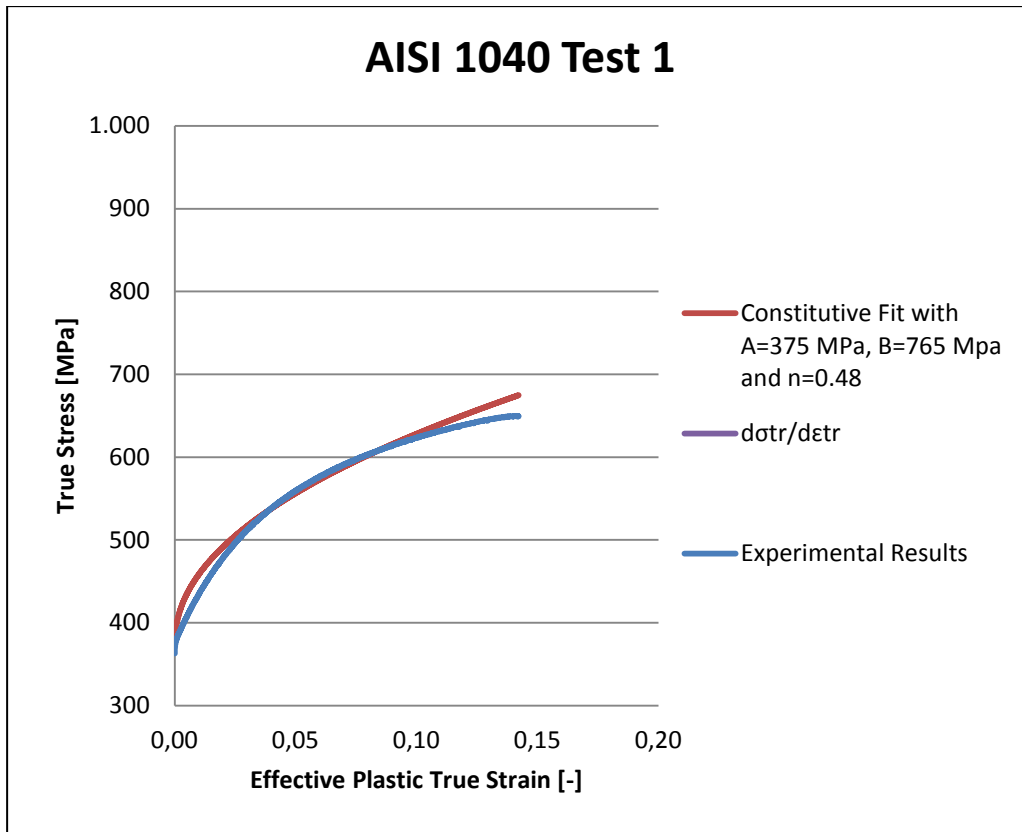
Figure A.12 : Constitutive fitting for AISI 1040 test 1 with parameter set 2.
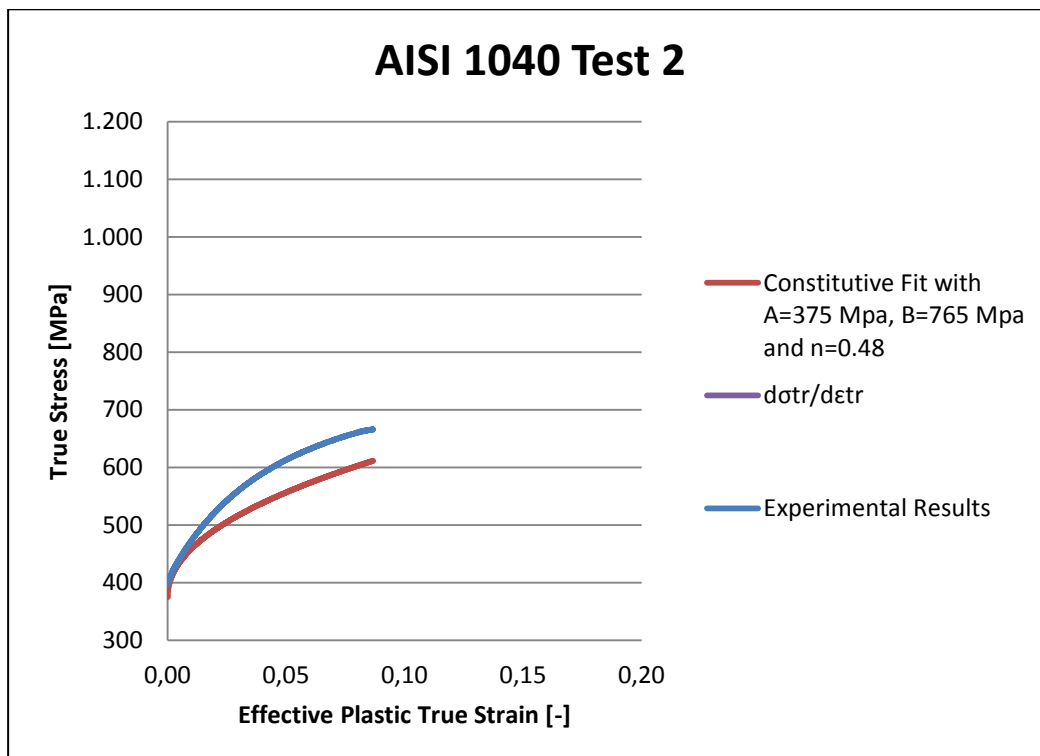
Figure A.13 : Constitutive fitting for AISI 1040 test 2 with parameter set 2.
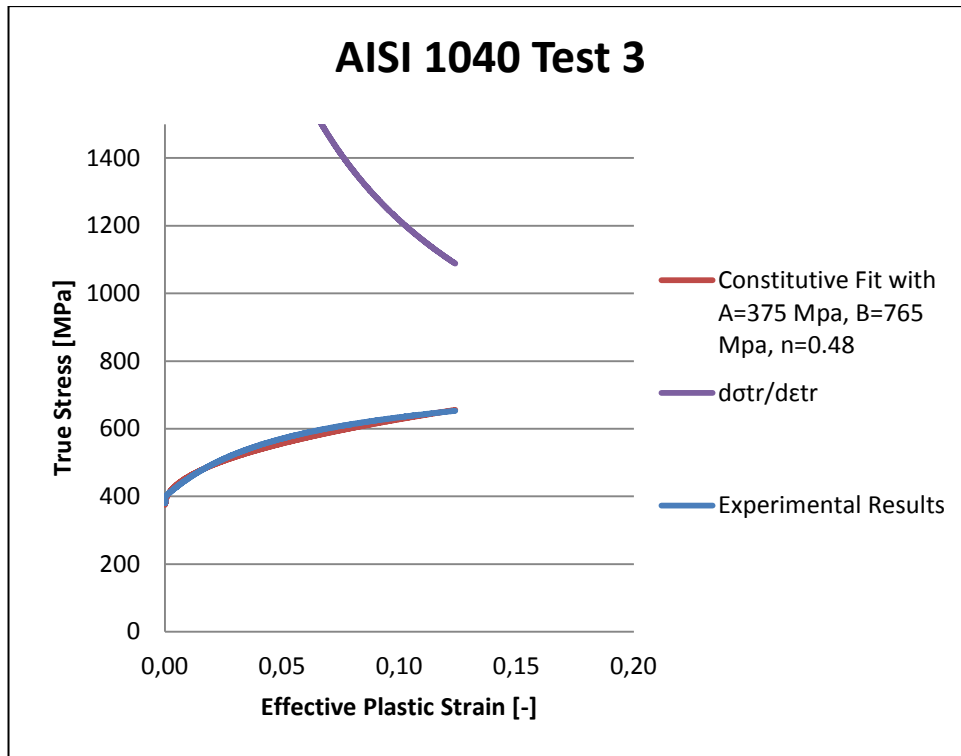
Figure A.14 : Constitutive fitting for AISI 1040 test 3 with parameter set 2.
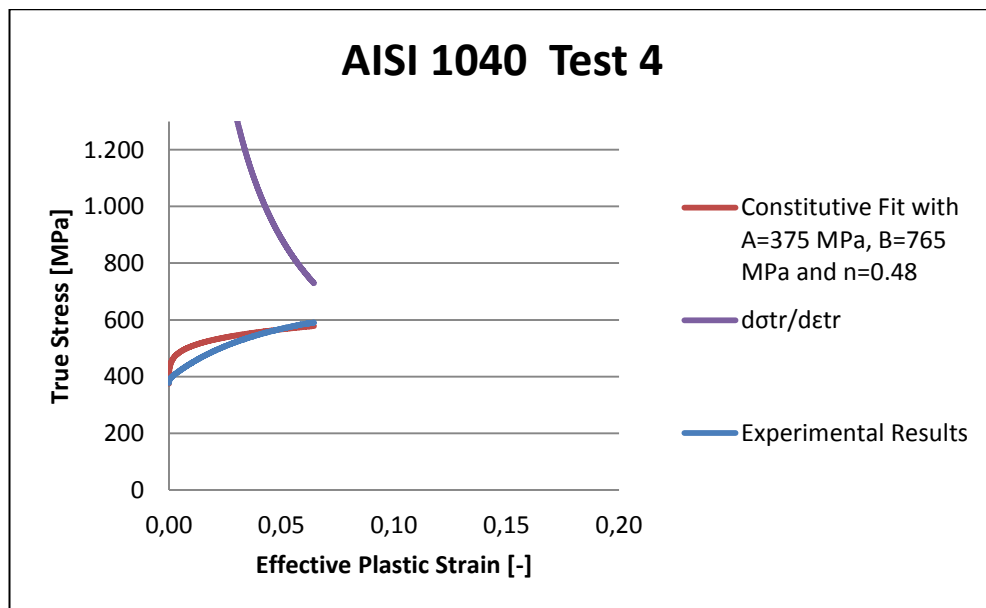
Figure A.15 : Constitutive fitting for AISI 1040 test 4 with parameter set 2.
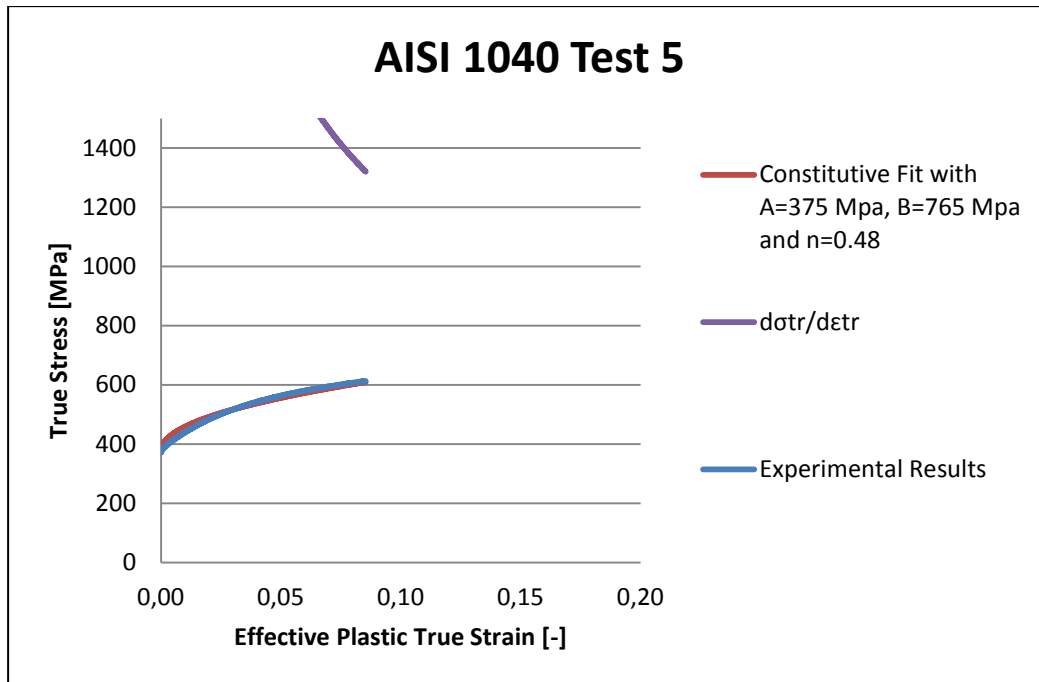
Figure A.16 : Constitutive fitting for AISI 1040 test 5 with parameter set 2.
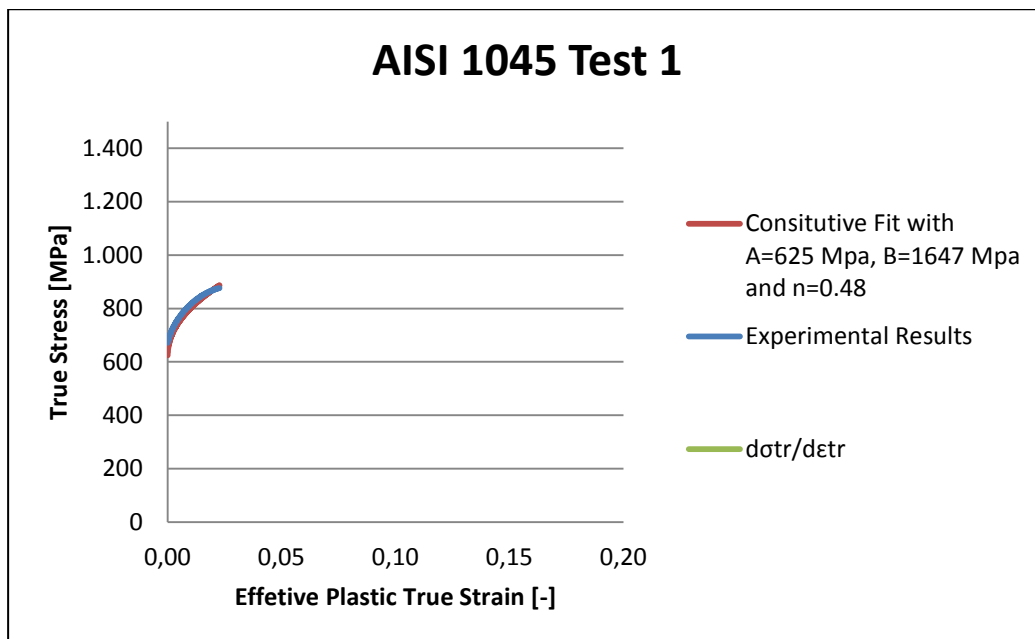
Figure A.17 : Constitutive fitting for AISI 1045 test 1 with parameter set 2.
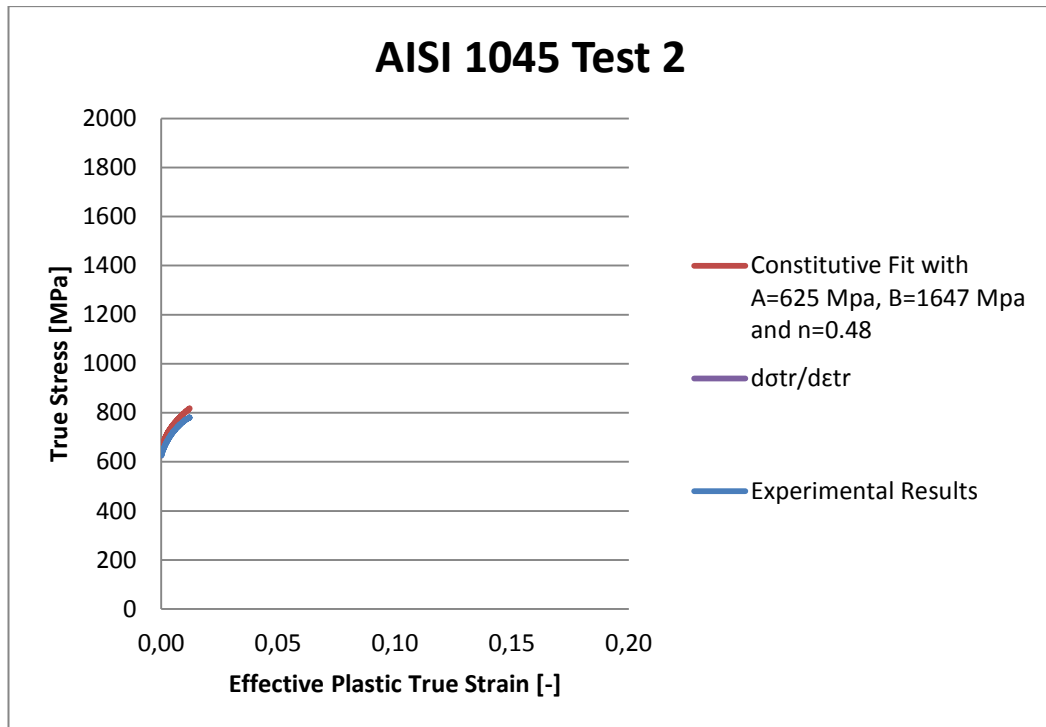
Figure A.18 : Constitutive fitting for AISI 1045 test 2 with parameter set 2.
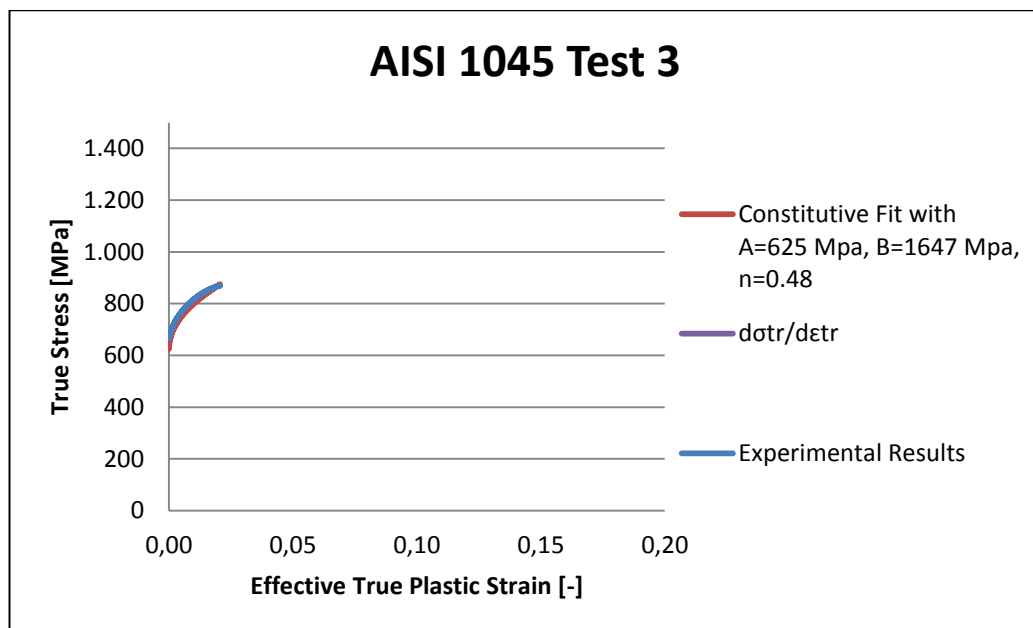
Figure A.19 : Constitutive fitting for AISI 1045 test 3 with parameter set 2.
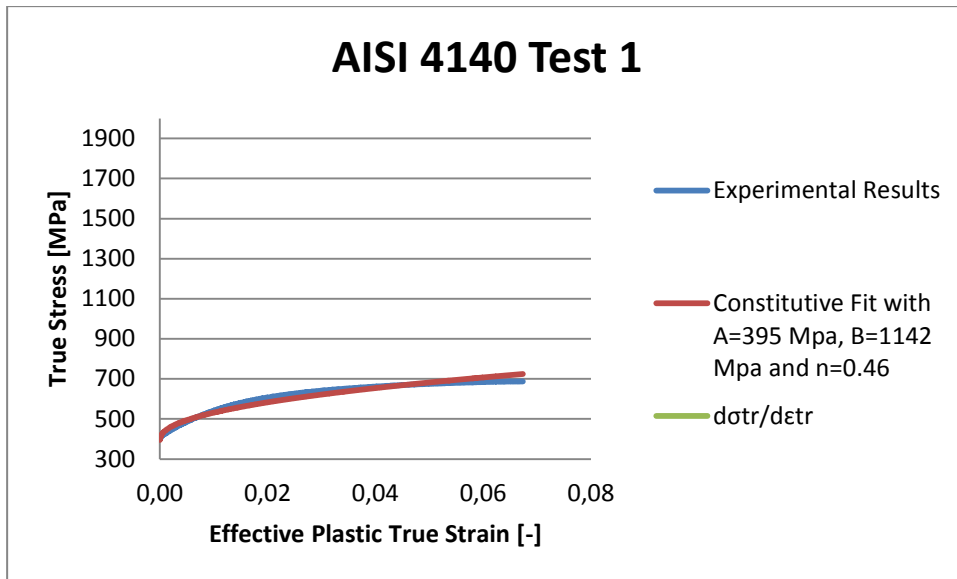
Figure A.20 : Constitutive fitting for AISI 4140 test 1 with parameter set 2.
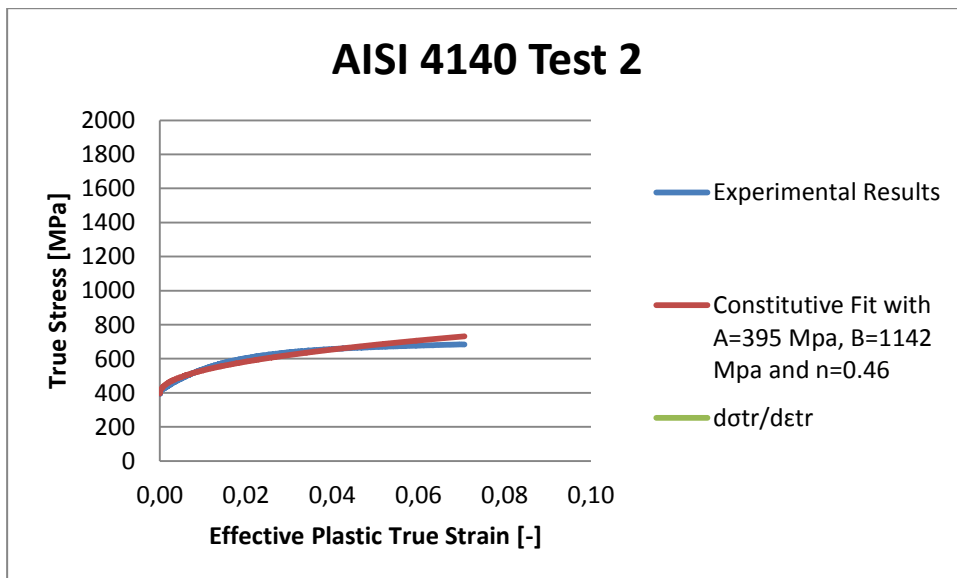
Figure A.21 : Constitutive fitting for AISI 4140 test 2 with parameter set 2.

Figure A.22 : Constitutive fitting for AISI 4140 test 3 with parameter set 2.

APPENDIX B

In this section, higher strain rate testing results were presented for two parameter sets. Since a large number of tests were performed for three materials, all of graphs were not given. Instead of this, test results were choosen for definite average strain rates such as $1500\,s^{-1}$, $2000\,s^{-1}$ and $3000\,s^{-1}$ and plotted for both parameter sets.

APPENDIX B.1 High Strain Rate Test Results for Parameter Set 1
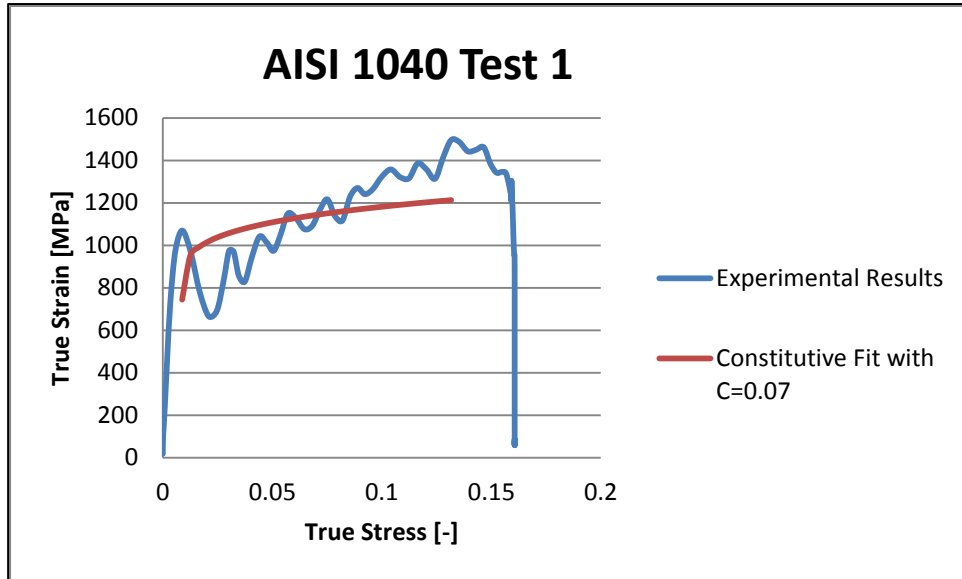
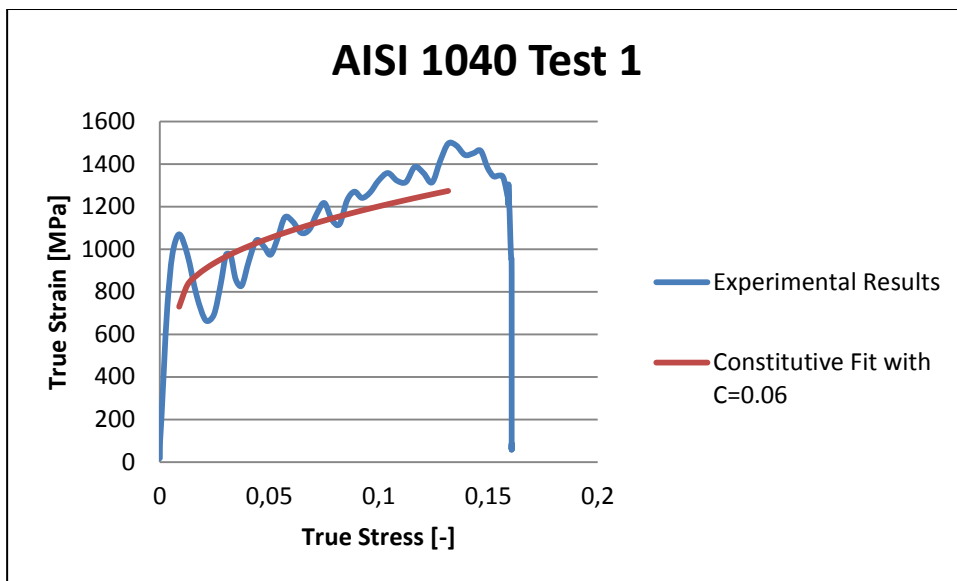**Figure B.1 :** Constitutive fit for AISI 1040 test 1 at strain rate of $1500\,s^{-1}$.
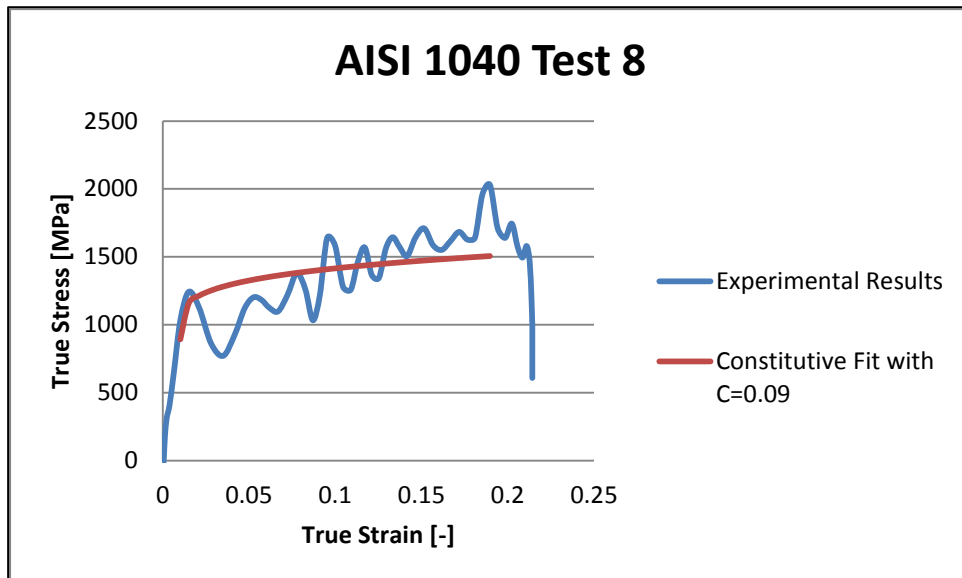
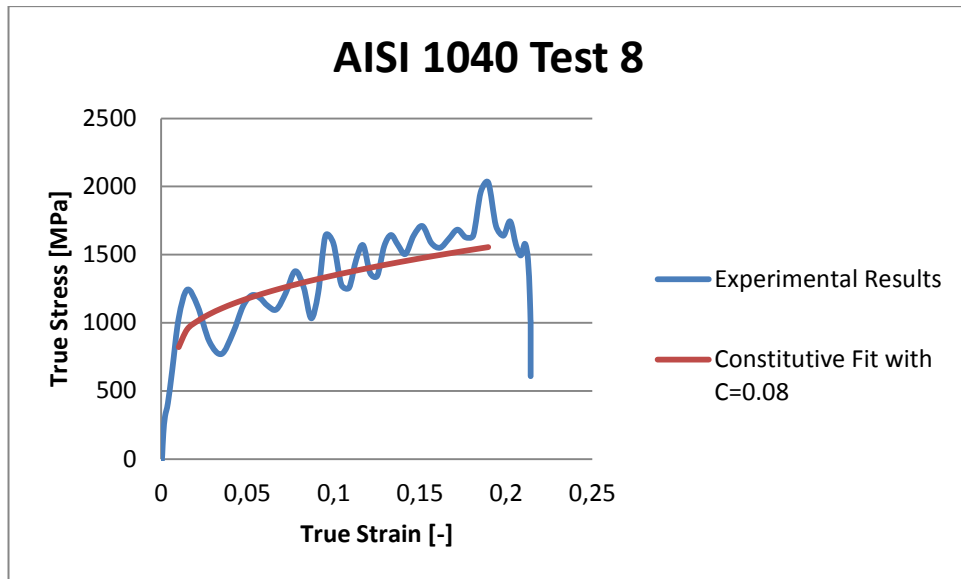**Figure B.2 :** Constitutive fit for AISI 1040 test 8 at strain rate of $2000\,s^{-1}$.
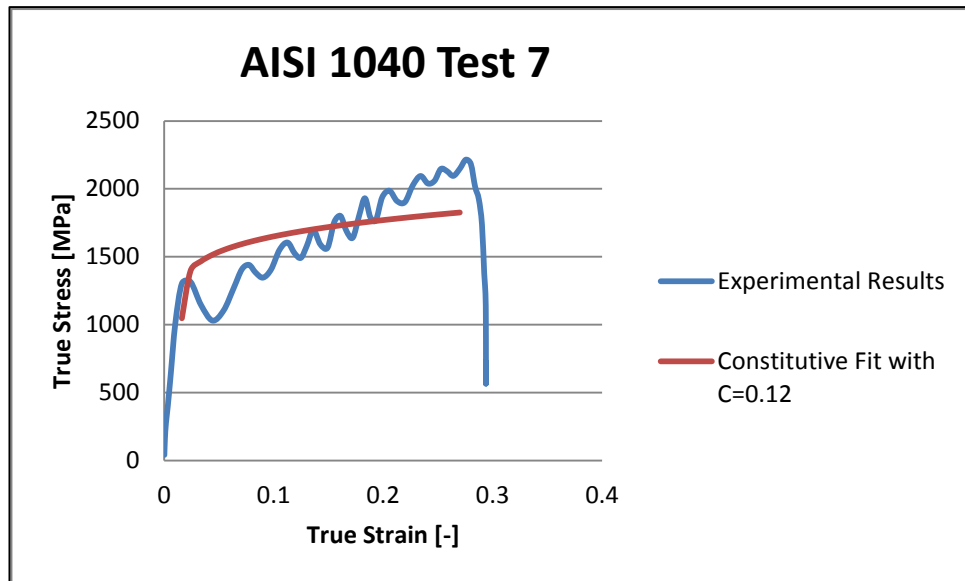
Figure B.3 : Constitutive fit for AISI 1040 test 7 at strain rate of $3000\,s^{-1}$.
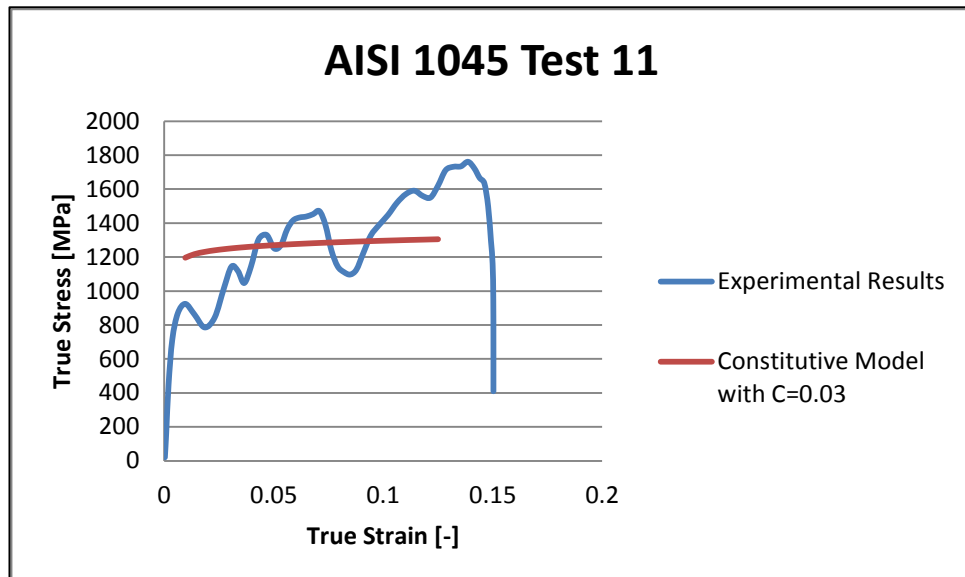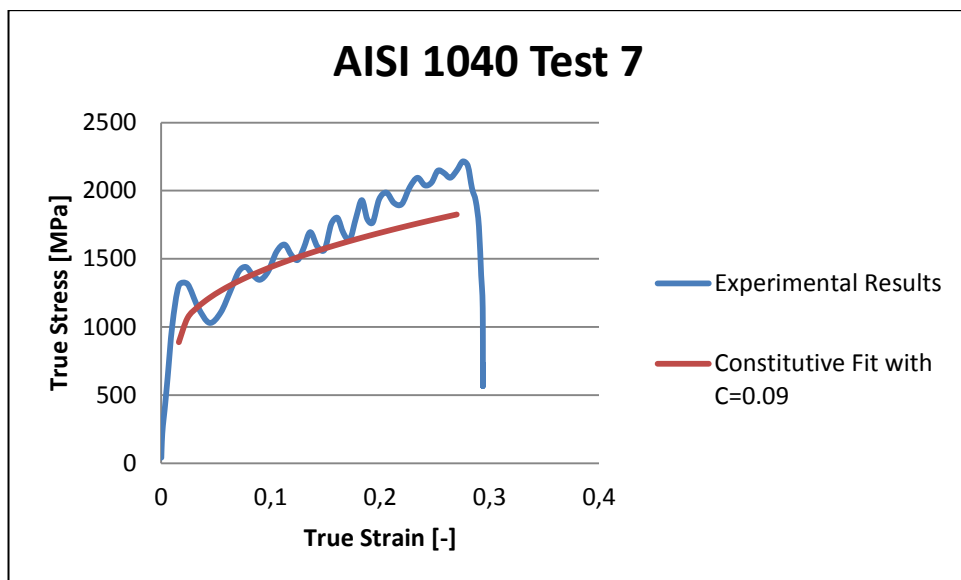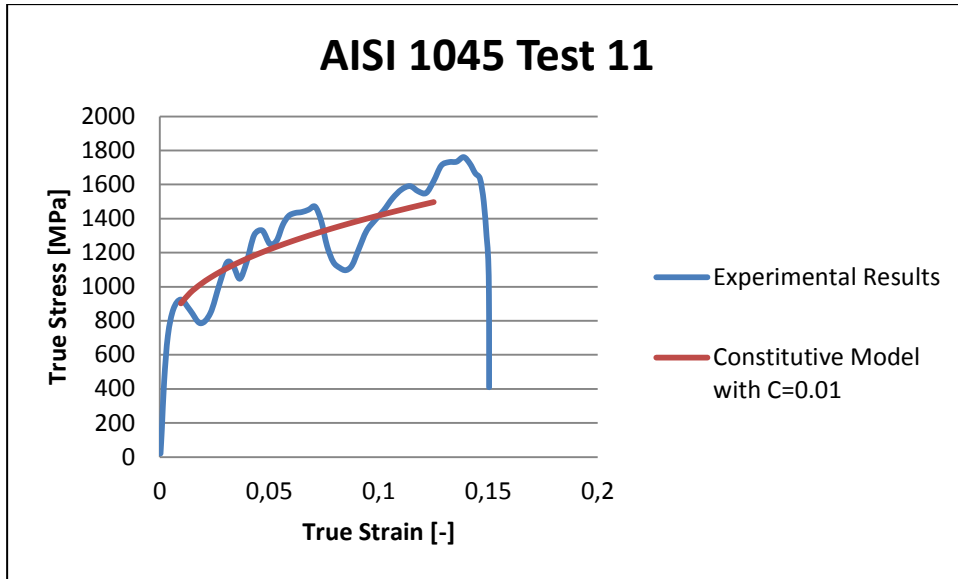

Figure B.4 : Constitutive fit for AISI 1045 test 11 at strain rate of $1500\,s^{-1}$.
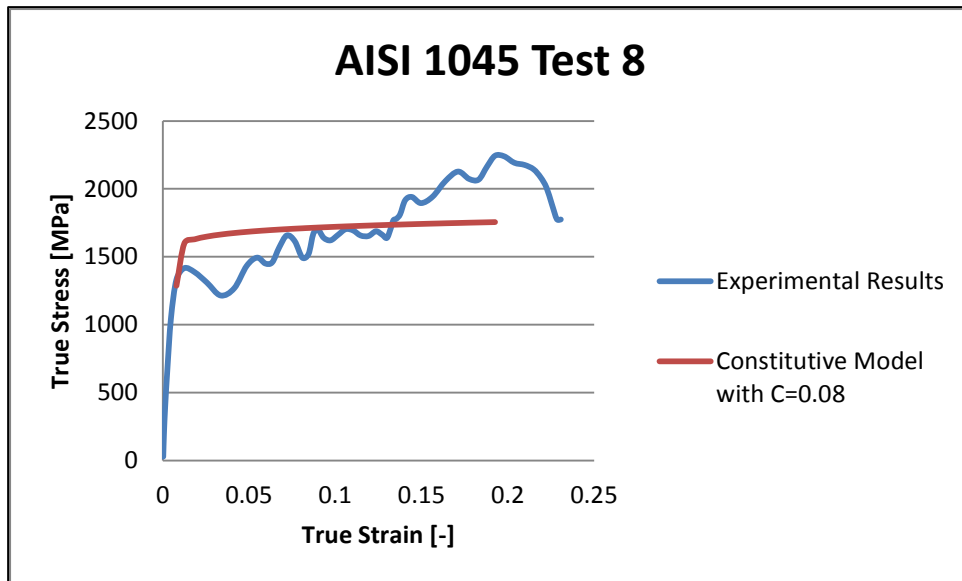
Figure B.5 : Constitutive fit for AISI 1045 test 8 at strain rate of $2000\,s^{-1}$.
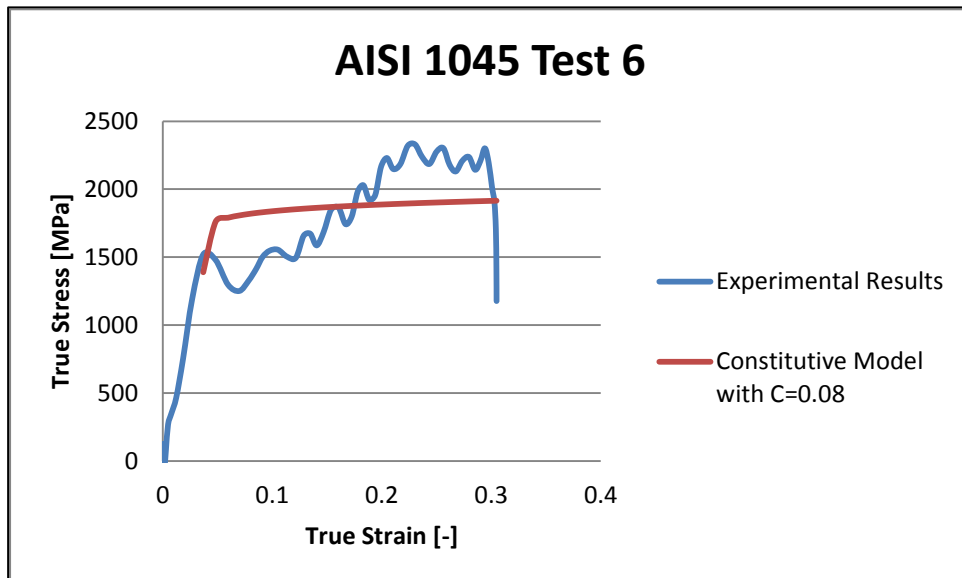
Figure B.6 : Constitutive fit for AISI 1045 test 6 at strain rate of $3000\,s^{-1}$.
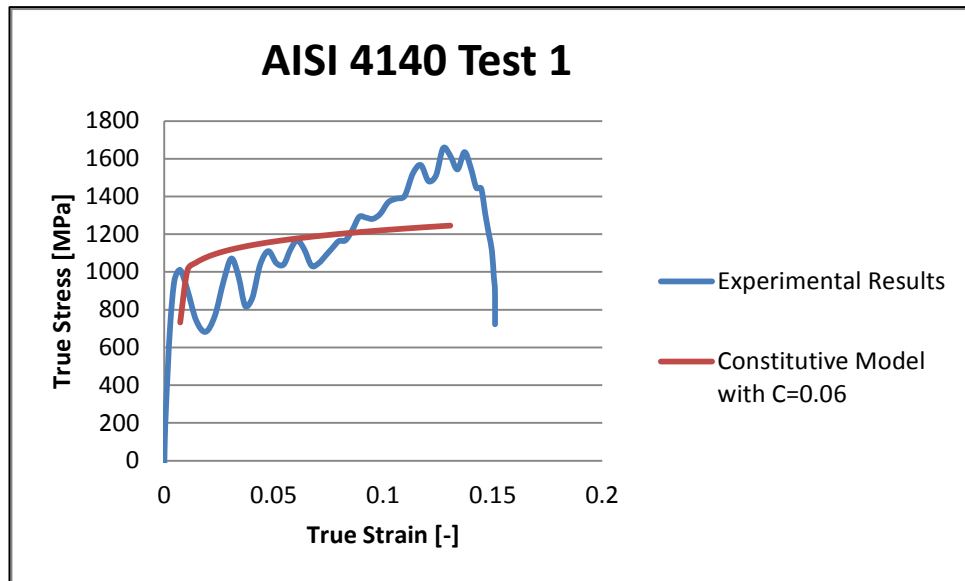
Figure B.7 : Constitutive fit for AISI 4140 test 1 at strain rate of $1500\,s^{-1}$.
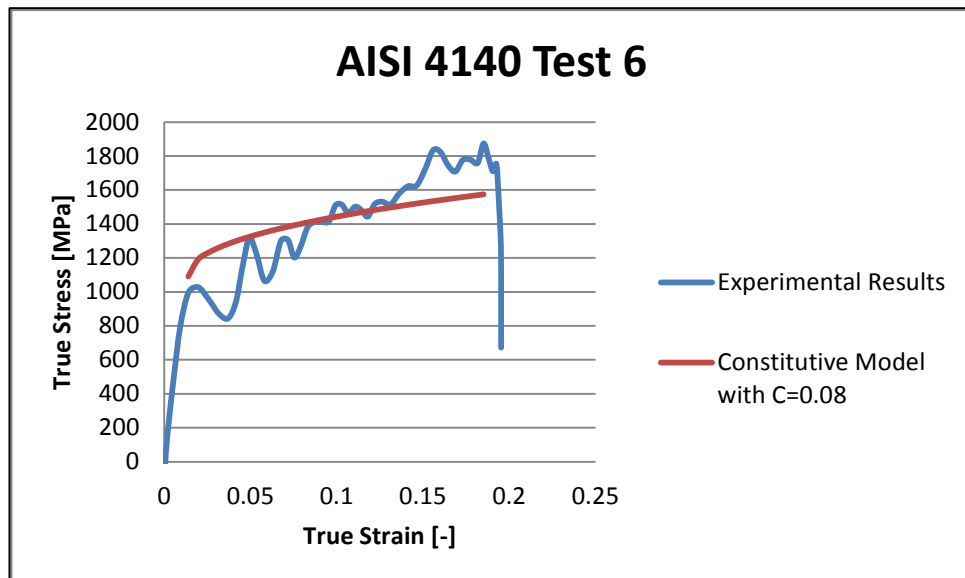
Figure B.8 : Constitutive fit for AISI 4140 test 6 at strain rate of $2000\,s^{-1}$.
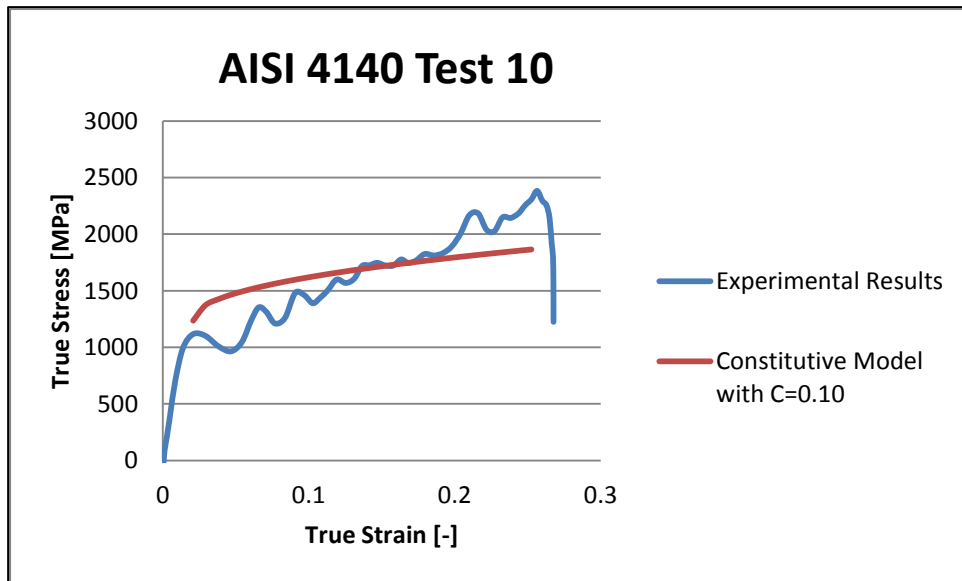
Figure B.9 : Constitutive fit for AISI 4140 test 10 at strain rate of $3000\,s^{-1}$.

APPENDIX B.2 High Strain Rate Test Results for Parameter Set 2

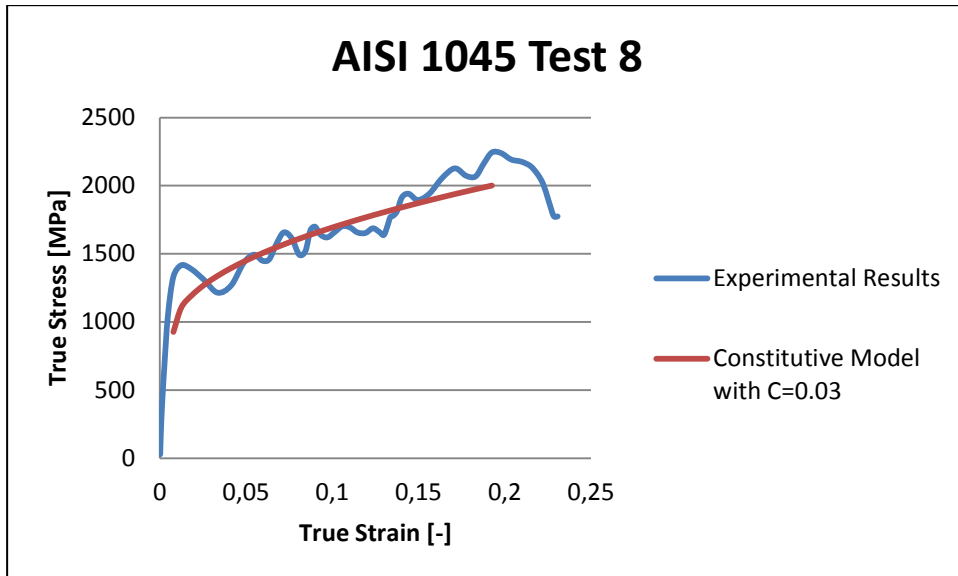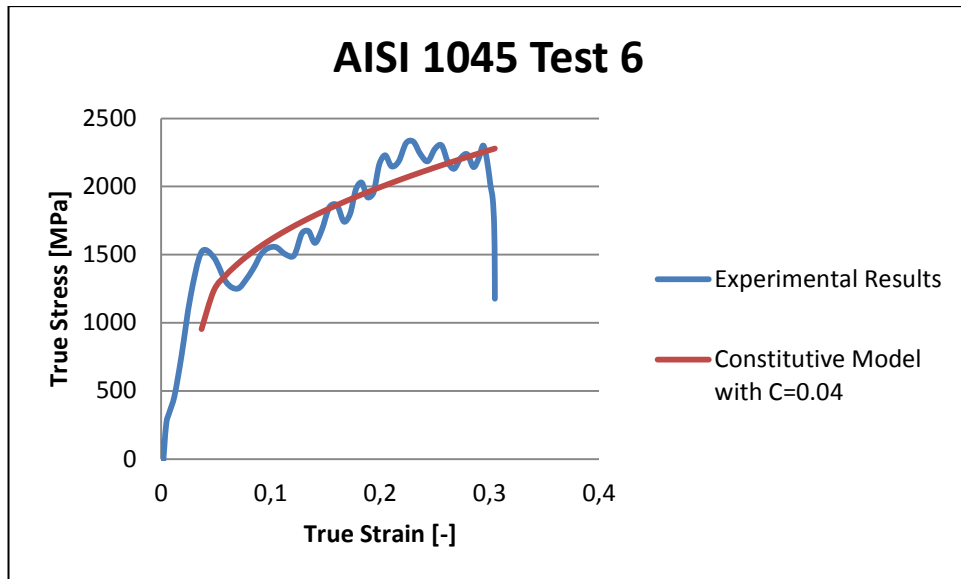**Figure B.10 :** Constitutive fit for AISI 1040 test 1 with parameter set 2 at strain rate of $1500\,s^{-1}$.

Figure B.11 : Constitutive fit for AISI 1040 test 8 with parameter set 2 at strain rate of $2000\, s^{-1}$.

Figure B.12 : Constitutive fit for AISI 1040 test 7 with parameter set 2 at strain rate of $3000\, s^{-1}$.

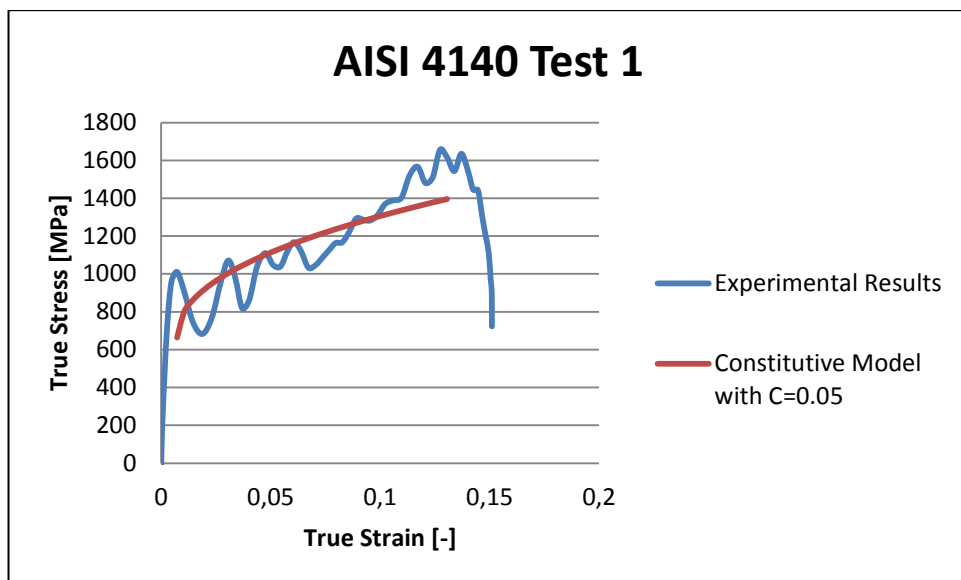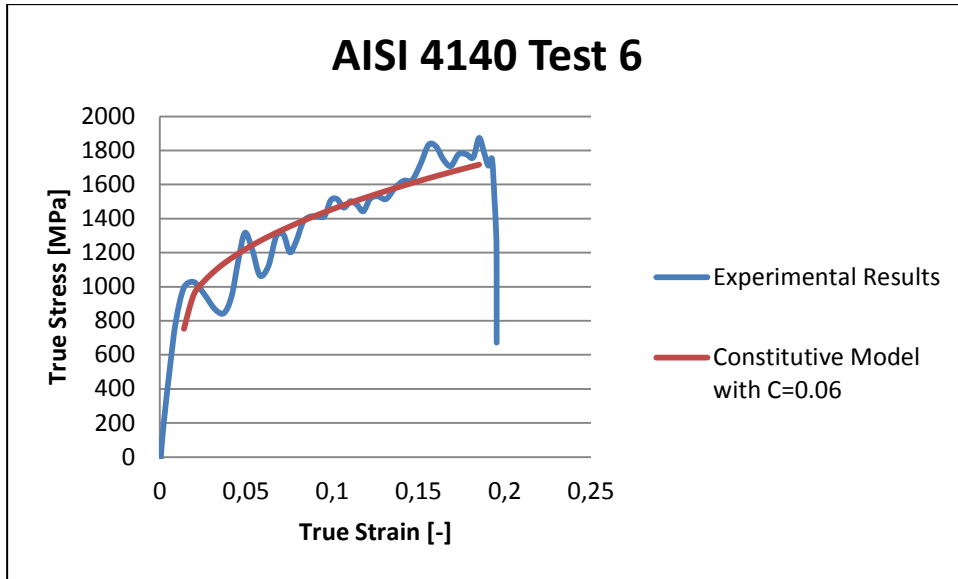**Figure B.13 :** Constitutive fit for AISI 1045 test 11 with parameter set 2 at strain rate of $1500\,s^{-1}$.

Figure B.14 : Constitutive fit for AISI 1045 test 8 with parameter set 2 at strain rate of $3000\,s^{-1}$.
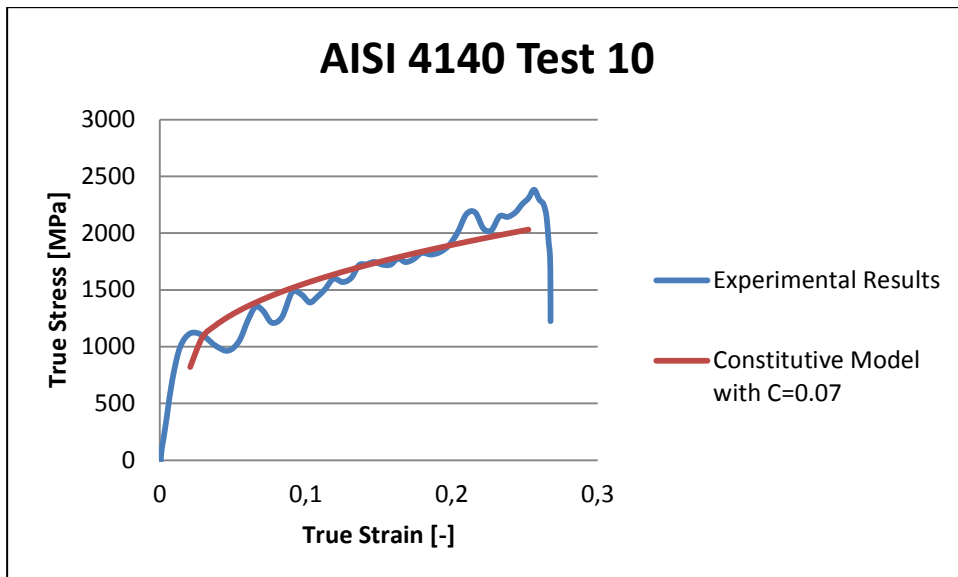
Figure B.15 : Constitutive fit for AISI 1045 test 6 with parameter set 2 at strain rate of $3000\,s^{-1}$.

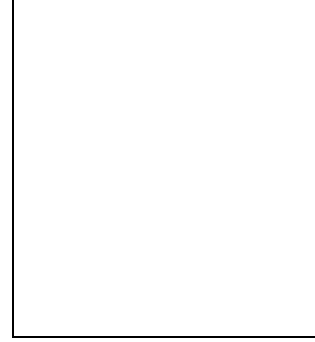**Figure B.16 :** Constitutive fit for AISI 4140 test 1 with parameter set 2 at strain rate of $1500\,s^{-1}$.

Figure B.17 : Constitutive fit for AISI 4140 test 6 with parameter set 2 at strain rate of $2000\,s^{-1}$.

Figure B.18 : Constitutive fit for AISI 4140 test 10 with parameter set 2 at strain rate of $3000\,s^{-1}$.

CURRICULUM VITAE

Name Surname:　　　**M. BURAK YEGİN**

Place and Date of Birth: Istanbul, 22.07.1986

E-Mail:　　　　　**byegin@ford.com.tr**

　　　　　　　　burakygn@hotmail.com

B.Sc.:　　　　　**Yeditepe University**

Professional Experience and Rewards: Mechanical Engineer at Ford Otosan

List of Publications and Patents: